UCSF
UC San Francisco Electronic Theses and Dissertations

Title

The Spatial Landscape of Extracellular Matrix Gene Expression in Healthy and Type 2 Diabetic Human Pancreas

Permalink

https://escholarship.org/uc/item/7x10s3kz

ISBN

9798189298271

Author

Meneses, Luisa Kimberly

Publication Date

2026-09-03

Supplemental Material

https://escholarship.org/uc/item/7x10s3kz#supplemental

Peer reviewed|Thesis/dissertation

eScholarship.org Powered by the California Digital Library
University of California

The Spatial Landscape of Extracellular Matrix Gene Expression in Healthy and Type 2 Diabetic Human Pancreas

by

Luisa Kimberly Meneses

DISSERTATION

Submitted in partial satisfaction of the requirements for degree of

DOCTOR OF PHILOSOPHY

in

Biochemistry and Molecular Biology

in the

GRADUATE DIVISION

of the

UNIVERSITY OF CALIFORNIA, SAN FRANCISCO

Approved:

DocuSigned by:

Guo Huang

9B69D521CB8C475...

Guo Huang

Chair

DocuSigned by:

Zev Gartner

Signed by:

Julie B. Sneddon

FD6D10EE42D14C8...

Julie B. Sneddon

Committee Members

Copyright 2026

By

Luisa Kimberly Meneses

Dedications/Acknowledgements

Throughout my scientific training at UCLA and UCSF, I have had the privilege of learning from outstanding mentors who have profoundly shaped my scientific journey. I am especially grateful to Dr. Zev Gartner for fostering an environment of innovation, rigorous thinking, and intellectual curiosity, and to Dr. Julie Sneddon for her invaluable guidance, generosity, and expertise in pancreatic biology. Their mentorship, encouragement, and support have been instrumental in both this dissertation and my growth as an independent scientist. I would also like to thank Dr. Brigitte Gomperts, who first introduced me to biomedical research as an undergraduate in her laboratory at UCLA. Her mentorship sparked my passion for scientific discovery and laid the foundation for my pursuit of a career in research. I am equally grateful to Dr. Tammy Rickabaugh, whose guidance, generosity, and reassurance during my time in the Gomperts laboratory greatly influenced my early development as a scientist. Even years later, her continued encouragement and willingness to check in have meant more to me than she knows.

To my parents, Liza and Ricardo, thank you for your unwavering love, encouragement, and countless sacrifices that made my education journey possible. Your belief in me gave me the confidence to pursue my goals, even during life's most challenging moments. I am forever grateful for your support and for everything you have done to help me reach this milestone. This is for you.

To my sisters, Alexa and Val, thank you for your endless love and support. You have always been my biggest cheerleaders and a constant source of strength throughout my academic journey. Whether celebrating milestones, offering words of

encouragement during difficult moments, or simply reminding me to laugh and enjoy life outside the lab, you have made this journey brighter and far less lonely. I am incredibly fortunate to have you by my side, and I will always be thankful for your love, friendship, and belief in me.

To my little brother, Mateo, watching you grow has been one of my greatest privileges, and your curiosity, resilience, and kind heart continue to inspire me every day. You remind me to appreciate the simple things in life and to always strive to be someone you can look up to. I hope this accomplishment shows you that with hard work, perseverance, and belief in yourself, anything is possible.

Finally, and most importantly, I would like to thank my fiancé, Anthony Flores. Thank you for your unconditional love, patience, and support throughout every stage of my Ph.D. You celebrated every success, helped me through every setback, and never stopped believing in me, even when I doubted myself. Your encouragement, kindness, and ability to bring balance and joy into my life have meant more than words can express. I could not have asked for a better partner to share this journey with, and I am deeply grateful for everything you have done for me and for our fur babies. This accomplishment is as much yours as it is mine.

The Spatial Landscape of Extracellular Matrix Gene Expression in Healthy and Type 2 Diabetic Human Pancreas

Luisa Kimberly Meneses

Abstract

The basement membranes surrounding human pancreatic islets and their vasculature are essential to β cell survival, polarity, and insulin secretion, yet the cells that build and maintain this extracellular matrix in the adult human pancreas, and the way it is remodeled in type 2 diabetes, have remained poorly defined. The prevailing model holds that endothelial cells are the principal source of the vascular basement membrane, but the close physical association of endothelial cells, pericytes, and fibroblasts has made it difficult to assign secreted matrix proteins to a cellular source, because conventional histology cannot identify the producing cell and dissociation-based sequencing discards spatial context. To resolve these questions, this work combined computational re-integration of publicly available human pancreas single-cell RNA-sequencing data with donor-resolved MERFISH spatial transcriptomics of non-diabetic and type 2 diabetic human pancreas, using a custom 300-gene panel that included 98 extracellular matrix genes. Islet boundaries were segmented manually, vascular populations were validated through spatial neighborhood and proximity analyses, and the single-cell and spatial datasets were treated as orthogonal analyses, with further validation against an anatomically resolved reference dataset, immunofluorescence, and RNA *in situ* hybridization. These analyses identify pericytes, rather than endothelial cells, as the predominant transcriptional source of vascular basement membrane genes, including *COL4A1*, *COL4A2*, *LAMA4*, and *LAMB2*, while

endothelial cells contribute the complementary components *HSPG2* and *LAMA5*. A spatially distinct islet-associated fibroblast population occupies the endocrine boundary and expresses a peri-islet matrix program enriched for *LAMB1* and *LAMC1*. Pericytes retain a conserved identity, while specializing between the endocrine and exocrine compartments. In type 2 diabetes, the endocrine vascular niche is remodeled, shifting the fibroblast-to-pericyte balance, reducing *PDGFRB* and basement membrane programs, and increasing contractile, stress, and inflammatory signatures. These findings support a cooperative, multicellular model in which endothelial cells, pericytes, and specialized fibroblasts build the human islet basement membrane, and they reveal its coordinated disruption in type 2 diabetes.

Table of Contents

List of Figures

List of Tables

List of Abbreviations

ACE: Angiotensin-converting enzyme

ACE2: Angiotensin-converting enzyme 2

ADAM9: ADAM metallopeptidase domain 9

ADIRF: Adipogenesis regulatory factor

ALB: Albumin

AQP1: Aquaporin 1

ARX: Aristaless related homeobox

BM: Basement membrane

BMI: Body mass index

BMP4: Bone morphogenetic protein 4

C1QB, C1QC: Complement C1q B/C chain

C1R, C1S: Complement C1r/C1s

C11orf96: Chromosome 11 open reading frame 96

CALD1: Caldesmon 1

CD4, CD8A: Cluster of differentiation 4 / 8 alpha

CD31: Cluster of differentiation 31 (PECAM1)

CD93: CD93 molecule

CDH5: Cadherin 5 (VE-cadherin)

CELA3B: Chymotrypsin-like elastase family member 3B

CFTR: Cystic fibrosis transmembrane conductance regulator

CHGA: Chromogranin A

CLDN5: Claudin 5

COL1A1, COL1A2: Collagen type I alpha 1/2 chain

COL3A1: Collagen type III alpha 1 chain

COL4A1, COL4A2, COL4A3: Collagen type IV alpha 1/2/3 chain

COL5A1, COL5A2: Collagen type V alpha 1/2 chain

COL6, COL6A1, COL6A2, COL6A3: Collagen type VI (alpha 1/2/3 chain)

COL12A1: Collagen type XII alpha 1 chain

COL13A1: Collagen type XIII alpha 1 chain

COL14A1: Collagen type XIV alpha 1 chain

COL18A1: Collagen type XVIII alpha 1 chain

CPM: Counts per million

CSPG4: Chondroitin sulfate proteoglycan 4 (NG2)

CTSB: Cathepsin B

CXCR4: C-X-C chemokine receptor type 4

DAPI: 4′,6-Diamidino-2-phenylindole

DCN: Decorin

DDIT4: DNA damage inducible transcript 4

DE: Differential expression

DGE: Differential gene expression

DEF8: Differentially expressed in FDCP 8 homolog

DHCR24: 24-Dehydrocholesterol reductase

DV200: RNA integrity metric (percentage of RNA fragments >200 nucleotides)

ECM: Extracellular matrix

EC: Endothelial cell

EGFL7: EGF-like domain multiple 7

EGR1: Early growth response 1

ERG: ETS-related gene

ESM1: Endothelial cell-specific molecule 1

FAM20C: FAM20C Golgi-associated secretory pathway kinase

FBLN1: Fibulin 1

FDR: False discovery rate

FFPE: Formalin-fixed, paraffin-embedded

FGA: Fibrinogen alpha chain

FJX1: Four-jointed box kinase 1

FLT1: Fms-related receptor tyrosine kinase 1 (VEGFR1)

FN1: Fibronectin 1

FOS: Fos proto-oncogene

FPKM: Fragments per kilobase of transcript per million mapped reads

FSTL1: Follistatin-like 1

GCG: Glucagon

GDF15: Growth differentiation factor 15

GEO: Gene Expression Omnibus

GHRL: Ghrelin

GLUT2: Glucose transporter 2 (SLC2A2)

GO: Gene Ontology

GSEA: Gene set enrichment analysis

H&E: Hematoxylin and eosin

HMOX1: Heme oxygenase 1

HOTAIRM1: HOXA transcript antisense RNA myeloid specific 1

HPAP: Human Pancreas Analysis Program

HSPG2: Heparan sulfate proteoglycan 2 (Perlecan)

IAF: Islet-associated fibroblast

IAPP: Islet amyloid polypeptide

ICOSLG: Inducible T-cell costimulator ligand

ID3: Inhibitor of DNA binding 3

IF: Immunofluorescence

IFI6: Interferon alpha inducible protein 6

IFI35: Interferon induced protein 35

IGFBP2: Insulin-like growth factor binding protein 2

IL-6: Interleukin 6

INS, INS1: Insulin

JAK/STAT3: Janus kinase/signal transducer and activator of transcription 3

JUN: Jun proto-oncogene

KDR: Kinase insert domain receptor (VEGFR2)

KRT19: Keratin 19

LAMA2, LAMA4, LAMA5: Laminin alpha 2/4/5 chain

LAMB1, LAMB2: Laminin beta 1/2 chain

LAMC1, LAMC2, LAMC3: Laminin gamma 1/2/3 chain

LGALS1: Galectin 1

LIMA1: LIM domain and actin binding 1

LRPAP1: LDL receptor-related protein associated protein 1

LSAMP: Limbic system-associated membrane protein

LUM: Lumican

LY96: Lymphocyte antigen 96

MAFA: MAF bZIP transcription factor A

MALDI: Matrix-assisted laser desorption/ionization

MCAM: Melanoma cell adhesion molecule

MERFISH: Multiplexed error-robust fluorescence *in situ* hybridization

MFGE8: Milk fat globule-EGF factor 8 protein

MSigDB: Molecular Signatures Database

MSL1: Mesenchymal subtype 1 (fibroblast-like)

MSL2: Mesenchymal subtype 2 (pericyte-like)

MYL9: Myosin light chain 9

MYO10: Myosin X

NCS1: Neuronal calcium sensor 1

ND: Non-diabetic

NES: Normalized enrichment score

NEUROD1: Neuronal differentiation 1

NG2: Neuron-glial antigen 2 (CSPG4)

NGN3: Neurogenin 3

NID1, NID2: Nidogen 1/2

NKX6.1: NK6 homeobox 1

NMT1: N-myristoyltransferase 1

OLFML2A: Olfactomedin-like 2A

PASK: PAS domain-containing serine/threonine kinase

PDGF: Platelet-derived growth factor

PDGF-B: Platelet-derived growth factor B chain

PDGFRB, PDGFRβ: Platelet-derived growth factor receptor beta

PDX1: Pancreatic and duodenal homeobox 1

PECAM1: Platelet endothelial cell adhesion molecule 1 (CD31)

PLVAP: Plasmalemma vesicle-associated protein

PNP: Purine nucleoside phosphorylase

PP / PPY: Pancreatic polypeptide (cells/hormone)

PRELP: Proline/arginine-rich end leucine-rich repeat protein

PROCR: Protein C receptor

QC: Quality control

RBM24: RNA binding motif protein 24

RGS5: Regulator of G protein signaling 5

RNAscope: RNA *in situ* hybridization assay platform

ROI: Region of interest

RRID: Research Resource Identifier

S100A6: S100 calcium binding protein A6

SCAD: Surfactant and chaotropic agent-assisted decellularization protocol

SDF2L1: Stromal cell-derived factor 2-like 1

SEC11C: SEC11 homolog C, signal peptidase complex subunit

SERPINA1: Serpin family A member 1

SERPINA3: Serpin family A member 3

SERPINF1: Serpin family F member 1

SFRP2: Secreted frizzled-related protein 2

SIDT2: SID1 transmembrane family member 2

SLC7A5: Solute carrier family 7 member 5

SOX18: SRY-box transcription factor 18

SST: Somatostatin

SSTR2: Somatostatin receptor 2

T2D: Type 2 diabetes

TCF7L2: Transcription factor 7-like 2

TGFBR3: Transforming growth factor beta receptor 3

TGF-β: Transforming growth factor beta

TGM2: Transglutaminase 2

THBD: Thrombomodulin

THBS1: Thrombospondin 1

TM4SF4: Transmembrane 4 L six family member 4

TMEM160: Transmembrane protein 160

TNRC18: Trinucleotide repeat containing 18

UMAP: Uniform Manifold Approximation and Projection

UNC5B: Unc-5 netrin receptor B

UPP1: Uridine phosphorylase 1

VEGFA: Vascular endothelial growth factor A

VEGFR2: Vascular endothelial growth factor receptor 2 (KDR)

VIM: Vimentin

VWF: Von Willebrand factor

List of Symbols

α cells: Glucagon-producing alpha cells

β cells: Insulin-producing beta cells

δ cells: Somatostatin-producing delta cells

γ cells: Pancreatic polypeptide-producing gamma cells

ε cells: Ghrelin-producing epsilon cells

α, β, γ (laminin chains): Laminin heterotrimer subunit chains

μm: Micrometer

nm: Nanometer

p: *p*-value (statistical significance)

r: Pearson correlation coefficient

ρ: Spearman correlation coefficient

z (z-score): Standardized score used for gene expression scaling and heatmap visualization.

Chapter 1 Introduction

1.1 The Human Pancreas

The human pancreas is a dual-function organ central to both digestion and metabolic homeostasis [1]. Located in the upper abdomen near the liver and stomach, and attached to the spleen, it operates simultaneously as an exocrine gland that produces digestive enzymes and as an endocrine organ that regulates systemic glucose metabolism through hormone secretion (**Fig. 1-1**) [1, 2]. Although these two functions have traditionally been studied in isolation, the endocrine and exocrine compartments comprise a single integrated tissue, sharing vasculature, stromal populations, extracellular matrix (ECM) networks, and neural inputs [2, 3]. The interactions among these elements maintain tissue homeostasis and coordinate the organ's response to changing nutritional and metabolic demands [2, 3].

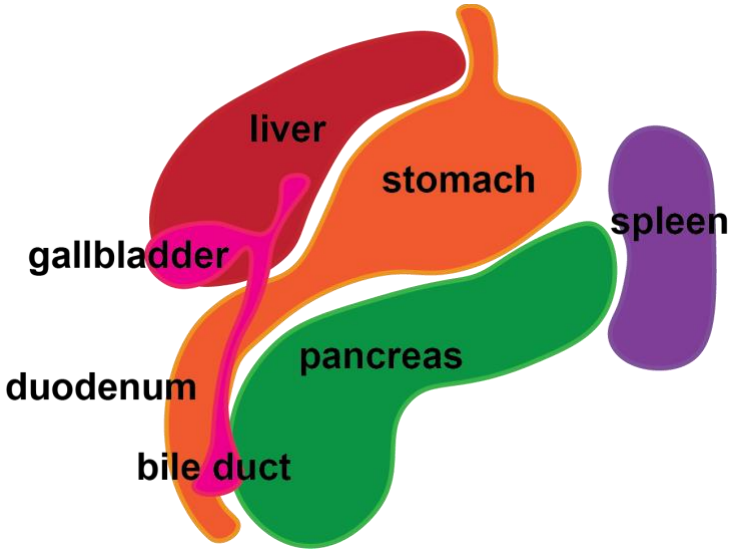

Figure 1-1: Gross anatomy of the human pancreas and the surrounding upper abdominal organs.

Schematic illustration showing the anatomical relationships between the pancreas (green), duodenum (orange), bile duct (magenta), gallbladder (magenta), liver (red), stomach (orange), and spleen (purple). The pancreas extends from the C-shaped duodenum toward the spleen and lies posterior to the stomach. The common bile duct passes through the head of the pancreas before emptying into the duodenum.

The two compartments differ strikingly in mass and organization. The exocrine pancreas accounts for roughly 98% of pancreatic mass and is built from acinar units and a branching ductal system that together synthesize and deliver digestive enzymes to the duodenum [2]. The endocrine pancreas comprises only 1 to 2% of pancreatic mass and is organized into islets of Langerhans, compact clusters of hormone-producing cells (**Fig. 1-2**) [4]. Despite their small volume and size (20-500 µm in diameter), islets exert a vast influence on whole-body metabolism through the regulated secretion of insulin (INS), glucagon (GCG), somatostatin (SST), pancreatic polypeptide (PPY), and other peptide hormones [4].

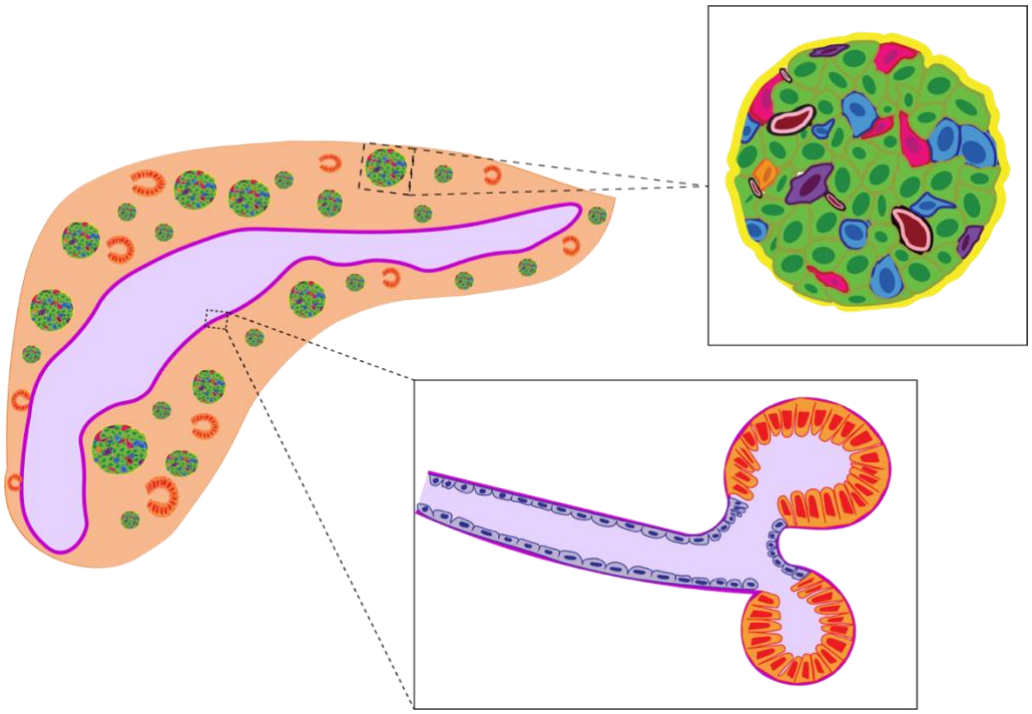

Figure 1-2: Schematic overview of the human pancreas and islet microenvironment.

Illustration of the pancreas showing major tissue compartments, including the pancreatic duct (purple), exocrine tissue, ducts, and scattered endocrine islets. The top inset highlights an individual pancreatic islet surrounded by a basement membrane and containing endocrine cells and support cells that together form the endocrine niche. The bottom inset highlights the structure of the exocrine compartment with ductal cells (purple) lining the duct and terminal acini composed of acinar cells (orange).

1.2 Cellular Composition of the Endocrine Niche

The endocrine pancreas is more than a cluster of hormone-producing cells. It includes a specialized structure in which endocrine, vascular, immune, and neural populations act together to sense metabolic demand and coordinate hormone secretion [4]. Endocrine cell function depends heavily on signals from neighboring vascular cells, which contribute not only to tissue architecture and perfusion but also to endocrine survival, maturation, and secretory activity [5–11].

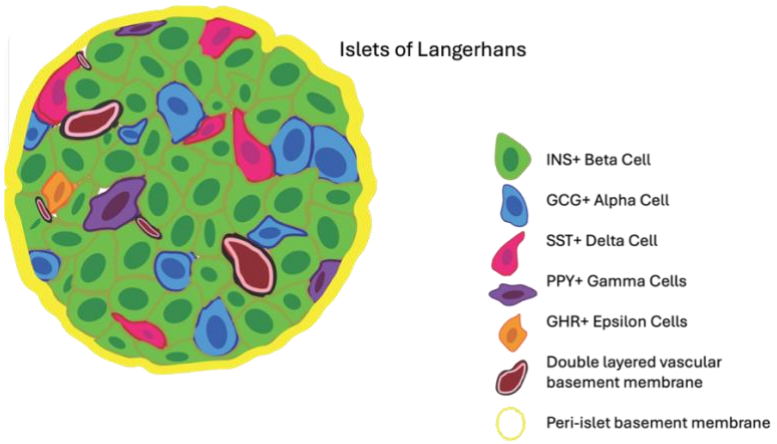

Figure 1-3: Schematic organization of the human pancreatic islet and its relationship to the surrounding ECM.

Insulin-producing β cells (green) are intermingled with glucagon-producing α cells (blue), somatostatin-producing δ cells (magenta), pancreatic polypeptide-producing cells (purple), and ghrelin-producing ε cells (orange). The islet is enclosed by the peri-islet BM (yellow outline) and contains a dense network of fenestrated capillaries surrounded by a double-layered vascular BM (red/black).

A key structural feature of this islet niche is the ECM, including the peri-islet basement membrane that surrounds each islet and the vascular basement membrane that ensheathes the dense intra-islet capillary network (**Fig. 1-3**) [12]. These basement membrane structures provide mechanical support while regulating cell adhesion, signaling, and communication between endocrine cells and their surrounding microenvironment [13].

1.2.1 Endocrine Cell Populations

Within the human pancreatic islet, β cells are the most abundant endocrine population (50-70%) and the principal cellular source of insulin [14]. β cells function as specialized glucose sensors and secrete insulin primarily when circulating glucose concentrations rise, particularly following a meal [15]. Glucose uptake and metabolism increase the intracellular ATP-to-ADP ratio, causing ATP-sensitive potassium channels to close, membrane depolarization, opening of voltage-dependent calcium channels, and calcium-triggered exocytosis of insulin-containing granules [16]. Although glucose is the principal physiological stimulus, insulin secretion is further potentiated by amino acids, fatty acids, autonomic input, and the incretin hormones GLP-1 and GIP [17]. Once released, insulin lowers circulating glucose by promoting glucose uptake and utilization in skeletal muscle and adipose tissue, stimulating glycogen and lipid synthesis, and suppressing hepatic glycogenolysis and gluconeogenesis [18].

β cells arise from multipotent pancreatic epithelial progenitors through a series of progressively restricted developmental states. Pancreatic progenitors first acquire endocrine competence through induction of the basic helix-loop-helix transcription factor *NGN3*, which is required for the generation of all major islet endocrine lineages [19]. Single-cell transcriptomic studies of the developing mouse pancreas and human embryonic stem cell differentiation models have further resolved this process into sequential *NGN3*-low, *NGN3*-high, and *FEV*-positive endocrine intermediates that precede the acquisition of mature hormone expression [19, 20]. These intermediate populations subsequently diverge along distinct α- and β-cell developmental trajectories, demonstrating that endocrine identity is established progressively rather

than through a single abrupt lineage decision. Commitment to the β-cell lineage is associated with coordinated activity of transcriptional regulators that include *PAX4*, *NKX2.2*, *PDX1*, and *NKX6.1*, whereas later functional maturation is supported by factors such as *MAFA* [20, 21]. This sequential transcriptional program establishes the machinery required for glucose sensing, insulin production, and regulated insulin secretion.

α cells are generally the second most abundant endocrine population and are the principal source of glucagon. In contrast to β cells, which are activated by elevated glucose, α cells increase glucagon secretion when circulating glucose concentrations fall, particularly during fasting, prolonged exercise, or hypoglycemia [22]. Glucagon secretion can also be stimulated by circulating amino acids, autonomic signals, and counter-regulatory hormones [22, 23]. At higher glucose concentrations, α-cell activity is restrained through a combination of intrinsic nutrient sensing and paracrine inhibition from neighboring islet cells [23]. Insulin and other β-cell-derived signals contribute to this inhibition, while somatostatin released from δ cells provides an additional potent restraint on glucagon secretion [22, 23].

Glucagon acts primarily on the liver to restore circulating glucose and preserve fuel availability during periods of nutrient deprivation [24]. Its most immediate effect is stimulation of hepatic glycogenolysis, through which stored glycogen is rapidly broken down and glucose is released into the circulation [24]. As fasting continues and hepatic glycogen stores become depleted, glucagon promotes gluconeogenesis from substrates such as lactate, glycerol, and glucogenic amino acids. Glucagon also suppresses hepatic glycogen synthesis and glycolysis, thereby directing hepatic metabolism toward

glucose production rather than glucose storage or utilization. In the setting of low insulin, glucagon additionally promotes hepatic fatty-acid oxidation and ketogenesis, generating alternative fuels that become increasingly important during prolonged fasting [23, 24]. Glucagon also regulates hepatic amino-acid uptake, catabolism, and ureagenesis, forming part of a reciprocal liver-α-cell feedback system that coordinates amino-acid and glucose homeostasis [22–24]. Thus, α-cell function extends beyond stimulating gluconeogenesis and includes the coordinated regulation of glycogen metabolism, amino-acid turnover, lipid oxidation, and ketone production.

Like β cells, α cells arise from *NGN3*-positive endocrine progenitors but follow a distinct lineage-specification program [19–21]. Acquisition of α-cell identity is promoted by transcriptional regulators including *ARX* and *MAFB*, which support glucagon expression and α-cell functional identity, whereas suppression of alternative endocrine programs helps stabilize the mature α-cell state [19, 20]. In adult human islets, α cells are dispersed throughout the endocrine compartment and frequently lie adjacent to β and δ cells. This arrangement creates extensive opportunities for reciprocal paracrine communication, allowing insulin, glucagon, and somatostatin secretion to be coordinated in response to changing nutrient availability.

δ cells produce somatostatin, a potent local inhibitor of both insulin and glucagon secretion [25]. Although less abundant than α and β cells, δ cells exert broad regulatory control through paracrine signaling [26]. Their influence is aided by a distinctive morphology in which long cytoplasmic projections extend toward multiple neighboring endocrine cells, increasing the spatial range over which somatostatin can act and

allowing a relatively small δ cell population to regulate a substantial portion of the islet [26].

δ cells are integrated into reciprocal feedback circuits with neighboring endocrine populations. In mature β cells, urocortin 3 is stored and released together with insulin in response to elevated glucose [27]. Urocortin 3 subsequently activates receptors on δ cells and potentiates somatostatin secretion, which feeds back onto β cells to restrain further insulin release as circulating glucose returns toward its physiological range [27]. This β cell–δ cell feedback loop therefore acts as a local brake that prevents excessive or prolonged insulin secretion and contributes to the precise matching of insulin output to metabolic demand.

More recent loss-of-function studies have demonstrated that δ cell signaling contributes directly to the regulation of systemic glucose homeostasis. In mice, genetic or pharmacological disruption of pancreatic δ cells or somatostatin signaling lowered the glucose concentration at which β cells began to respond, increased insulin secretion in response to a given glucose challenge and produced a sustained reduction in the glycemic set point [28]. These findings establish δ cells as active determinants of the threshold and magnitude of β cell responses rather than merely passive inhibitors of hormone secretion. Together, the extensive morphology and reciprocal signaling relationships of δ cells enable this relatively small endocrine population to coordinate islet output and stabilize circulating glucose concentrations.

Two smaller populations complete the endocrine compartment. PPY-producing γ cells, also called pancreatic polypeptide or PP cells, secrete pancreatic polypeptide in response to food intake, vagal stimulation, exercise, and hypoglycemia. Pancreatic

polypeptide contributes to the coordination of digestive and metabolic responses by inhibiting pancreatic exocrine secretion and modulating gastrointestinal motility and gastric emptying. Peripheral pancreatic polypeptide also promotes satiety and reduces food intake, while delayed gastric emptying can slow the postprandial rise in circulating glucose and insulin [25, 29–31].

Ghrelin-producing ε cells represent an even rarer endocrine population. During human pancreatic development, ε cells can constitute a substantial fraction of the emerging endocrine compartment and are frequently positioned around developing islets. Their abundance declines markedly after birth, however, and they account for less than 1% of endocrine cells in the adult human pancreas [25, 32, 33]. Ghrelin is best known as an orexigenic hormone that stimulates appetite and contributes to the regulation of energy balance and glucose homeostasis. Because most circulating ghrelin is produced by the gastrointestinal tract, the very small ε cell population in the adult pancreas is unlikely to contribute substantially to systemic ghrelin concentrations. Instead, pancreatic ε cells may act primarily through local signaling within the islet. In isolated human islets, ghrelin suppresses glucose-stimulated insulin secretion, indicating that ε cells may influence the threshold and magnitude of the β cell response to glucose [34]. Experimental studies in β cell lines and rodent models further suggest that acylated and unacylated ghrelin can promote β cell proliferation and survival and protect against apoptosis and metabolic stress, although the extent to which adult human pancreatic ε cells provide this protective signal *in vivo* remains unresolved [35, 36]. Although γ and ε cells contribute relatively little to total endocrine mass, their regulation of digestive activity, appetite, islet hormone secretion, and potentially

endocrine-cell survival further illustrates the cellular and functional diversity of the human islet (**Fig. 1-3**).

1.2.2 Vascular-Associated Cell Populations

The pancreatic vascular basement membrane forms a specialized interface between endothelial cells, pericytes, and endocrine cells, supporting vessel stability while also regulating endocrine cell function (**Fig. 1-4).**

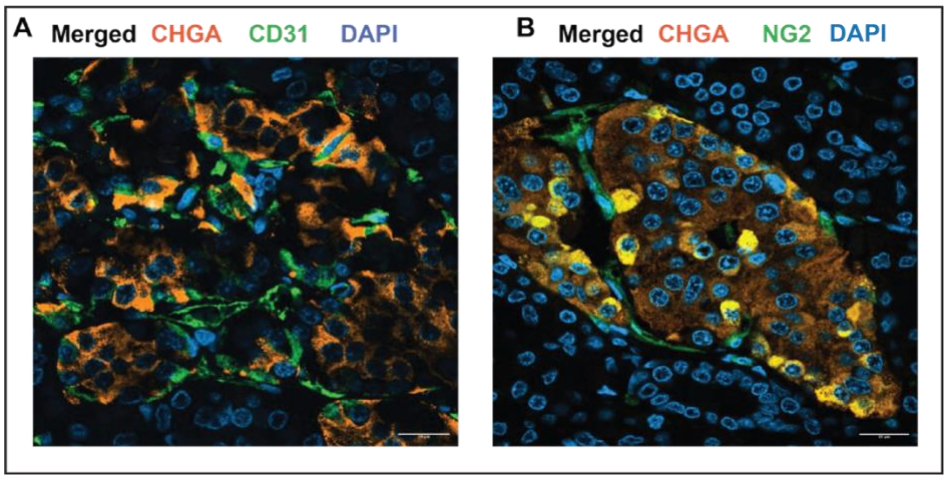

Figure 1-4: Representative immunofluorescence image of the human islet vasculature and its associated cell types.

(**A**) Representative immunofluorescence images of human pancreatic tissue stained for pan-endocrine marker CHGA (orange), CD31 (green), and DAPI (blue). CD31 immunostaining highlights the dense endothelial capillary network surrounding and penetrating the islet. Scale bar = 20 μm.
(**B**) Representative immunofluorescence images of human pancreatic tissue stained for CHGA (orange), NG2 (green), and DAPI (blue). NG2 immunostaining identifies pericytes closely associated with the islet microvasculature. Scale bar = 20 μm.

1.2.2.1 Endothelial Cells

Endothelial cells line the islet capillary network and form the interface between the circulating blood and the endocrine parenchyma (**Fig. 1-4A**) [11]. In both human and rodent endothelial cells are identified by the pan-endothelial markers *PECAM1*, *VWF*, *CDH5*, and *KDR*, together with *ERG* and *CLDN5*, but within the islet they adopt a specialized phenotype distinct from endothelium elsewhere in the pancreas [37, 38].

Recent single-cell profiling of the adult human pancreas has further shown that islet endothelial cells adopt a transcriptional phenotype distinct from endothelial cells in the exocrine compartment [38]. This human islet-enriched signature includes structural and vascular genes such as *COL13A1*, *ESM1*, *PLVAP*, *UNC5B*, and *LAMA4*; angiocrine-associated genes such as *THBS1* and *CXCR4*; and metabolic genes such as *ACE* and *PASK*, reflecting the specialized demands of the human endocrine microenvironment [38]. A defining structural feature of islet endothelium is its extensive fenestration [37, 39–41]. Quantitative descriptions of fenestra abundance have been derived largely from rodent studies, in which islet capillaries contain approximately ten times the density of fenestrae found in the surrounding exocrine vasculature [37]. These transcellular pores are spanned by diaphragms containing the protein encoded by PLVAP and contribute to the high permeability of islet capillaries [37]. Fenestrated capillaries are also present in human islets, although their density, distribution, and ultrastructural organization are not necessarily identical to those observed in rodents [37, 40]. Functionally, endothelial permeability facilitates the rapid exchange of glucose, oxygen, and other circulating signals between the blood and endocrine tissue while allowing newly secreted insulin and other hormones to enter the circulation with minimal delay [37, 40].

In both species, endothelial specialization is accompanied by a dense islet vascular supply [3, 42]. Rodent islets contain a highly convoluted intra-islet capillary network that places most endocrine cells near a vessel. Human islets are likewise richly vascularized, but their vascular architecture is generally less dense and less tortuous than that of mouse islets [43]. Despite these species-specific architectural differences, human β cells frequently lie adjacent to capillaries, minimizing diffusion distances and

bringing the endocrine cell surface into close association with the vascular basement membrane [44]. Studies performed predominantly in rodents indicate that this vascular contact contributes to glucose sensing, β cell polarity, and the preferential targeting of insulin secretion toward the bloodstream [45–47]. Similar polarized relationships have been observed in human islets, although the precise cellular organization is more heterogeneous than in the mouse [44, 48].

Much of the mechanistic understanding of how the islet endothelial phenotype is established and maintained comes from genetically modified mouse models. In mice, β cells express high levels of vascular endothelial growth factor A (VEGFA) during development and adult life, and VEGFA signaling through endothelial VEGFR2 promotes the recruitment, proliferation, survival, and fenestration of islet endothelial cells [49–52]. β cell-specific deletion of VEGFA in mice reduces intra-islet vascular density, eliminates or markedly decreases endothelial fenestration, lowers islet blood flow, and impairs glucose-stimulated insulin secretion [53, 54]. Withdrawal of local VEGFA signaling also causes fenestrae to regress, indicating that a continuous endocrine-derived VEGFA signal is required to maintain the specialized rodent islet vasculature [49]. Human β cells also express VEGFA, and human islet endothelial cells express its receptors, suggesting that a comparable signaling axis operates in the human pancreas; however, direct functional evidence in humans remains more limited [38].

The relationship between endocrine and endothelial cells is reciprocal. Developmental studies in the rodent systems have shown that blood vessels contribute to pancreatic specification, endocrine differentiation, and the induction of insulin

expression [54]. In adult rodent islets, endothelial cells produce angiocrine and extracellular-matrix signals that support β cell identity and function [7, 55]. Reported factors include hepatocyte growth factor, thrombospondins, connective tissue growth factor, endothelins, and laminins, which have been associated with β cell proliferation, survival, insulin biosynthesis, and functional maturation [56, 57]. Human pancreatic endothelial cells express several of these factors, and studies using isolated human islets or human endothelial-endocrine coculture systems support the existence of similar reciprocal signaling [57–59]. Nevertheless, the individual functions assigned to these angiocrine factors have been established most extensively in experimental rodent models. The current evidence therefore supports a conserved bidirectional dialogue in which endocrine cells shape the vasculature through signals such as VEGFA, while endothelial cells influence endocrine cells through soluble, angiocrine, and matrix-bound cues.

A central component of this dialogue is the vascular basement membrane. In both human and rodent islets, endothelial cells contribute selected basement-membrane constituents, including specific laminin chains [7, 38]. Rodent studies have shown that vascular laminins bind integrins on adjacent β cells, helping establish cell polarity, direct insulin-granule trafficking toward the capillary, and activate prosurvival signaling pathways [46, 60–63]. Human β cells also express basement-membrane-binding integrins and associate closely with vascular basement membranes, supporting the relevance of these mechanisms to human islet biology [12, 44]. However, the human islet basement membrane has a more complex and distinctly bilayered

organization, and its cellular sources and molecular composition cannot be inferred directly from mouse studies [48].

Islet endothelial cells additionally participate in immune surveillance, barrier regulation, and the control of local perfusion. Evidence from both human tissue and rodent models shows that pancreatic endothelial cells express adhesion molecules involved in leukocyte recruitment and trafficking, although most functional studies of immune-cell entry into islets have been conducted in mice [64–67]. Similarly, endothelial-derived vasoactive mediators, including nitric oxide and endothelin-1, are thought to adjust local vascular tone and match islet blood flow to metabolic and secretory demand, but the underlying mechanisms have again been characterized primarily in rodents [68]. Thus, although mouse studies have provided the mechanistic framework for understanding islet endothelial biology, human islets differ in vascular density, capillary organization, basement-membrane architecture, and endothelial transcriptional state. These differences make direct investigation of human islet endothelium essential rather than assuming that all features of the mouse vascular niche are conserved in humans.

1.2.2.2 Pericytes

Pericytes are mural cells that wrap closely around the endothelium of the islet capillary network, are embedded within the vascular basement membrane, and form direct physical and signaling contacts with endothelial cells (**Fig. 1-4B**) [69]. In the pancreas they occupy a periendothelial position, extend long cytoplasmic processes along the vessel, and can be identified by NG2 (encoded by CSPG4), PDGFRB, DES,

and α-smooth muscle actin, together with RGS5, a marker whose expression scales with pericyte coverage of the vasculature [69–71].

The recruitment and retention of pericytes are governed by platelet-derived growth factor (PDGF) signaling [11, 72]. Endothelial cells secrete PDGF-B, which binds PDGFRβ on the pericyte surface to drive pericyte proliferation, migration, and investment of the vessel wall, and complete loss of either Pdgfb or Pdgfrb in mice produces a near-total absence of pericytes and embryonic lethality [73]. Although these foundational experiments were performed largely in the brain and other vascular beds, they established endothelial PDGF-B as a central regulator of pericyte recruitment and maintenance. Importantly, this conclusion was strengthened using a tamoxifen-inducible, endothelial-specific Cre model in which Pdgfb was deleted in two-month-old mice, after the cerebral vasculature and its pericyte coverage had already formed. The subsequent, slowly progressive loss of brain pericytes demonstrated that endothelial PDGF-B is required not only for their recruitment during vascular development but also for maintaining pericyte coverage in the mature cerebral microvasculature. Whether adult islet pericytes exhibit the same continuous dependence has not been tested directly, but their expression of PDGFRβ and close association with PDGF-B-producing endothelial cells suggest that this pathway may similarly contribute to their maintenance [73–77].

A long-standing view holds that the principal function of the islet pericyte is the regulation of capillary perfusion [78, 79]. Direct study of mouse islets has confirmed that pericytes control local capillary diameter and blood flow, mediating the acute functional hyperemia that increases islet perfusion in response to a glucose challenge [78].

Through their contractile machinery and their integration of vasoactive signals, pericytes match perfusion, oxygen delivery, and hormone clearance to secretory demand, a function of particular importance in a tissue where insulin output must adapt within seconds [78, 80].

More recent mouse experiments have shown that islet pericytes are not merely vascular regulators but active supporters of β cells [9, 70, 81–84]. Using a diphtheria toxin-based transgenic system to deplete pancreatic pericytes *in vivo*, the Landsman laboratory found that pericyte loss reduces islet insulin content and expression, impairs glucose-stimulated insulin secretion, and is accompanied by reduced expression of genes associated with mature β cell function [83, 84]. Critically, the secretion defect persisted in isolated islets studied outside the body, demonstrating that pericytes support β cell maturity directly rather than only by controlling blood flow [81]. Mouse pancreatic pericytes produce BMP4 during the postnatal period, and this niche-derived BMP4 promotes β cell maturation by supporting core β cell gene expression, insulin production, and glucose-stimulated insulin [81, 82]. Islet pericytes therefore contribute to both the functional maturation of β cells and the expansion of β cell mass during development.

A growing body of work links these trophic effects to the matrix that pericytes produce. Mouse pancreatic pericytes express multiple components of the interstitial and basement membrane matrices, including collagen IV, laminins, proteoglycans, fibronectin, and nidogen, and they generate substantially higher levels of the α2 and α4 laminin chains than other islet cells, chains that build the peri-islet and vascular basement membranes [70]. Culturing islet cells on a pericyte-type laminin, Laminin-421,

induces expression of the β cell genes *INS1*, *MAFA*, and *GLUT2* and improves glucose-stimulated insulin secretion [70]. These findings reframe the pericyte as a significant source of the islet basement membrane and connect its matrix output directly to β cell identity and function, a relationship central to this dissertation.

Taken as a whole, the islet pericyte has been reported as a multifunctional cell spanning contractile regulation of blood flow, paracrine support of β cell maturation and proliferation, and active production of the islet basement membrane, rather than a passive structural support. An important caveat is that nearly all this mechanistic evidence derives from mouse models, and the genetic tools underlying it are not pericyte-specific. The vascular regulation studies rely principally on a NG2 reporter and CreER lines to visualize and manipulate pericytes [85]. NG2 also marks other mural cells, including vascular smooth muscle cells, so NG2-based labeling and calcium imaging cannot fully exclude a contribution from non-pericyte perivascular cells to the observed capillary responses [78]. The paracrine and maturation studies rest on the Nkx3.2-Cre; iDTR system, which carries a comparable limitation [70, 81–84]. Nkx3.2 marks the broader embryonic pancreatic mesenchyme rather than a pericyte-restricted lineage; indeed, the same Cre line has been used by the Landsman group to ablate the entire mesenchymal compartment of the developing pancreas in earlier work [86]. The line also drives recombination outside the pancreas, in joint and gastrointestinal mesenchyme, which underscores that Nkx3.2 lineage-tracing captures a developmental mesenchymal origin rather than a pericyte-specific marker in the mature organ [82]. The matrix production data derive from bulk or population-level profiling of these same imprecisely defined populations [70]. Because adult Nkx3.2- and NG2-lineage cells

encompass pericytes alongside other stromal or mural derivatives, none of these systems can cleanly isolate pericyte-specific contributions to β cell maturation, blood flow regulation, or matrix production from effects mediated by co-depleted or co-labeled non-pericyte populations sharing the same developmental or marker profile.

1.2.2.3 Fibroblasts/Mesenchyme

Fibroblasts are major stromal producers of the ECM, expressing the fibrillar collagens, proteoglycans, and glycoproteins that define tissue architecture [87]. They synthesize the interstitial network of collagens I, III, and V together with fibronectin, the small leucine-rich proteoglycans decorin (DCN) and lumican (LUM), matricellular proteins, and they continually remodel this matrix through secreted proteases and their inhibitors [87]. Through the matrix they build, fibroblasts govern tissue mechanics, set the pathways available for cell migration, and act as a reservoir and presenter of growth factors, placing these cells at the center of stromal organization in the pancreas [87, 88].

Far from being a uniform population, pancreatic fibroblasts are heterogeneous and spatially organized [89, 90]. Pancreatic fibroblasts arise from the embryonic mesenchyme surrounding the developing pancreatic epithelium, which is derived primarily from the splanchnic layer of the lateral plate mesoderm adjacent to the foregut endoderm [91]. Mouse lineage-tracing studies using constitutive and temporally inducible Isl1-Cre reporters have shown that ISL1-expressing splanchnic mesenchymal cells present during early pancreatic specification give rise to most tissue-resident fibroblasts in the adult pancreas, including interstitial and perivascular stromal cells [91]. Within this broader lineage, the peripheral WT1-expressing pancreatic mesothelium acts as an additional mesenchymal progenitor compartment: inducible Wt1-CreER

tracing demonstrated that embryonic mesothelial cells generate several transcriptionally distinct *DCN*, *NTM*, and *ACE2*+ mesenchymal populations during pancreatic organogenesis [92]. Other stromal lineages become progressively restricted during development; for example, Nkx3.2-Cre lineage tracing identified NKX3.2-expressing embryonic pancreatic mesenchyme as a major source of adult pancreatic pericytes [82]. Thus, the adult pancreatic stroma does not arise from a single homogeneous fibroblast precursor but from spatially and transcriptionally distinct populations within the splanchnic mesenchymal lineage.

A recurring theme in stromal biology is that fibroblast identity is dictated largely by anatomical location and local signals [93]. Subepithelial fibroblasts in the intestine maintain epithelial stem cells, papillary and reticular fibroblasts impose distinct properties on the dermis, and boundary-associated fibroblasts have been described around many epithelial and vascular structures [94–97]. In the pancreas this principle predicts the existence of fibroblast subsets specialized to niches, and one such niche lies at the interface between the endocrine and exocrine compartments [98]. A subset of fibroblasts is enriched at the islet boundary, occupying the narrow zone around the islet rather than the general interstitium [98].

The molecular identity of this islet-associated population overlaps with that of other mesenchymal cells, which has historically complicated its classification [99–101]. Fibroblasts, pancreatic stellate cells, and mesenchymal stromal cells share many markers, including *PDGFRB*, *COL1A1*, *COL1A2*, *DCN*, and *LUM*, and a given population may be labeled a fibroblast, a stellate cell, or a mesenchymal cell depending on the study and the methods used [38, 99–101]. This overlap reflects genuine

biological relatedness within the pancreatic mesenchyme rather than simple ambiguity, but it means that transcription alone is often insufficient to define a stromal population [102]. Anatomical context becomes essential, since the reproducible localization of a population, such as enrichment at the islet boundary, can distinguish a specialized fibroblast from a generic interstitial one even when their marker profiles are similar [38].

Unlike pericytes, which are embedded within the vascular wall and tied to the endothelium, fibroblasts associate with the broader interstitial matrix network and are not restricted to the vasculature [85]. This distinction matters for the central question of how the islet basement membrane is built. If pericytes and endothelial cells assemble the vascular basement membrane immediately surrounding the capillary, a distinct fibroblast population at the islet boundary could supply the separate peri-islet matrix that delimits the endocrine compartment, dividing the labor of matrix production among several specialized stromal populations. Whether such a specialized islet fibroblast exists in the human pancreas, where it resides, and which matrix components it produces are questions this dissertation addresses directly.

1.2.3 Immune and Neural Populations

Immune and neural populations complete the endocrine niche [103]. Resident macrophages are the dominant immune cells in the islet and localize near endocrine cells and vessels, where they clear debris, regulate local inflammation, and help maintain tissue integrity. A smaller subset of immune cells includes T cells, dendritic cells, and mast cells occupying distinct islet positions that become more prominent during disease [103–111]. The islet is also richly innervated by sympathetic, parasympathetic, and sensory fibers that couple endocrine output to systemic state.

Sympathetic signaling generally promotes glucagon and suppresses insulin, parasympathetic signaling enhances insulin release with feeding, and sensory neurons relay local conditions to the central nervous system [112–115].

1.3 Cellular Composition of the Exocrine Microenvironment

Although the islets dominate attention because of their metabolic role, the exocrine pancreas constitutes most of the organ and performs the equally essential work of digestion [2]. The exocrine pancreas is comprised of a continuous glandular network of epithelial, vascular, stromal, immune, and neural cells within a shared matrix, and its cellular composition and ECM organization differ from the endocrine niche in ways that likely reflect their distinct functions [116].

1.3.1 Epithelial Cell Populations

The exocrine epithelium comprises mainly acinar and ductal cells. Acinar cells are the dominant population and synthesize digestive enzymes, including proteases, lipases, and amylases [116]. Organized as polarized units around a central lumen and packed with rough endoplasmic reticulum and secretory granules, acinar cells release enzymes into the lumen for transport to the duodenum, a synthetic load that demands substantial vascular and stromal support (**Fig. 1-1**) [116]. Ductal cells form the branching network that carries and modifies these secretions, as well as regulate the bicarbonate and fluid output needed to neutralize gastric acid and optimize enzyme activity [116]. Anchored to a specialized ECM that separates epithelium from stroma, ductal cells also maintain epithelial polarity and contribute to repair and local signaling [117]. Together these populations establish the functional architecture of the exocrine pancreas [116].

1.3.2 Vascular-Associated Cell Populations

Exocrine endothelial cells share canonical markers with their endocrine counterparts, including *PECAM1*, *VWF*, and *CDH5*, but form more continuous, less permeable capillaries rather than the highly fenestrated vessels of the islet [38, 118]. This difference reflects function, since the exocrine pancreas mainly relies on sustained nutrient delivery for enzyme synthesis rather than the rapid hormone exchange that islets require [118, 119]. These vessels are likewise supported by a vascular ECM and contribute to local signaling and repair [118, 119].

Exocrine pericytes resemble endocrine pericytes in gene marker expression and position but appear adapted to a different setting [38]. Embedded within a dense interstitial matrix rather than supporting fenestrated endocrine capillaries, they express broad ECM genes, pointing to a broader role in tissue organization [70]. This contrast reinforces the emerging view that pericyte identity is not fixed but tuned to local microenvironmental demands [85, 120].

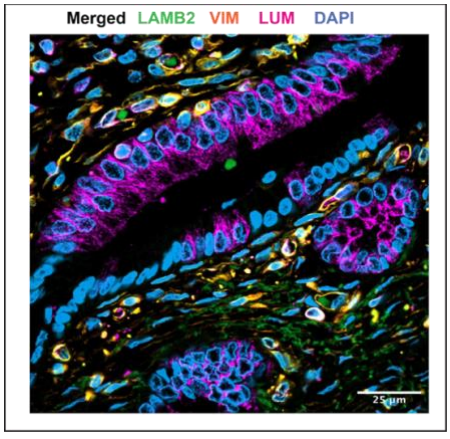

Figure 1-5: Immunofluorescence image of human pancreatic exocrine vasculature.

Representative immunofluorescence image of human pancreatic tissue stained for LAMB2 (green), vimentin (VIM) (orange), lumican (LUM) (magenta), and DAPI (blue). LAMB2 localizes predominantly along basement membrane structures surrounding pancreatic ducts and blood vessels, while LUM marks stromal extracellular matrix and VIM labels mesenchymal cells. Scale bar = 25 µm.

Fibroblasts are among the most abundant stromal cells in the exocrine pancreas and the principal producers of interstitial matrix [89, 121]. Distributed through the parenchyma and concentrated around ducts, vessels, and connective tissue, they synthesize fibrillar collagens, together with glycoproteins and proteoglycans that build a matrix (**Fig. 1-5**) [121]. Through secreted growth factors, cytokines, and matrix, they also influence repair and injury responses, making them central regulators of the exocrine microenvironment and, in disease, important contributors to fibrosis [89, 121].

1.3.3 Immune and Neural Components

Immune cells are more abundant in the exocrine pancreas than in the endocrine compartment [122, 123]. Macrophages, dendritic cells, and lymphocytes monitor tissue integrity and coordinate responses to injury, and through secreted cytokines and matrix-modifying enzymes, they also participate in matrix remodeling, an activity that becomes prominent during exocrine repair and fibrosis [122, 123]. Extensive autonomic and sensory innervation regulates enzyme secretion, ductal fluid transport, and local blood flow, and these neural signals can in turn influence stromal and vascular populations, helping exocrine tissue adapt to changing demand [124].

1.4 The Pancreatic Vasculature

1.4.1 Islet Vascular Architecture

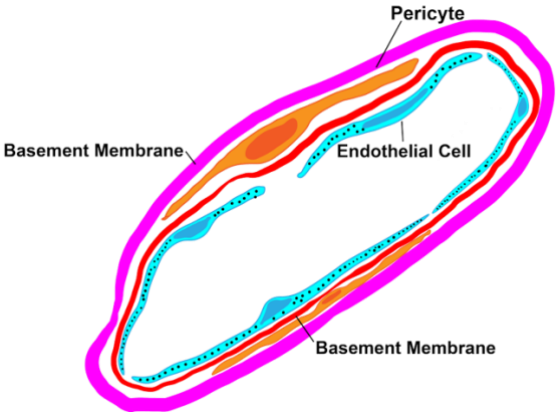

Figure 1-6: Schematic of the human islet vascular basement membrane.

Illustration of a pancreatic islet basement membrane and blood vessel showing endothelial cells lining the vessel lumen, surrounding pericytes, and basement membrane layers associated with the vascular wall. Black dots indicate endothelial fenestrations.

Despite comprising only 1-2% of pancreatic mass, islets receive a share of pancreatic blood flow ten times greater than neighboring exocrine tissue [125]. Circulating glucose must reach endocrine cells rapidly for accurate sensing, and newly secreted hormones must enter the bloodstream with minimal delay [126]. To meet these demands, each islet is penetrated by its own capillary network, supplied by one or more dedicated arterioles, that brings vessels into close apposition with the endocrine cells, so that nearly every cell lies against a capillary and its vascular basement membrane (**Fig. 1-6**) [3, 8, 127]mate vascular contact also serves the high metabolic demand of endocrine cells, which sustain some of the highest oxygen consumption rates in the body [128]. Because oxygen reaches the islet interior largely by diffusion from intra-islet capillaries, viability depends on the number and spatial distribution of those vessels, and computational models show islet oxygenation to be sensitive to capillary density [125, 129].

The architecture of the human islet differs in important ways from the rodent islet, which has shaped most of what is known about islet vascular biology. Rodent islets are richly vascularized and follow a core-mantle plan, with β cells occupying the core between a dense intra-islet capillary network [130, 131]. Human islets instead intermingle their endocrine cell types throughout the islet and carry a markedly sparser vasculature [43]. Quantitative morphometry shows roughly five-fold fewer capillaries per islet area in human than in mouse islets, and the human intra-islet capillaries are significantly less convoluted [43]. The human islet vascular network is thus simpler and less dense than the mouse network, even though both arrangements keep endocrine cells in close contact with vessels [43].

Comparison across species reinforces the point that islet vascular organization tracks with islet cytoarchitecture [132]. Non-human primates share with humans a heterogeneous islet cytoarchitecture in which β, α, and δ cells are intermingled throughout the islet rather than segregated into a β cell core and a non-β cell mantle, and this shared organization extends to the intra-islet vasculature and innervation, with sympathetic fibers targeting the islet vessels much as in the human [133, 134]. Pig islets are an instructive intermediate, since their endocrine cells are organized into several smaller subunits, yet their dense, integrated capillary network closely resembles that of human islets, which together with their human-like islet size and physiology has made the pig a favored large-animal and xenotransplantation model [135]. Broader surveys spanning monkeys, rabbits, and birds reveal considerable diversity in endocrine composition, including a δ-cell-predominant organization in the bird pancreas and an inverted β-to-non-β cell ratio in some non-human primates and marsupials, even as

overall islet size distributions overlap closely across mammals [132, 134, 136]. Across these non-rodent species, the recurring theme is an intermingled endocrine architecture served by a capillary network integrated with the surrounding tissue, in contrast to the stereotyped, densely and tortuously vascularized core-mantle islet of the mouse and rat.

Across all these species the defining structural feature of the islet vasculature is the same: the network places endocrine cells directly against the vascular basement membrane, the matrix interface that is the focus of this dissertation [133, 137–139]. Because the human islet establishes this contact through a sparser and less tortuous network than the rodent, and because that network remodels in type 2 diabetes, characterizing the human islet vasculature and its associated matrix directly, rather than by extrapolation from rodent models, is essential [43, 44, 140].

1.4.2 Exocrine Vascular Architecture

The exocrine vasculature is built to sustain the high biosynthetic output of enzyme-producing acini rather than the rapid hormone exchange of the islet [118, 119]. In the human pancreas, interlobular arteries running within the connective tissue septa give rise to intralobular arterioles that branch into capillary plexuses within individual acini, with separate periductal capillary networks surrounding the larger interlobular ducts [138]. These capillary beds drain through intralobular and interlobular venules that ultimately return blood to the portal circulation [138].

A defining architectural feature is that the exocrine capillary bed is not wholly independent of the islet [118, 141]. Efferent venules leaving intralobular islets continue into the capillary networks of the surrounding acini, forming an insulo-acinar portal system in which acinar tissue is perfused by blood that has already passed through the

islet [141]. The two capillary networks are therefore arranged in series, a configuration that provides the anatomical basis for endocrine influence over exocrine function [141]. Not all acini are supplied this way, since some receive blood directly from arterioles through an independent acinar route, so the exocrine compartment is fed by both portal and direct arterial supplies [141].

Quantitatively, the exocrine bed is more sparsely vascularized and less highly perfused than the islet [141]. Like islet perfusion, exocrine blood flow is metabolically regulated and modulated by local endothelial mediators, the nervous system, and gastrointestinal hormones, matching nutrient and oxygen delivery to the demands of enzyme synthesis [118, 141].

1.5 Extracellular Matrix Biology in the Human Pancreas

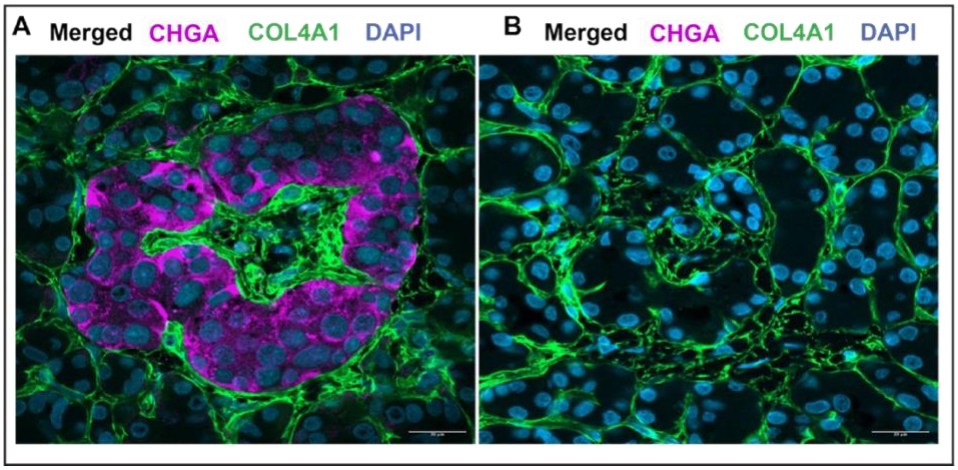

Figure 1-7: Representative immunofluorescence images of human pancreatic ECM organization.

(**A**) Representative immunofluorescence images of human pancreatic islet tissue stained for CHGA (magenta), COL4A1 (green), and DAPI (blue). Endocrine islet shows enrichment of COL4A1 surrounding CHGA+ endocrine cells and throughout the islet-associated vasculature. 40x; Scale bar = 20 μm. (**B**) Representative immunofluorescence images of human pancreatic exocrine tissue stained for CHGA (magenta), COL4A1 (green), and DAPI (blue). Exocrine tissue adjacent to the islet in (A) demonstrates COL4A1 localization along the vascular basement membrane surrounding exocrine acini. 40x; Scale bar = 20 μm.

The pancreatic ECM constitutes a three-dimensional protein network in a state of dynamic communication with the cells it surrounds, transmitting chemical and mechanical cues that regulate islet proliferation, differentiation, adhesion, and insulin secretion (**Fig. 1-7**) [142]. Naba and colleagues formalized this network as the matrisome, a curated set of core structural proteins (collagens, glycoproteins, proteoglycans) and matrisome-associated proteins (ECM regulators, ECM-affiliated proteins, secreted factors) defined both computationally and through direct proteomic characterization of tissue [143, 144].

Ma *et al*. set out to comprehensively characterize the ECM composition of the human pancreas, a tissue that has been difficult to profile because ECM proteins resist standard extraction methods [145]. The authors developed a surfactant and chaotropic agent-assisted sequential extraction protocol (SCAD), which they applied to native and decellularized human pancreas from both fetal and adult donors. They then identified 33 isoforms spanning 19 collagen types, including the fibrillar collagens I, II, III, V, and XI, the network-forming collagen IV, and the beaded-filament collagen VI, alongside multiple laminin isoforms and fibronectin [145].

Comparing fetal and adult tissue, the authors found enrichment in adult pancreas of collagens I, III, V, VI, VII, XVI, and XXVIII along with SERPINA3 [145]. This adult-enriched signature is consistent with functional data cited by the same study showing that collagen I promotes differentiation of pancreatic precursor cells toward a glucose-responsive phenotype and that collagen VI supports the viability of human pancreatic islets in culture, linking the observed compositional shift to postnatal β cell maturation [145].

Li and colleagues extended this developmental framework across a broader age range, profiling fetal, juvenile, young adult, and older adult human pancreas and quantifying 117 ECM proteins by isobaric labeling [146]. Hierarchical clustering distinguished fetal, juvenile, and adult matrisome signatures, with the largest compositional shifts occurring between fetal and postnatal tissue and comparatively few differences between young and older adults [146]. Of the ECM protein categories, collagens proved the most stable across development, with only 37% of quantified collagens changing significantly in abundance, while glycoproteins, ECM regulators, and ECM-affiliated proteins were far more dynamic, with 74 to 90% of proteins in these categories showing significant developmental change [146]. Together, these two studies establish that the collagen scaffold of the human pancreas is laid down early and remains comparatively stable, while the surrounding glycoprotein and regulatory layers continue to be remodeled through postnatal maturation [145, 146].

Both datasets characterize bulk tissue or whole-organ scaffolds rather than resolving which cell types produce or occupy specific matrix niches *in situ*. This spatial gap, particularly the question of which stromal populations generate the peri-islet and peri-vascular basement membranes captured in these proteomic surveys, motivates the spatial transcriptomic approach developed in this dissertation.

1.5.1 Basement Membranes

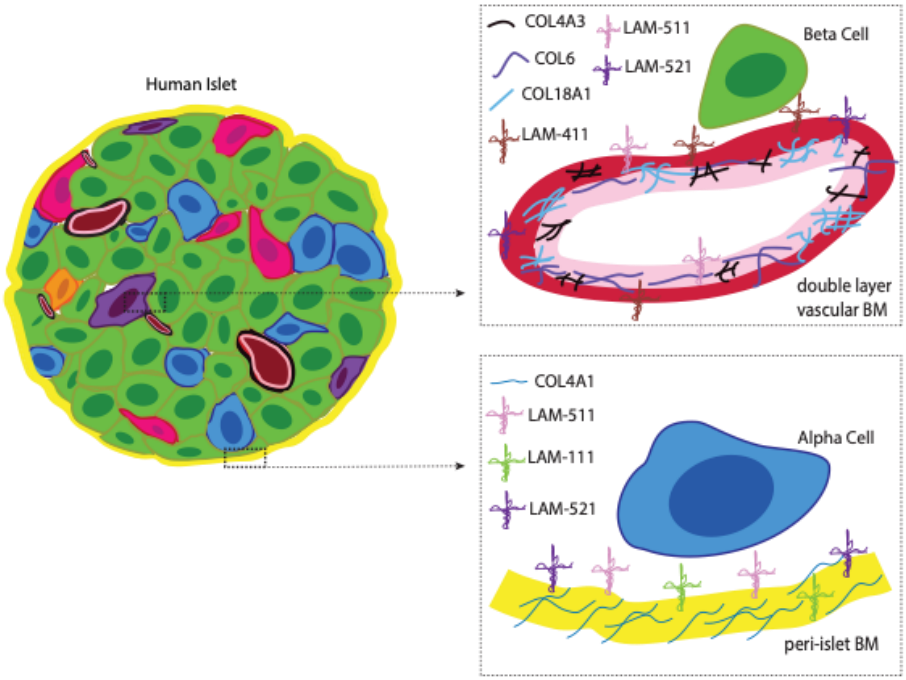

Figure 1-8: Organization and molecular composition of the human islet basement membranes.

The intra-islet vasculature is surrounded by a characteristic double-layered vascular basement membrane composed of basement membrane proteins including collagen IV (COL4A1 and COL4A2), laminin-411 (LAM-411), laminin-511 (LAM-511), laminin-521 (LAM-521), collagen XVIII (COL18A1), and collagen VI (COL6). The peri-islet basement membrane, which separates the endocrine and exocrine compartments, is enriched in collagen IV (COL4A1) together with laminin-111 (LAM-111), laminin-511 (LAM-511), and laminin-521 (LAM-521).

Basement membranes are thin, sheet-like specializations of the matrix that underlie epithelial and endothelial layers and surround vessels and other cell types [147, 148]. Though only 50 to 100 nm thick, they are essential to tissue organization and actively regulate adhesion, polarity, differentiation, migration, and survival while serving as permeability barriers and growth factor reservoirs [147, 149]. The islet vascular basement membrane supports endothelial and mural cells, while the peri-islet basement membrane separates endocrine from exocrine tissues (**Fig. 1-8**) [12]. Nearly all basement membranes assemble from four protein families, collagen IV, laminins, nidogens, and heparan sulfate proteoglycans, which self-organize into an

interconnected meshwork providing both mechanical stability and signaling capacity [12, 13, 147, 148, 150–154].

Collagen IV is the principal structural component and the scaffold on which other basement membrane proteins assemble [155, 156]. In the pancreas, collagen IV is enriched in vascular and peri-islet basement membranes, where it anchors endothelial cells and pericytes, and increasing evidence indicates that its production is not restricted to endothelial cells but extends to vascular-supportive stromal populations, particularly pericytes [12, 48, 70].

Laminins are the second major component and are required for basement membrane assembly [157–159]. These heterotrimeric glycoproteins of one α, one β, and one γ chain form at least sixteen isoforms with tissue-specific distributions, polymerizing into a network that is linked to the collagen IV scaffold by nidogens [159]. Beyond structure they regulate epithelial polarity, endothelial differentiation, stem cell maintenance, and angiogenesis through integrins, dystroglycan, and syndecans [160]. Their isoforms are distributed by compartment such as laminin-511 and laminin-521, which contain the α5 chain encoded by *LAMA5.* These laminins are known to be enriched in vascular basement membranes and required for endothelial stability, while other isoforms populate the peri-islet and ductal basement membranes [12, 48, 161].

Nidogens, also called entactins, are conserved glycoproteins that act as molecular bridges [162]. The two isoforms, nidogen-1 and nidogen-2, encoded by *NID1* and *NID2*, do not polymerize on their own but bind collagen IV, laminins, and perlecan simultaneously, physically connecting the collagen and laminin networks [163]. Deletion of either isoform alone produces relatively mild phenotypes, consistent with functional

compensation between the two proteins. In contrast, combined deletion of Nid1 and Nid2 in mice causes tissue-selective basement-membrane defects that are most severe in the developing lung and heart, including disruption of pulmonary epithelial and microvascular basement membranes and discontinuities in myocardial capillary basement membranes, resulting in death shortly after birth. Renal glomerular basement membranes remain largely intact, although tubular basement membranes can be thickened, discontinuous, or absent, and subsequent studies have also identified abnormalities in limb development [162]. In the pancreas, they are present throughout vascular basement membranes, helping maintain the continuity of the endocrine vascular niche and nidogen-1 has been known to restore islet functionality in hypoxic conditions [163].

The fourth family, heparan sulfate proteoglycans, is represented in the islet basement membrane primarily by perlecan, encoded by *HSPG2*, with collagen XVIII also contributing [164, 165]. Structurally, perlecan binds laminins, collagen IV, and nidogens to reinforce the membrane, while its heparan sulfate chains bind water and regulate diffusion [165]. In islets, perlecan supports endothelial function and vascular stability and influences endocrine survival through growth factor signaling [166]. Collagen XVIII gives rise to the anti-angiogenic peptide endostatin, illustrating how basement membrane proteins double as precursors of bioactive signals [166, 167]. Proteolytic cleavage of its carboxy-terminal non-collagenous domain releases endostatin, inhibits angiogenesis by restricting endothelial proliferation and migration and promoting endothelial apoptosis, acting in part through binding to integrins, heparan sulfate, and components of the vascular basement membrane [167]. Endostatin is

elevated in the circulation in diabetes and is associated with diabetic nephropathy, retinopathy, and cardiovascular disease, where it is regarded as a marker of microvascular injury and impaired angiogenic repair [168–170]. Because collagen XVIII is a component of the vascular basement membrane and a substrate for the same remodeling enzymes that are dysregulated in diabetes, changes in its expression offer a direct route by which basement membrane remodeling could feed back on endothelial behavior in the diabetic islet.

1.5.2 Stromal Extracellular Matrix Regulation of Endocrine Function

The matrix is an active regulator of endocrine biology (**Fig. 1-9**). β cells actively maintained within a physiological matrix retain better viability, secretory capacity, and mature gene expression than those on plastic, showing that endocrine function depends on the biochemical and mechanical properties of the surrounding environment as well as on soluble and cell-cell signals [5, 70, 171–173].

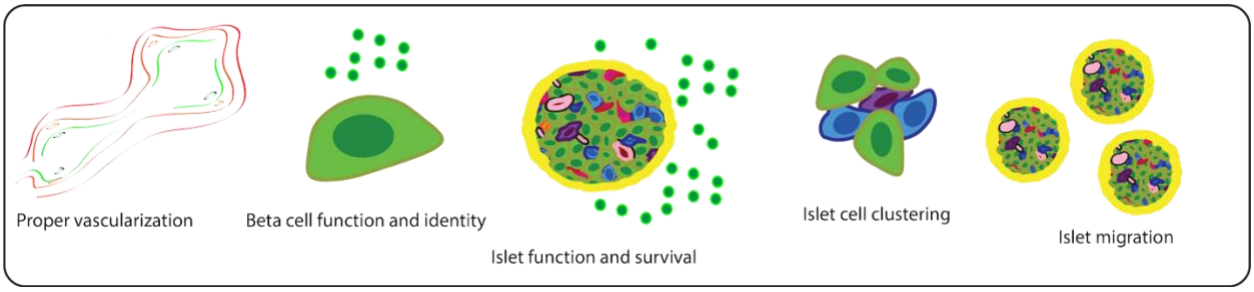

Figure 1-9: Functional roles of the pancreatic islet microenvironment.

Schematic summary showing key roles of the islet niche in pancreas development and function, including vascularization, β cell function and identity, islet function and survival, endocrine cell clustering, and islet migration.

The principal mediator of the beta cell-ECM interface is an integrin system that β cells express, specifically α3, α5, α6, β1, and β3 subunits, which engage basement membrane components around the islet vasculature [60–62, 174–179]. β1 specifically has been shown to be essential, since its deletion in β cells disrupts islet architecture,

impairs glucose-stimulated insulin secretion, reduces proliferation, and compromises survival and identity [60–62, 174–179]. Through focal adhesion kinase, integrin-linked kinase, downstream PI3K-AKT and MAPK signaling, and crosstalk with growth factor receptors, integrin engagement links matrix composition to β cell survival, insulin biosynthesis, and metabolic adaptation, while also allowing β cells to sense matrix stiffness through mechanotransduction [180].

The matrix also supplies survival signals that protect endocrine cells from apoptosis [176, 181]. β cells normally remain anchored to the vascular basement membrane through integrins, and losing this contact triggers anoikis, the apoptosis of detached anchorage-dependent cells [182]. The matrix also protects endocrine cells indirectly by sequestering growth factors within heparan sulfate proteoglycans and regulating their local availability [183]. The clinical relevance is clear in islet isolation, where enzymatic digestion strips basement membrane proteins and increases apoptosis, and where restoring matrix contact through scaffolds, decellularized matrix, or basement membrane coatings improves survival [172, 184–186].

The matrix also shapes hormone secretion directly. β cells are polarized, contacting the vascular basement membrane at their basal surface, and laminins and collagen IV organize the cytoskeleton and granule trafficking that direct insulin release toward adjacent capillaries rather than into the interstitium [47, 63]. Integrin signaling supports this by positioning the exocytotic machinery at the vascular interface, and disrupting basement membrane contact degrades polarity and glucose-stimulated secretion even when insulin synthesis is intact [60, 187].

1.5.3 Cellular Sources of the Pancreatic Extracellular Matrix

For decades endothelial cells were considered the principal source of vascular basement membrane, a view grounded in developmental studies showing that β cells do not produce basement membrane and instead need to signal to endothelial cells to secrete collagen IV and laminins required to form the intra-islet vascular basement membrane [7]. The supporting evidence, however, came largely from mouse developmental biology and bulk tissue analyses that could not resolve contributions from neighboring stromal cells, leaving the relative role of endothelial cells uncertain [7, 13, 70]. Single-cell transcriptomics has reframed the picture, showing that fibroblasts, pericytes, smooth muscle cells, and other specialized mesenchymal cells express matrix gene programs at expression levels that often exceed those of endothelial cells [38, 70, 99, 100]. Fibroblasts remain the dominant producers of fibrillar matrix, including collagens I, III, and V, fibronectin, decorin, and lumican, and are themselves heterogeneous [38, 100]. Pericytes have emerged as especially important, expressing collagen IV, laminins, and nidogens at high levels, a pattern observed across brain, kidney, retina, and lung that suggests basement membrane production is a conserved mural cell function [97, 188–195]. These observations point to a cooperative model in which endothelial cells, pericytes, and specialized fibroblasts contribute complementary components of the vascular and peri-islet basement membranes rather than any one population acting alone. Resolving the relative contribution of each cell type requires a method that can localize matrix gene expression within intact tissue, a need that motivates the integrated single-cell and spatial transcriptomic approach taken in this dissertation.

1.6 Extracellular Matrix Remodeling in Type 2 Diabetes

Type 2 diabetes is marked by progressive β cell dysfunction against a background of insulin resistance and chronic metabolic stress [196]. Although endocrine research has focused on intrinsic β cell defects, the surrounding microenvironment also changes substantially. This remodeling is not passive accumulation but a dynamic imbalance between synthesis and degradation driven by hyperglycemia, oxidative stress, inflammation, and altered signaling, affecting endothelial cells, pericytes, fibroblasts, and immune cells together [43, 197–200].

1.6.1 Islet Fibrosis

Fibrosis is among the most recognized forms of diabetic ECM remodeling [121, 201, 202]. Diabetic islets show increased deposition of interstitial collagens, fibronectin, and other matrix proteins with expansion of the surrounding stroma, and although its extent varies between individuals, excess matrix is consistently associated with impaired β cell function [43, 44, 140, 197, 198, 200, 203]. By stiffening the matrix and disrupting architecture, fibrosis alters the pathways that regulate β cell proliferation, differentiation, and secretion, and increased collagen may also widen the distance between endocrine cells and capillaries, impairing exchange [98, 201, 202]. The responsible cells are not fully defined. Fibroblasts have been the presumed mediators, but vascular-associated populations also appear to contribute [121, 202].

1.6.2 Basement Membrane Thickening

Basement membrane thickening is a defining feature of diabetic microvascular disease across the kidney, retina, nerve, and muscle, and is increasingly recognized in

the pancreatic microvasculature [204–206]. Diabetic capillaries accumulate collagen IV, laminins, fibronectin, and heparan sulfate proteoglycans, expanding the vascular basement membrane [153]. Once seen as a benign response to hyperglycemia, thickening is now understood to impair diffusion, alter mechanics and endothelial signaling, and disrupt communication among vascular and endocrine cells, with changes in integrin signaling that can compromise insulin secretion and survival [43, 44, 203, 207].

1.6.3 Vascular Dysfunction

The pancreatic vasculature remodels substantially in diabetes [2, 11, 140, 200, 208]. Endothelial dysfunction, marked by reduced nitric oxide, impaired angiogenic signaling, altered permeability, and blunted vascular responsiveness, compromises perfusion and the efficiency of glucose sensing and hormone delivery, and it disrupts the reciprocal endothelial-endocrine signaling that maintains islet homeostasis [2, 11, 140, 200, 208].

1.6.4 Pericyte Remodeling

Pericytes have emerged as central, and metabolically vulnerable, participants in the microvascular pathology of type 2 diabetes [209]. Because their physiological roles are to stabilize the microvasculature, regulate capillary perfusion, and respond to changes in their local environment, they are directly exposed to the metabolic disturbances that define the disease, including hyperglycemia, hyperinsulinemia, and dyslipidemia [85, 209]. Pericyte loss and dysfunction are now recognized as common threads linking the major microvascular complications of type 2 diabetes across the

retina, kidney, peripheral nerve, and skeletal muscle, and the same vulnerability extends to the pancreatic islet [209].

The diabetic environment injures pericytes through several converging biochemical pathways. Chronic hyperglycemia, often accompanied by dyslipidemia in type 2 diabetes, activates several canonical pathways of diabetic microvascular injury, including increased polyol pathway flux, formation of advanced glycation end products, protein kinase C activation, and elevated intracellular reactive oxygen species [210, 211]. Together, these processes damage endothelial cells and their respective pericytes, weakening the reciprocal signaling required for vascular stability. In pericytes specifically, oxidative and glycative stress promotes apoptosis, impairs cellular longevity, and impairs vascular support [212].

The downstream consequences follow a recurring pattern across tissues that is directly relevant to the pancreas. In the retina, the earliest morphological change of diabetes is loss of pericyte coverage, and pericyte loss weakens capillaries and produces the microaneurysms characteristic of diabetic retinopathy [213, 214]. In endoneurial capillaries located within peripheral nerves, pericyte degeneration is accompanied by reduplication and thickening of the vascular basement membrane. *In vitro*, advanced glycation end products stimulate human peripheral-nerve pericytes to increase their production of fibronectin and collagen IV, suggesting that abnormal pericyte matrix deposition may contribute to basement-membrane hypertrophy and disruption of the blood–nerve barrier in diabetic neuropathy [215, 216]. Comparable pericyte degeneration with basement membrane thickening is seen in diabetic skeletal muscle [217]. A consistent theme is that diabetic pericytes both die and, where they

persist, shift toward an activated, matrix-depositing phenotype that thickens the surrounding basement membrane.

Evidence from rodent pancreas indicates that islet pericytes are indeed remodeled in type 2 diabetes [202]. Ultrastructural studies of insulin-resistant and diabetic rodents describe a widening of the islet-exocrine interface accompanied by pericyte hypercellularity and elongated cytoplasmic processes, with these expanded pericytes depositing collagen and contributing to islet fibrosis [212]. In human patients with type 2 diabetes, pericyte coverage of the intra-islet capillaries is reduced, and the degree of pericyte loss is inversely related to disease duration, paralleling the fibrosis and amyloid deposition seen in diabetic islets [78]. The transcription factor *TCF7L2*, encoded by the strongest common genetic risk locus for type 2 diabetes, is expressed by pancreatic pericytes and supports β cell function through pericyte-derived signals, so that loss of pericyte *TCF7L2* function impairs glucose homeostasis [81, 84].

Across these processes, type 2 diabetes emerges not as an isolated failure of β cells but as a coordinated remodeling of the endocrine vascular niche, in which fibrosis, basement membrane thickening, endothelial dysfunction, and pericyte activation act together to destabilize the microenvironment that sustains endocrine function. A central obstacle to understanding this remodeling is that the specific cellular sources of the altered matrix, and the way they differ between the endocrine and exocrine compartments, cannot be resolved by the methods that have defined the field to date. The following section examines the strengths and limitations of those methods.

1.7 Limitations of Current Approaches

Defining the cellular sources and spatial organization of the pancreatic matrix requires methods that resolve both which cells make matrix proteins and where those cells lie within intact tissue. Each established approach has contributed to current understanding while leaving part of this question unanswered.

1.7.1 Histology

Conventional histology and immunohistochemistry methods have defined pancreatic architecture for over a century, revealing the organization of islets, vessels, and matrix, with electron microscopy resolving basement membrane ultrastructure and endothelial fenestrations [12, 48, 133]. The main limitation of these methods is dimensionality, since only a few markers can be examined at once, which makes it difficult to define cell phenotypes or distinguish related stromal populations. Also, the commercial availability of specific, reliable, and reproducible ECM antibodies remains limited [218]. Because secreted matrix proteins accumulate in shared extracellular space, protein localization alone also cannot identify which cell originally synthesized a given component.

1.7.2 Bulk Sequencing

Bulk RNA-sequencing has enabled transcriptome-wide comparison of healthy and diabetic tissue and identified disease-associated changes in matrix, inflammatory, and vascular genes [70]. By averaging expression across many cells, however, it obscures individual cell types, so in a tissue as heterogeneous as the pancreas it

cannot assign a change in expression of a basement membrane gene to endothelial cells, pericytes, or fibroblasts [70].

1.7.3 Single-Cell RNA-Sequencing

Single-cell RNA-sequencing transformed the field by profiling individual cells, uncovering stromal heterogeneity, defining endocrine states, and showing that multiple vascular-associated populations express matrix genes, directly challenging the assumption that endothelial cells are the sole source of vascular basement membrane [38, 70, 99, 100]. Its drawback is the loss of spatial information, because dissociation reveals what genes a cell expresses but not where it resides, whether it associates with vessels or islets, or how neighbors cooperate to build matrix. Furthermore, fragile cells may be lost during dissociation, and a cell's transcriptome can be altered by the enzymatic and manual dissociation needed to acquire single-cell suspension for sequencing [38, 219–221].

1.8 Study Rationale and Objectives

Decades of work have first, established the extracellular matrix, including the basement membrane, as an integral, active component of the endocrine niche and second, have shown that endothelial cells and pericytes support vascular stability and endocrine function. Yet how the vascular matrix is built and maintained in the adult human pancreas remains poorly understood. The endothelial-centric model arose from developmental and histological studies that could not resolve neighboring stromal contributions. Single-cell RNA-sequencing has revealed that fibroblasts and pericytes express extensive matrix programs but cannot elucidate where these cells reside or how their programs differ between compartments. Diabetic remodeling compounds this

knowledge gap, since most studies focus on β cell dysfunction or quantify overall fibrosis without identifying which stromal populations drive the altered production, deposition, and organization of basement-membrane and interstitial matrix components. High-resolution spatial transcriptomics, integrated with single-cell analysis, now makes it possible to identify matrix-producing cells while preserving their architectural relationships to vessels, endocrine cells, and stroma. This dissertation uses that combination to define the cellular architecture of the adult human pancreatic vascular niche and its remodeling in type 2 diabetes, addressing four key questions:

1) Which cells express the genes that encode vascular basement membrane proteins in the adult human pancreas? Although endothelial cells have been considered the primary source, the relative contributions of endothelial cells, pericytes, fibroblasts, and other stromal populations are unresolved. Determining the cellular origins of collagen IV, laminins, and other components is fundamental to understanding how the pancreatic vascular niche is established and maintained.
2) How do the endocrine and exocrine vascular niches differ? The two compartments perform different functions and show different vascular architectures, but whether their vascular-supportive cells carry distinct transcriptional identities and matrix programs has been largely unexplored. Defining these differences is essential to understanding how specialized matrix environments support endocrine function.
3) What are the roles of pericytes and fibroblasts in the human pancreatic vascular niche? Pericytes are classically tied to vascular stability and

fibroblasts to interstitial matrix, but both may do more. Whether pericytes contribute substantially to vascular basement membrane synthesis, and whether a specialized fibroblast population exists within the endocrine compartment, are open questions whose answers require resolving the identity, location, and matrix programs of these cells.

4) How are vascular-supportive niches remodeled in type 2 diabetes? Diabetes alters the endocrine microenvironment through matrix remodeling, vascular dysfunction, and β cell failure, but the specific populations that remodel, and whether they differ between compartments, are poorly defined. Characterizing these changes may reveal mechanisms of diabetic microvascular dysfunction and identify stromal targets for preserving islet function.

To address these questions, this dissertation leverages integrated single-cell RNA-sequencing with high-resolution MERFISH spatial transcriptomics to build a cellular and spatial atlas of the adult human pancreatic vascular niche, identifying matrix-expressing populations, mapping their organization across the endocrine and exocrine compartments, and determining how they are remodeled in type 2 diabetes. The chapter that follows presents this work, beginning with the cellular sources of the vascular basement membrane in the healthy human pancreas and proceeding to their spatial organization and remodeling in type 2 diabetes.

1.9 References

1. Atkinson MA, Campbell-Thompson M, Kusmartseva I, Kaestner KH (2020) Organisation of the human pancreas in health and in diabetes. Diabetologia 2020 63:10 63(10):1966–1973. https://doi.org/10.1007/S00125-020-05203-7

2. Rickels MR, Norris AW, Hull RL (2020) A tale of two pancreases: exocrine pathology and endocrine dysfunction. Diabetologia 2020 63:10 63(10):2030–2039. https://doi.org/10.1007/S00125-020-05210-8

3. Henry BM, Skinningsrud B, Saganiak K, Pękala PA, Walocha JA, Tomaszewski KA (2019) Development of the human pancreas and its vasculature — An integrated review covering anatomical, embryological, histological, and molecular aspects. Annals of Anatomy - Anatomischer Anzeiger 221:115–124. https://doi.org/10.1016/J.AANAT.2018.09.008

4. Walker JT, Saunders DiC, Brissova M, Powers AC (2021) The Human Islet: Mini-Organ With Mega-Impact. Endocr Rev 42(5):605–657. https://doi.org/10.1210/ENDREV/BNAB010

5. Lammert E, Thorn P (2020) The Role of the Islet Niche on Beta Cell Structure and Function. J Mol Biol 432(5):1407–1418. https://doi.org/10.1016/J.JMB.2019.10.032

6. Huising MO, Lee S, van der Meulen T (2018) Evidence for a Neogenic Niche at the Periphery of Pancreatic Islets. BioEssays 40(11):1800119. https://doi.org/10.1002/BIES.201800119

7. Nikolova G, Jabs N, Konstantinova I, et al (2006) The Vascular Basement Membrane: A Niche for Insulin Gene Expression and β Cell Proliferation. Dev Cell 10(3):397–405. https://doi.org/10.1016/J.DEVCEL.2006.01.015

8. Cleaver O, Dor Y (2012) Vascular instruction of pancreas development. Development (Cambridge) 139(16):2833–2843. https://doi.org/10.1242/DEV.065953

9. Burganova G, Bridges C, Thorn P, Landsman L (2021) The Role of Vascular Cells in Pancreatic Beta-Cell Function. Front Endocrinol (Lausanne) 12:442. https://doi.org/10.3389/FENDO.2021.667170/BIBTEX

10. Brissova M, Aamodt K, Brahmachary P, et al (2014) Islet Microenvironment, Modulated by Vascular Endothelial Growth Factor-A Signaling, Promotes β Cell Regeneration. Cell Metab 19(3):498–511. https://doi.org/10.1016/J.CMET.2014.02.001

11. Richards OC, Raines SM, Attie AD (2010) The Role of Blood Vessels, Endothelial Cells, and Vascular Pericytes in Insulin Secretion and Peripheral Insulin Action. Endocr Rev 31(3):343–363. https://doi.org/10.1210/ER.2009-0035

12. Virtanen I, Banerjee M, Palgi J, et al (2008) Blood vessels of human islets of Langerhans are surrounded by a double basement membrane. Diabetologia 51(7):1181–1191. https://doi.org/10.1007/S00125-008-0997-9

13. Nikolova G, Strilic B, Lammert E (2007) The vascular niche and its basement membrane. Trends Cell Biol 17(1):19–25. https://doi.org/10.1016/J.TCB.2006.11.005

14. Sasaki S, Lee MYY, Wakabayashi Y, et al (2022) Spatial and transcriptional heterogeneity of pancreatic beta cell neogenesis revealed by a time-resolved reporter system. Diabetologia 2022 1–18. https://doi.org/10.1007/S00125-022-05662-0

15. Striegel DA, Hara M, Periwal V (2015) The Beta Cell in Its Cluster: Stochastic Graphs of Beta Cell Connectivity in the Islets of Langerhans. PLoS Comput Biol 11(8):e1004423–e1004423. https://doi.org/10.1371/journal.pcbi.1004423

16. Trexler AJ, Taraska JW (2017) Regulation of insulin exocytosis by calcium-dependent protein kinase C in beta cells. Cell Calcium 67:1. https://doi.org/10.1016/J.CECA.2017.07.008

17. Yamanouchi D (2025) The Roles of Incretin Hormones GIP and GLP-1 in Metabolic and Cardiovascular Health: A Comprehensive Review. Int J Mol Sci 27(1):27. https://doi.org/10.3390/IJMS27010027

18. Elizabeth Mann 1 MS 2, and MDB 2 (2020) Secretion of Insulin in Response to Diet and Hormones. Pancreapedia: The Exocrine Pancreas Knowledge Base. https://doi.org/10.3998/PANC.2020.16

19. Bastidas-Ponce A, Tritschler S, Dony L, et al (2019) Comprehensive single cell mRNA profiling reveals a detailed roadmap for pancreatic endocrinogenesis. Development 146(12). https://doi.org/10.1242/DEV.173849

20. Krentz NAJ, Lee MYY, Xu EE, et al (2018) Single-Cell Transcriptome Profiling of Mouse and hESC-Derived Pancreatic Progenitors. Stem Cell Reports 11(6):1551. https://doi.org/10.1016/J.STEMCR.2018.11.008

21. Byrnes LE, Wong DM, Subramaniam M, et al (2018) Lineage dynamics of murine pancreatic development at single-cell resolution. Nat Commun 9(1). https://doi.org/10.1038/S41467-018-06176-3

22. Rix I, Nexøe-Larsen C, Bergmann NC, Lund A, Knop FK (2019) Glucagon Physiology. Can J Diabetes 34(3):187–188. https://doi.org/10.1016/S1499-2671(10)43015-4

23. Andersen DB, Holst JJ (2022) Peptides in the regulation of glucagon secretion. Peptides (NY) 148:170683. https://doi.org/10.1016/J.PEPTIDES.2021.170683

24. Zeigerer A, Sekar R, Kleinert M, Nason S, Habegger KM, Müller TD (2021) Glucagon's Metabolic Action in Health and Disease. Compr Physiol 11(2):1759. https://doi.org/10.1002/CPHY.C200013

25. Da Silva Xavier G (2018) The Cells of the Islets of Langerhans. Journal of Clinical Medicine 2018, Vol 7, 7(3). https://doi.org/10.3390/JCM7030054

26. Arrojo e Drigo R, Jacob S, García-Prieto CF, et al (2019) Structural basis for delta cell paracrine regulation in pancreatic islets. Nat Commun 10(1). https://doi.org/10.1038/S41467-019-11517-X

27. Van Der Meulen T, Donaldson CJ, Cáceres E, et al (2015) Urocortin3 mediates somatostatin-dependent negative feedback control of insulin secretion. Nat Med 21(7):769–776. https://doi.org/10.1038/NM.3872

28. Huang JL, Pourhosseinzadeh MS, Lee S, et al (2024) Paracrine signalling by pancreatic δ cells determines the glycaemic set point in mice. Nat Metab 6(1):61–77. https://doi.org/10.1038/S42255-023-00944-2

29. Batterham RL, Le Roux CW, Cohen MA, et al (2003) Pancreatic polypeptide reduces appetite and food intake in humans. J Clin Endocrinol Metab 88(8):3989–3992. https://doi.org/10.1210/JC.2003-030630

30. Schmidt PT, Näslund E, Grybäck P, et al (2005) A role for pancreatic polypeptide in the regulation of gastric emptying and short-term metabolic control. J Clin Endocrinol Metab 90(9):5241–5246. https://doi.org/10.1210/JC.2004-2089

31. Lonovics J, Guzman S, Devitt PG, et al (1981) Action of pancreatic polypeptide on exocrine pancreas and on release of cholecystokinin and secretin. Endocrinology 108(5):1925–1930. https://doi.org/10.1210/ENDO-108-5-1925

32. Andralojc KM, Mercalli A, Nowak KW, et al (2009) Ghrelin-producing epsilon cells in the developing and adult human pancreas. Diabetologia 52(3):486–493. https://doi.org/10.1007/S00125-008-1238-Y

33. Gutierrez GD, Kim J, Lee AH, et al (2018) Gene Signature of the Human Pancreatic ε Cell. Endocrinology 159(12):4023–4032. https://doi.org/10.1210/EN.2018-00833

34. Lindqvist A, Shcherbina L, Prasad RB, et al (2020) Ghrelin suppresses insulin secretion in human islets and type 2 diabetes patients have diminished islet ghrelin cell number and lower plasma ghrelin levels. Mol Cell Endocrinol 511. https://doi.org/10.1016/j.mce.2020.110835

35. Wang W, Liu Y, Chen Y, et al (2010) Inhibition of Foxo1 mediates protective effects of ghrelin against lipotoxicity in MIN6 pancreatic beta-cells. Peptides (NY) 31(2):307–314. https://doi.org/10.1016/J.PEPTIDES.2009.11.011

36. Granata R, Settanni F, Trovato L, et al (2006) Unacylated as well as acylated ghrelin promotes cell survival and inhibit apoptosis in HIT-T15 pancreatic beta-cells. J Endocrinol Invest 29(9). https://doi.org/10.1007/BF03347367

37. Olsson R, Carlsson PO (2006) The pancreatic islet endothelial cell: Emerging roles in islet function and disease. Int J Biochem Cell Biol 38(4):492–497. https://doi.org/10.1016/J.BIOCEL.2005.06.021

38. Craig-Schapiro R, Li G, Chen K, et al (2025) Single-cell atlas of human pancreatic islet and acinar endothelial cells in health and diabetes. Nature Communications 2025 16:1 16(1):1338-. https://doi.org/10.1038/s41467-024-55415-3

39. Brissova M, Fowler M, Wiebe P, et al (2004) Intraislet Endothelial Cells Contribute to Revascularization of Transplanted Pancreatic Islets. Diabetes 53(5):1318–1325. https://doi.org/10.2337/DIABETES.53.5.1318

40. Narayanan S, Loganathan G, Dhanasekaran M, et al (2017) Intra-islet endothelial cell and β-cell crosstalk: Implication for islet cell transplantation. World J Transplant 7(2):117. https://doi.org/10.5500/WJT.V7.I2.117

41. Johansson M, Mattsson G, Andersson A, Jansson L, Carlsson PO (2006) Islet Endothelial Cells and Pancreatic β-Cell Proliferation: Studies in Vitro and during Pregnancy in Adult Rats. Endocrinology 147(5):2315–2324. https://doi.org/10.1210/EN.2005-0997

42. Ballian N, Brunicardi FC (2007) Islet Vasculature as a Regulator of Endocrine Pancreas Function. World Journal of Surgery 2007 31:4 31(4):705–714. https://doi.org/10.1007/S00268-006-0719-8

43. Brissova M, Shostak A, Fligner CL, et al (2015) Human Islets Have Fewer Blood Vessels than Mouse Islets and the Density of Islet Vascular Structures Is Increased in Type 2 Diabetes. Journal of Histochemistry and Cytochemistry 63(8):637–645. https://doi.org/10.1369/0022155415573324

44. Cottle L, Gan WJ, Gilroy I, et al (2021) Structural and functional polarisation of human pancreatic beta cells in islets from organ donors with and without type 2 diabetes. Diabetologia 64(3):618. https://doi.org/10.1007/S00125-020-05345-8

45. Jevon D, Cottle L, Hallahan N, et al (2024) Capillary contact points determine beta cell polarity, control secretion and are disrupted in the db/db mouse model of diabetes. Diabetologia 67(8):1683–1697. https://doi.org/10.1007/S00125-024-06180-X

46. Low JT, Zavortink M, Mitchell JM, et al (2014) Insulin secretion from beta cells in intact mouse islets is targeted towards the vasculature. Diabetologia 57(8):1655–1663. https://doi.org/10.1007/S00125-014-3252-6

47. Gan WJ, Zavortink M, Ludick C, et al (2017) Cell polarity defines three distinct domains in pancreatic β-cells. J Cell Sci 130(1):143–151. https://doi.org/10.1242/JCS.185116

48. Otonkoski T, Banerjee M, Korsgren O, Thornell LE, Virtanen I (2008) Unique basement membrane structure of human pancreatic islets: Implications for β-cell growth and differentiation. Diabetes Obes Metab 10(SUPPL. 4):119–127. https://doi.org/10.1111/J.1463-1326.2008.00955.X

49. Lammert E, Gu G, McLaughlin M, et al (2003) Role of VEGF-A in Vascularization of Pancreatic Islets. Current Biology 13(12):1070–1074. https://doi.org/10.1016/S0960-9822(03)00378-6

50. Kamba T, Tam BYY, Hashizume H, et al (2006) VEGF-dependent plasticity of fenestrated capillaries in the normal adult microvasculature. Am J Physiol Heart Circ Physiol 290(2). https://doi.org/10.1152/AJPHEART.00133.2005

51. Xiong Y, Scerbo MJ, Seelig A, et al (2020) Islet vascularization is regulated by primary endothelial cilia via vegf-a-dependent signaling. Elife 9:1–27. https://doi.org/10.7554/ELIFE.56914

52. Cai Q, Brissova M, Reinert RB, et al (2012) Enhanced expression of VEGF-A in β cells increases endothelial cell number but impairs islet morphogenesis and β cell proliferation. Dev Biol 367(1):40–54. https://doi.org/10.1016/J.YDBIO.2012.04.022

53. Reinert RB, Brissova M, Shostak A, et al (2013) Vascular endothelial growth factor-a and islet vascularization are necessary in developing, but not adult, pancreatic islets. Diabetes 62(12):4154–4164. https://doi.org/10.2337/DB13-0071/-/DC1

54. Lammert E, Cleaver O, Melton D (2001) Induction of pancreatic differentiation by signals from blood vessels. Science 294(5542):564–567. https://doi.org/10.1126/SCIENCE.1064344

55. Johansson Å, Lau J, Sandberg M, Borg LAH, Magnusson PU, Carlsson PO (2009) Endothelial cell signalling supports pancreatic beta cell function in the rat. Diabetologia 52(11):2385–2394. https://doi.org/10.1007/S00125-009-1485-6/

56. Drott CJ, Olerud J, Emanuelsson H, Christoffersson G, Carlsson PO (2012) Sustained Beta-Cell Dysfunction but Normalized Islet Mass in Aged Thrombospondin-1 Deficient Mice. PLoS One 7(10):e47451. https://doi.org/10.1371/JOURNAL.PONE.0047451

57. Aplin AC, Aghazadeh Y, Mohn OG, Hull-Meichle RL (2024) Role of the Pancreatic Islet Microvasculature in Health and Disease. J Histochem Cytochem 72(11–12):711–728. https://doi.org/10.1369/00221554241299862

58. Spelios MG, Afinowicz LA, Tipon RC, Akirav EM (2018) Human EndoC-βH1 β-cells form pseudoislets with improved glucose sensitivity and enhanced GLP-1 signaling in the presence of islet-derived endothelial cells. Am J Physiol Endocrinol Metab 314(5):E512–E521. https://doi.org/10.1152/AJPENDO.00272.2017

59. Porter JM, Yitayew M, Tabrizian M (2023) Renewable Human Cell Model for Type 1 Diabetes Research: EndoC- β H5/HUVEC Coculture Spheroids. J Diabetes Res 2023. https://doi.org/10.1155/2023/6610007

60. Gan WJ, Do OH, Cottle L, et al (2018) Local Integrin Activation in Pancreatic β Cells Targets Insulin Secretion to the Vasculature. Cell Rep 24(11):2819-2826.e3. https://doi.org/10.1016/J.CELREP.2018.08.035

61. Bosco D, Meda P, Halban PA, Rouiller DG (2000) Importance of cell-matrix interactions in rat islet beta-cell secretion in vitro: role of alpha6beta1 integrin. Diabetes 49(2):233–243. https://doi.org/10.2337/DIABETES.49.2.233

62. Diaferia GR, Jimenez-Caliani AJ, Ranjitkar P, et al (2013) β1 integrin is a crucial regulator of pancreatic β-cell expansion. Development 140(16):3360–3372. https://doi.org/10.1242/DEV.098533

63. Bonner-Weir S (1988) Morphological evidence for pancreatic polarity of beta-cell within islets of Langerhans. Diabetes 37(5):616–621. https://doi.org/10.2337/DIAB.37.5.616

64. Li Y, Gunderson RC, Xu Z, et al (2024) Mucosal Addressin Cell Adhesion Molecule-1 Mediates T Cell Migration into Pancreas-Draining Lymph Nodes for Initiation of the Autoimmune Response in Type 1 Diabetes. Int J Mol Sci 25(21). https://doi.org/10.3390/IJMS252111350

65. Yang XD, Michie SA, Tisch R, Karin N, Steinman L, McDevitt HO (1994) A predominant role of integrin alpha 4 in the spontaneous development of autoimmune diabetes in nonobese diabetic mice. Proc Natl Acad Sci U S A 91(26):12604–12608. https://doi.org/10.1073/PNAS.91.26.12604

66. Yagi N, Yokono K, Amano K, et al (1995) Expression of intercellular adhesion molecule 1 on pancreatic beta-cells accelerates beta-cell destruction by cytotoxic T-cells in murine autoimmune diabetes. Diabetes 44(7):744–752. https://doi.org/10.2337/DIAB.44.7.744

67. Martin TM, Burke SJ, Batdorf HM, et al (2022) ICAM-1 Abundance Is Increased in Pancreatic Islets of Hyperglycemic Female NOD Mice and Is Rapidly Upregulated by NF-κB in Pancreatic β-Cells. J Immunol 209(3):569–581. https://doi.org/10.4049/JIMMUNOL.2200065

68. En YL, Persson AEG, Bodin B, et al (2007) Endothelin-1 and pancreatic islet vasculature: studies in vivo and on isolated, vascularly perfused pancreatic islets.

Am J Physiol Endocrinol Metab 292(6). https://doi.org/10.1152/AJPENDO.00640.2006

69. Harari N, Sakhneny L, Khalifa-Malka L, et al (2019) Pancreatic pericytes originate from the embryonic pancreatic mesenchyme. Dev Biol 449(1):14–20. https://doi.org/10.1016/J.YDBIO.2019.01.020

70. Sakhneny L, Epshtein A, Landsman L (2021) Pericytes contribute to the islet basement membranes to promote beta-cell gene expression. Scientific Reports 2021 11:1 11(1):1–10. https://doi.org/10.1038/s41598-021-81774-8

71. Cho H, Kozasa T, Bondjers C, Betsholtz C, Kehrl JH (2003) Pericyte-specific expression of Rgs5: implications for PDGF and EDG receptor signaling during vascular maturation. The FASEB journal : official publication of the Federation of American Societies for Experimental Biology 17(3):440–442. https://doi.org/10.1096/FJ.02-0340FJE

72. Chen H, Gu X, Liu Y, et al (2011) PDGF signalling controls age-dependent proliferation in pancreatic β-cells. Nature 478(7369):349–355. https://doi.org/10.1038/NATURE10502

73. Xiang D-N, Feng Y-F, Wang J, et al (2019) Platelet-derived growth factor-BB promotes proliferation and migration of retinal microvascular pericytes by up-regulating the expression of C-X-C chemokine receptor types 4. Exp Ther Med 18(5):4022. https://doi.org/10.3892/ETM.2019.8016

74. Lee SJ, Kim S, Jo DH, et al (2021) Specific ablation of PDGFRβ-overexpressing pericytes with antibody-drug conjugate potently inhibits pathologic ocular neovascularization in mouse models. Communications Medicine 2021 1:1 1(1):1–12. https://doi.org/10.1038/s43856-021-00059-3

75. Kapuria S, Bai H, Fierros J, et al (2022) Heterogeneous pdgfrb+ cells regulate coronary vessel development and revascularization during heart regeneration. Development 149(4): dev199752. https://doi.org/10.1242/DEV.199752/VIDEO-3

76. Olson LE, Soriano P (2011) PDGFRβ Signaling Regulates Mural Cell Plasticity and Inhibits Fat Development. Dev Cell 20(6):815–826. https://doi.org/10.1016/J.DEVCEL.2011.04.019

77. Song S, Ewald AJ, Stallcup W, Werb Z, Bergers G (2005) PDGFRβ+ perivascular progenitor cells in tumours regulate pericyte differentiation and vascular survival. Nature Cell Biology 2005 7:9 7(9):870–879. https://doi.org/10.1038/ncb1288

78. Almaça J, Weitz J, Rodriguez-Diaz R, Pereira E, Caicedo A (2018) The Pericyte of the Pancreatic Islet Regulates Capillary Diameter and Local Blood Flow. Cell Metab 27(3):630-644.e4. https://doi.org/10.1016/J.CMET.2018.02.016

79. Tamayo A, Gonçalves LM, Rodriguez-Diaz R, et al (2022) Pericyte Control of Blood Flow in Intraocular Islet Grafts Impacts Glucose Homeostasis in Mice. Diabetes 71(8):1679. https://doi.org/10.2337/DB21-1104

80. Almaça J, Caicedo A (2020) Blood flow in the pancreatic islet: Not so isolated anymore. Diabetes 69(7):1336–1338. https://doi.org/10.2337/DBI20-0016

81. Sakhneny L, Mueller L, Schonblum A, et al (2021) The postnatal pancreatic microenvironment guides β cell maturation through BMP4 production. Dev Cell 56(19):2703-2711.e5. https://doi.org/10.1016/J.DEVCEL.2021.08.014

82. Epshtein A, Rachi E, Sakhneny L, Mizrachi S, Baer D, Landsman L (2017) Neonatal pancreatic pericytes support & beta-cell proliferation. https://doi.org/10.1016/j.molmet.2017.07.010

83. Sasson A, Rachi E, Sakhneny L, et al (2016) Islet Pericytes Are Required for β-Cell Maturity. Diabetes 65(10):3008–3014. https://doi.org/10.2337/DB16-0365

84. Sakhneny L, Rachi E, Epshtein A, et al (2018) Pancreatic Pericytes Support β-Cell Function in a Tcf7l2-Dependent Manner. Diabetes 67(3):437–447. https://doi.org/10.2337/DB17-0697

85. Armulik A, Genové G, Betsholtz C (2011) Pericytes: developmental, physiological, and pathological perspectives, problems, and promises. Dev Cell 21(2):193–215. https://doi.org/10.1016/J.DEVCEL.2011.07.001

86. Landsman L, Nijagal A, Whitchurch TJ, et al (2011) Pancreatic mesenchyme regulates epithelial organogenesis throughout development. PLoS Biol 9(9). https://doi.org/10.1371/JOURNAL.PBIO.1001143

87. Rhee S (2009) Fibroblasts in three dimensional matrices: cell migration and matrix remodeling. Exp Mol Med 41(12):858. https://doi.org/10.3858/EMM.2009.41.12.096

88. Grinnell F (2003) Fibroblast biology in three-dimensional collagen matrices. Trends Cell Biol 13(5):264–269. https://doi.org/10.1016/S0962-8924(03)00057-6

89. Garcia PE, Scales MK, Allen BL, Di Magliano MP (2020) Pancreatic Fibroblast Heterogeneity: From Development to Cancer. Cells 9(11):2464. https://doi.org/10.3390/CELLS9112464

90. Croft W, Pearce H, Margielewska-Davies S, et al (2023) Spatial determination and prognostic impact of the fibroblast transcriptome in pancreatic ductal adenocarcinoma. Elife 12:e86125. https://doi.org/10.7554/ELIFE.86125

91. Han L, Wu Y, Fang K, et al (2023) The splanchnic mesenchyme is the tissue of origin for pancreatic fibroblasts during homeostasis and tumorigenesis. Nature Communications 2023 14:1 14(1):1-. https://doi.org/10.1038/s41467-022-34464-6

92. Scavuzzo MA, Szlachcic WJ, Hill MC, et al (2025) Pancreatic organogenesis mapped through space and time. Exp Mol Med 57(1):204–220. https://doi.org/10.1038/S12276-024-01384-Y

93. Lendahl U, Muhl L, Betsholtz C (2022) Identification, discrimination and heterogeneity of fibroblasts. Nature Communications 2022 13:1 13(1):3409-. https://doi.org/10.1038/s41467-022-30633-9

94. Dranoff JA, Wells RG (2010) Portal fibroblasts: Underappreciated mediators of biliary fibrosis. Hepatology 51(4):1438. https://doi.org/10.1002/HEP.23405

95. Plikus M V., Wang X, Sinha S, et al (2021) Fibroblasts: origins, definitions, and functions in health and disease. Cell 184(15):3852. https://doi.org/10.1016/J.CELL.2021.06.024

96. Woodley DT (2017) Distinct Fibroblasts in the Papillary and Reticular Dermis: Implications for Wound Healing. Dermatol Clin 35(1):95–100. https://doi.org/10.1016/j.det.2016.07.004

97. Hung C, Linn G, Chow YH, et al (2013) Role of lung Pericytes and resident fibroblasts in the pathogenesis of pulmonary fibrosis. Am J Respir Crit Care Med 188(7):820–830. https://doi.org/10.1164/RCCM.201212-2297OC

98. Nilsson J, Fardoos R, Hansen L, et al (2019) Recruited fibroblasts reconstitute the peri-islet membrane: a longitudinal imaging study of human islet grafting and revascularisation. Diabetologia 2019 63:1 63(1):137–148. https://doi.org/10.1007/S00125-019-05018-1

99. Patil AR, Schug J, Naji A, Kaestner KH, Faryabi RB, Vahedi G (2023) Single-cell expression profiling of islets generated by the Human Pancreas Analysis Program. Nat Metab 5(5):713. https://doi.org/10.1038/S42255-023-00806-X

100. Tosti L, Hang Y, Debnath O, et al (2021) Single-Nucleus and In Situ RNA–Sequencing Reveal Cell Topographies in the Human Pancreas. Gastroenterology 160(4):1330-1344.e11. https://doi.org/10.1053/J.GASTRO.2020.11.010

101. Jones RC, Karkanias J, Krasnow MA, et al (2022) The Tabula Sapiens: A multiple-organ, single-cell transcriptomic atlas of humans. Science (1979) 376(6594). https://doi.org/10.1126/SCIENCE.ABL4896

102. Muhl L, Genové G, Leptidis S, et al (2020) Single-cell analysis uncovers fibroblast heterogeneity and criteria for fibroblast and mural cell identification and discrimination. Nature Communications 2020 11:1 11(1):3953-. https://doi.org/10.1038/s41467-020-17740-1

103. Guo J, Fu W (2020) Immune regulation of islet homeostasis and adaptation. J Mol Cell Biol 12(10):764–774. https://doi.org/10.1093/jmcb/mjaa009

104. Cruz AF, Rohban R, Esni F (2020) Macrophages in the pancreas: Villains by circumstances, not necessarily by actions. Immun Inflamm Dis 8(4):807–824. https://doi.org/https://doi.org/10.1002/iid3.345

105. Calderon B, Carrero JA, Ferris ST, et al (2015) The pancreas anatomy conditions the origin and properties of resident macrophages. Journal of Experimental Medicine 212(10):1497–1512. https://doi.org/10.1084/jem.20150496

106. Weitz JR, Makhmutova M, Almaça J, et al (2018) Mouse pancreatic islet macrophages use locally released ATP to monitor beta cell activity. Diabetologia 61(1):182–192. https://doi.org/10.1007/S00125-017-4416-Y

107. Saunders DC, Aamodt KI, Richardson TM, et al (2021) Coordinated interactions between endothelial cells and macrophages in the islet microenvironment

promote β cell regeneration. npj Regenerative Medicine 2021 6:1 6(1):1–13. https://doi.org/10.1038/s41536-021-00129-z

108. Weitz JR, Jacques-Silva C, Qadir MMF, et al (2020) Secretory Functions of Macrophages in the Human Pancreatic Islet Are Regulated by Endogenous Purinergic Signaling. Diabetes 69(6):1206–1218. https://doi.org/10.2337/DB19-0687

109. Ying W, Lee YS, Dong Y, et al (2018) Expansion of Islet-Resident Macrophages Leads to Inflammation Affecting β Cell Proliferation and Function in Obesity. Cell Metab 29(2):457. https://doi.org/10.1016/J.CMET.2018.12.003

110. Carrero JA, McCarthy DP, Ferris ST, et al (2017) Resident macrophages of pancreatic islets have a seminal role in the initiation of autoimmune diabetes of NOD mice. Proc Natl Acad Sci U S A 114(48):E10418–E10427. https://doi.org/10.1073/PNAS.1713543114

111. Sunami E, Kanazawa H, Hashizume H, Takeda M, Hatakeyama K, Ushiki T (2001) Morphological characteristics of Schwann cells in the islets of Langerhans of the murine pancreas. Arch Histol Cytol 64(2):191–201. https://doi.org/10.1679/AOHC.64.191

112. Burris RE, Hebrok M (2007) Pancreatic innervation in mouse development and β-cell regeneration. Neuroscience 150(3):592–602. https://doi.org/10.1016/J.NEUROSCIENCE.2007.09.079

113. Persson-Sjögren S, Zashihin A, Forsgren S (2001) Nerve cells associated with the endocrine pancreas in young mice: An ultrastructural analysis of the neuroinsular complex type I. Histochemical Journal 33(6):373–378. https://doi.org/10.1023/A:1012439510709

114. Cerf ME (2011) Islet organogenesis, angiogenesis and innervation. Cell Biol Int 35(11):1065–1078. https://doi.org/10.1042/CBI20100780/

115. Rodriguez-Diaz R, Abdulreda MH, Formoso AL, et al (2011) Innervation patterns of autonomic axons in the human endocrine pancreas. Cell Metab 14(1):45–54. https://doi.org/10.1016/J.CMET.2011.05.008

116. Pandiri AR (2013) Overview of Exocrine Pancreatic Pathobiology. Toxicol Pathol 42(1):207. https://doi.org/10.1177/0192623313509907

117. Kadono G, Ishihara T, Yamaguchi T, et al (2004) Immunohistochemical localization of type IV collagen alpha chains in the basement membrane of the pancreatic duct in human normal pancreas and pancreatic diseases. Pancreas 29(1):61–66. https://doi.org/10.1097/00006676-200407000-00057

118. Rizk AA, Dybala MP, Rodriguez KC, Rupnik MS, Hara M (2023) Pancreatic regional blood flow links the endocrine and exocrine diseases. J Clin Invest 133(15):e166185. https://doi.org/10.1172/JCI166185

119. Yousef El-Gohary1 GG (2018) Structure of Islets and Vascular Relationship to the Exocrine Pancreas. Pancreapedia: The Exocrine Pancreas Knowledge Base. https://doi.org/10.3998/PANC.2017.10

120. Alarcon-Martinez L, Yemisci M, Dalkara T (2021) Pericyte morphology and function. Histol Histopathol 36(6):633–643. https://doi.org/10.14670/HH-18-314

121. Kattner N, Bashir A, Shaw JAM (2026) The emerging role of pancreatic exocrine fibrosis as a common aetiological driver of islet dysfunction and diabetes: opportunities for novel disease-modifying interventions. Diabetologia 2026 69:5 69(5):1118–1132. https://doi.org/10.1007/S00125-026-06678-6

122. Rodriguez-Calvo T, Ekwall O, Amirian N, Zapardiel-Gonzalo J, Von Herrath MG (2014) Increased immune cell infiltration of the exocrine pancreas: A possible contribution to the pathogenesis of type 1 diabetes. Diabetes 63(11):3880–3890. https://doi.org/10.2337/DB14-0549/-/DC1

123. Murtaugh LC, Keefe MD (2015) Regeneration and repair of the exocrine pancreas. Annu Rev Physiol 77(Volume 77, 2015):229–249. https://doi.org/10.1146/ANNUREV-PHYSIOL-021014-071727

124. Love JA, Yi E, Smith TG (2007) Autonomic pathways regulating pancreatic exocrine secretion. Autonomic Neuroscience 133(1):19–34. https://doi.org/10.1016/J.AUTNEU.2006.10.001

125. Jansson L, Carlsson P (2019) Pancreatic Blood Flow with Special Emphasis on Blood Perfusion of the Islets of Langerhans. Compr Physiol 9(2):799–837. https://doi.org/10.1002/J.2040-4603.2019

126. Henderson JR, Moss MC (1985) A morphometric study of the endocrine and exocrine capillaries of the pancreas. Quarterly Journal of Experimental Physiology 70(3):347–356. https://doi.org/10.1113/EXPPHYSIOL.1985.SP002920

127. Muratore M, Santos C, Rorsman P (2021) The vascular architecture of the pancreatic islets: A homage to August Krogh. Comp Biochem Physiol A Mol Integr Physiol 252. https://doi.org/10.1016/j.cbpa.2020.110846

128. Akram J, Menezes P, Idris NI, et al (2025) Metabolic Stress and Adaptation in Pancreatic β-Cells to Hypoxia: Mechanisms, Modulators, and Implications for Transplantation. Cells 14(24):2014. https://doi.org/10.3390/CELLS14242014

129. Papas KK, De Leon H, Suszynski TM, Johnson RC (2019) Oxygenation strategies for encapsulated islet and beta cell transplants. Adv Drug Deliv Rev 139:139–156. https://doi.org/10.1016/J.ADDR.2019.05.002

130. Kim A, Miller K, Jo J, Kilimnik G, Wojcik P, Hara M Islet architecture: A comparative study. https://doi.org/10.4161/isl.1.2.9480

131. Adams MT, Blum B (2022) Determinants and dynamics of pancreatic islet architecture. https://doi.org/101080/1938201420222030649 14(1):82–100. https://doi.org/10.1080/19382014.2022.2030649

132. Steiner DJ, Kim A, Miller K, Hara M (2010) Pancreatic islet plasticity: Interspecies comparison of islet architecture and composition. Islets 2(3). https://doi.org/10.4161/ISL.2.3.11815

133. Cabrera O, Berman DM, Kenyon NS, Ricordi C, Berggren PO, Caicedo A (2006) The unique cytoarchitecture of human pancreatic islets has implications for islet cell function. Proc Natl Acad Sci U S A 103(7):2334–2339. https://doi.org/10.1073/PNAS.0510790103

134. Arrojo e Drigo R, Ali Y, Diez J, Srinivasan DK, Berggren PO, Boehm BO (2015) New insights into the architecture of the islet of Langerhans: a focused cross-species assessment. Diabetologia 58(10):2218–2228. https://doi.org/10.1007/S00125-015-3699-0

135. Cohrs CM, Chen C, Jahn SR, et al (2017) Vessel network architecture of adult human islets promotes distinct cell-cell interactions in situ and is altered after transplantation. Endocrinology 158(5):1373–1385. https://doi.org/10.1210/EN.2016-1184

136. Abdulreda MH, Rodriguez-Diaz R, Cabrera O, Caicedo A, Berggren PO (2016) The different faces of the pancreatic islet. Adv Exp Med Biol 938:11–24. https://doi.org/10.1007/978-3-319-39824-2_2

137. Jansson L, Barbu A, Bodin B, et al (2016) Pancreatic islet blood flow and its measurement. Ups J Med Sci 121(2):81. https://doi.org/10.3109/03009734.2016.1164769

138. Purice GI, Onose G (2012) Microanatomical study of the human pancreatic made on necroptic pieces. J Med Life 5(Spec Issue):102

139. In’t Veld P, Marichal M (2010) Microscopic anatomy of the human islet of Langerhans. Adv Exp Med Biol 654:1–19. https://doi.org/10.1007/978-90-481-3271-3_1

140. Song WW, Ergul A (2006) Type-2 diabetes-induced changes in vascular extracellular matrix gene expression: relation to vessel size. Cardiovasc Diabetol 5. https://doi.org/10.1186/1475-2840-5-3

141. Dybala MP, Kuznetsov A, Motobu M, et al (2020) Integrated Pancreatic Blood Flow: Bidirectional Microcirculation Between Endocrine and Exocrine Pancreas. Diabetes 69(7):1439. https://doi.org/10.2337/DB19-1034

142. Asthana A, Tamburrini R, Chaimov D, et al (2021) Comprehensive characterization of the human pancreatic proteome for bioengineering applications. Biomaterials 270:120613. https://doi.org/10.1016/J.BIOMATERIALS.2020.120613

143. Naba A, Clauser KR, Mani DR, Carr SA, Hynes RO (2017) Quantitative proteomic profiling of the extracellular matrix of pancreatic islets during the angiogenic switch and insulinoma progression. Scientific Reports 2017 7:1 7(1):40495-. https://doi.org/10.1038/srep40495

144. Naba A, Clauser KR, Hoersch S, Liu H, Carr SA, Hynes RO (2012) The matrisome: In silico definition and in vivo characterization by proteomics of normal and tumor extracellular matrices. Molecular and Cellular Proteomics 11(4). https://doi.org/10.1074/mcp.M111.014647

145. Ma F, Tremmel DM, Li Z, et al (2019) In Depth Quantification of Extracellular Matrix Proteins from Human Pancreas. J Proteome Res 18(8):3156–3165. https://doi.org/10.1021/ACS.JPROTEOME.9B00241

146. Li Z, Tremmel DM, Ma F, et al (2021) Proteome-wide and matrisome-specific alterations during human pancreas development and maturation. Nature Communications 2021 12:1 12(1):1–12. https://doi.org/10.1038/s41467-021-21261-w

147. Kragl M, Lammert E (2010) Basement membrane in pancreatic islet function. Adv Exp Med Biol 654:217–234. https://doi.org/10.1007/978-90-481-3271-3_10

148. Yurchenco PD (2011) Basement membranes: Cell scaffoldings and signaling platforms. Cold Spring Harb Perspect Biol 3(2):1–27. https://doi.org/10.1101/CSHPERSPECT.A004911

149. Weber LM, Hayda KN, Anseth KS (2008) Cell-matrix interactions improve β-cell survival and insulin secretion in three-dimensional culture. Tissue Eng Part A 14(12):1959–1968. https://doi.org/10.1089/TEN.TEA.2007.0238

150. Sekiguchi R, Yamada KM (2018) Basement Membranes in Development and Disease. Curr Top Dev Biol 130:143–191. https://doi.org/10.1016/BS.CTDB.2018.02.005

151. Yousif LF, Di Russo J, Sorokin L (2013) Laminin isoforms in endothelial and perivascular basement membranes. Cell Adh Migr 7(1):101–110. https://doi.org/10.4161/CAM.22680

152. Kalluri R (2003) Basement membranes: structure, assembly and role in tumour angiogenesis. Nature Reviews Cancer 2003 3:6 3(6):422–433. https://doi.org/10.1038/nrc1094

153. Williamson JR, Kilo C (1977) Current status of capillary basement membrane disease in diabetes mellitus. Diabetes 26(1):69–73. https://doi.org/10.2337/DIAB.26.1.65

154. Brandhorst D, Brandhorst H, Lee Layland S, Acreman S, Schenke-Layland K, Johnson PRV (2022) Basement membrane proteins improve human islet survival in hypoxia: Implications for islet inflammation. Acta Biomater 137:92–102. https://doi.org/10.1016/J.ACTBIO.2021.10.013

155. Boudko SP, Danylevych N, Hudson BG, Pedchenko VK (2017) Basement membrane collagen IV: Isolation of functional domains. Methods Cell Biol 143:171. https://doi.org/10.1016/BS.MCB.2017.08.010

156. Ricard-Blum S (2011) The Collagen Family. Cold Spring Harb Perspect Biol 3(1):1–19. https://doi.org/10.1101/CSHPERSPECT.A004978

157. Lee J, Gross JM (2007) Laminin β1 and γ1 containing laminins are essential for basement membrane integrity in the zebrafish eye. Invest Ophthalmol Vis Sci 48(6):2483–2490. https://doi.org/10.1167/IOVS.06-1211

158. Radner S, Banos C, Bachay G, et al (2013) β2 and γ3 laminins are critical cortical basement membrane components: Ablation of Lamb2 and Lamc3 genes disrupts

cortical lamination and produces dysplasia. Dev Neurobiol 73(3):209–229. https://doi.org/10.1002/DNEU.22057

159. Goddi A, Schroedl L, Brey EM, Cohen RN (2021) Laminins in metabolic tissues. Metabolism 120:154775. https://doi.org/10.1016/J.METABOL.2021.154775

160. Ponce ML, Kleinman HK (2003) Identification of redundant angiogenic sites in laminin α1 and γ1 chains. Exp Cell Res 285(2):189–195. https://doi.org/10.1016/S0014-4827(03)00056-9

161. Kuncha J, Darden CM, Liu Y, Lawrence M, Sebastian Danobeitia J, Naziruddin B (2025) Correlation of Pancreatic Laminin Alpha 5 Expression With Clinical Outcomes in Total Pancreatectomy With Islet Autotransplantation. Cell Transplant 34:09636897251317048. https://doi.org/10.1177/09636897251317048

162. Bader BL, Smyth N, Nedbal S, et al (2005) Compound Genetic Ablation of Nidogen 1 and 2 Causes Basement Membrane Defects and Perinatal Lethality in Mice. Mol Cell Biol 25(15):6846. https://doi.org/10.1128/MCB.25.15.6846-6856.2005

163. Ho MSP, Böse K, Mokkapati S, Nischt R, Smyth N (2008) Nidogens-Extracellular matrix linker molecules. Microsc Res Tech 71(5):387–395. https://doi.org/10.1002/JEMT.20567

164. Iozzo R V. (2005) Basement membrane proteoglycans: from cellar to ceiling. Nature Reviews Molecular Cell Biology 2005 6:8 6(8):646–656. https://doi.org/10.1038/nrm1702

165. Hiebert LM (2021) Heparan Sulfate Proteoglycans in Diabetes. Semin Thromb Hemost 47(3):261–273. https://doi.org/10.1055/S-0041-1724118/ID/JR02864-14/BIB

166. Brandhorst D, Brandhorst H, Acreman S, Johnson PRV (2024) Perlecan: An Islet Basement Membrane Protein with Protective Anti-Inflammatory Characteristics. Bioengineering 11(8):828. https://doi.org/10.3390/BIOENGINEERING11080828

167. Marneros AG, Olsen BR (2005) Physiological role of collagen XVIII and endostatin. FASEB J 19(7):716–728. https://doi.org/10.1096/FJ.04-2134REV

168. Carlsson AC, Östgren CJ, Länne T, Larsson A, Nystrom FH, Ärnlöv J (2016) The association between endostatin and kidney disease and mortality in patients with type 2 diabetes. Diabetes Metab 42(5):351–357. https://doi.org/10.1016/j.diabet.2016.03.006

169. Sodha NR, Clements RT, Boodhwani M, et al (2008) Endostatin and angiostatin are increased in diabetic patients with coronary artery disease and associated with impaired coronary collateral formation. Am J Physiol Heart Circ Physiol 296(2):H428. https://doi.org/10.1152/AJPHEART.00283.2008

170. Zhou J, Xie Z (2022) Endostatin Inhibits Blood-Retinal Barrier Breakdown in Diabetic Rats by Increasing the Expression of ICAM-1 and VCAM-1 and Decreasing the Expression of VEGF. Comput Math Methods Med 2022:5105866. https://doi.org/10.1155/2022/5105866

171. Kaido T, Yebra M, Cirulli V, Rhodes C, Diaferia G, Montgomery AM (2006) Impact of defined matrix interactions on insulin production by cultured human beta-cells: effect on insulin content, secretion, and gene transcription. Diabetes 55(10):2723–2729. https://doi.org/10.2337/DB06-0120

172. Wang RN, Rosenberg L (1999) Maintenance of beta-cell function and survival following islet isolation requires re-establishment of the islet-matrix relationship. J Endocrinol 163(2):181–190. https://doi.org/10.1677/JOE.0.1630181

173. Banerjee M, Virtanen I, Palgi J, Korsgren O, Otonkoski T (2012) Proliferation and plasticity of human beta cells on physiologically occurring laminin isoforms. Mol Cell Endocrinol 355(1):78–86. https://doi.org/10.1016/J.MCE.2012.01.020

174. Parnaud G, Hammar E, Rouiller DG, Armanet M, Halban PA, Bosco D (2006) Blockade of beta1 integrin-laminin-5 interaction affects spreading and insulin secretion of rat beta-cells attached on extracellular matrix. Diabetes 55(5):1413–1420. https://doi.org/10.2337/DB05-1388

175. Mamidi A, Prawiro C, Seymour PA, et al (2018) Mechanosignalling via integrins directs fate decisions of pancreatic progenitors. Nature 2018 564:7734 564(7734):114–118. https://doi.org/10.1038/s41586-018-0762-2

176. Pinkse GGM, Bouwman WP, Jiawan-Lalai R, Terpstra OT, Bruijn JA, De Heer E (2006) Integrin signaling via RGD peptides and anti-beta1 antibodies confers resistance to apoptosis in islets of Langerhans. Diabetes 55(2):312–317. https://doi.org/10.2337/DIABETES.55.02.06.DB04-0195

177. Cirulli V, Beattie GM, Klier G, et al (2000) Expression and Function of v 3 and v 5 Integrins in the Developing Pancreas: Roles in the Adhesion and Migration of Putative Endocrine Progenitor Cells. J Cell Biol 150(6):1445–1459

178. Miao G, Zhao Y, Li Y, et al (2013) Basement membrane extract preserves islet viability and activity in vitro by up-regulating α3 integrin and its signal. Pancreas 42(6):971–976. https://doi.org/10.1097/MPA.0B013E318287CFE0

179. Wang R, Li J, Lyte K, Yashpal NK, Fellows F, Goodyer CG (2005) Role for β1 integrin and its associated α3, α5, and α6 subunits in development of the human fetal pancreas. Diabetes 54(7):2080–2089. https://doi.org/10.2337/DIABETES.54.7.2080

180. Townsend SE, Gannon M (2019) Extracellular Matrix–Associated Factors Play Critical Roles in Regulating Pancreatic β-Cell Proliferation and Survival. Endocrinology 160(8):1885–1894. https://doi.org/10.1210/EN.2019-00206

181. Venieratos PD, Drossopoulou GI, Kapodistria KD, Tsilibary EC, Kitsiou P V. (2010) High glucose induces suppression of insulin signalling and apoptosis via upregulation of endogenous IL-1β and suppressor of cytokine signalling-1 in mouse pancreatic beta cells. Cell Signal 22(5):791–800. https://doi.org/10.1016/J.CELLSIG.2010.01.003

182. Hammar E, Parnaud G, Bosco D, et al (2004) Extracellular Matrix Protects Pancreatic β-Cells Against ApoptosisRole of Short- and Long-Term Signaling

Pathways. Diabetes 53(8):2034–2041. https://doi.org/10.2337/DIABETES.53.8.2034

183. Santos da Silva T, Silva-Júnior LN da, Horvath-Pereira B de O, et al (2024) The Role of the Pancreatic Extracellular Matrix as a Tissue Engineering Support for the Bioartificial Pancreas. Biomimetics 2024, Vol 9, 9(10). https://doi.org/10.3390/BIOMIMETICS9100598

184. Meyer T, Chodnewska I, Czub S, et al (1998) Extracellular Matrix Proteins in the Porcine Pancreas: A Structural Analysis for Directed Pancreatic Islet Isolation. Transplant Proc 30(2):354. https://doi.org/10.1016/S0041-1345(97)01302-X

185. Cross SE, Vaughan RH, Willcox AJ, et al (2017) Key Matrix Proteins Within the Pancreatic Islet Basement Membrane Are Differentially Digested During Human Islet Isolation. American Journal of Transplantation 17(2):451–461. https://doi.org/10.1111/AJT.13975

186. Irving-Rodgers HF, Choong FJ, Hummitzsch K, Parish CR, Rodgers RJ, Simeonovic CJ (2014) Pancreatic Islet basement membrane loss and remodeling after mouse islet isolation and transplantation: Impact for allograft rejection. Cell Transplant 23(1):59–72. https://doi.org/10.3727/096368912X659880/ASSET/IMAGES/LARGE/10.3727_096368912X659880-FIG2.JPEG

187. Barillaro M, Schuurman M, Wang R (2022) β1-Integrin-A Key Player in Controlling Pancreatic Beta-Cell Insulin Secretion via Interplay With SNARE Proteins. Endocrinology 164(1). https://doi.org/10.1210/ENDOCR/BQAC179

188. Yamazaki T, Mukouyama YS (2018) Tissue Specific Origin, Development, and Pathological Perspectives of Pericytes. Front Cardiovasc Med 5. https://doi.org/10.3389/FCVM.2018.00078

189. Brown LS, Foster CG, Courtney JM, King NE, Howells DW, Sutherland BA (2019) Pericytes and neurovascular function in the healthy and diseased brain. Front Cell Neurosci 13:282. https://doi.org/10.3389/FNCEL.2019.00282/BIBTEX

190. Bergers G, Song S (2005) The role of pericytes in blood-vessel formation and maintenance. Neuro Oncol 7(4):452–464. https://doi.org/10.1215/S1152851705000232

191. Hartmann DA, Berthiaume AA, Grant RI, et al (2021) Brain capillary pericytes exert a substantial but slow influence on blood flow. Nature Neuroscience 2021 24:5 24(5):633–645. https://doi.org/10.1038/s41593-020-00793-2

192. Paquet-Fifield S, Li J, Kaur P, et al (2009) A role for pericytes as microenvironmental regulators of human skin tissue regeneration. J Clin Invest 119(9):2795–2806. https://doi.org/10.1172/JCI38535

193. Sava P, Ramanathan A, Dobronyi A, et al (2017) Human pericytes adopt myofibroblast properties in the microenvironment of the IPF lung. JCI Insight 2(24). https://doi.org/10.1172/JCI.INSIGHT.96352

194. Bak K, Kim H, Garland JS, et al (2025) Matrix Gla Protein Expression in Pericytes and Myofibroblasts Contributes to Renal Fibrosis. Am J Pathol 196(3):669. https://doi.org/10.1016/J.AJPATH.2025.12.003

195. Alex L, Tuleta I, Hernandez SC, et al (2023) Cardiac Pericytes Acquire a Fibrogenic Phenotype and Contribute to Vascular Maturation after Myocardial Infarction. Circulation 148(11):882–898. https://doi.org/10.1161/CIRCULATIONAHA.123.064155;PAGE:STRING:ARTICLE/CHAPTER

196. Xourafa G, Korbmacher M, Roden M (2024) Inter-organ crosstalk during development and progression of type 2 diabetes mellitus. Nat Rev Endocrinol 20(1):27–49. https://doi.org/10.1038/S41574-023-00898-1

197. Eguchi K, Nagai R (2017) Islet inflammation in type 2 diabetes and physiology. J Clin Invest 127(1):14. https://doi.org/10.1172/JCI88877

198. Sun Y, Zhang Z, Wang Y, et al (2025) Hidden pathway: the role of extracellular matrix in type 2 diabetes mellitus–related sarcopenia. Front Endocrinol (Lausanne) 16:1560396. https://doi.org/10.3389/FENDO.2025.1560396

199. Hayden MR, Patel K, Habibi J, et al (2008) Attenuation of Endocrine-Exocrine Pancreatic Communication in Type 2 Diabetes: Pancreatic Extracellular Matrix Ultrastructural Abnormalities. J Cardiometab Syndr 3(4):234–243. https://doi.org/10.1111/J.1559-4572.2008.00024.X

200. Hayden MR, Sowers JR, Tyagi SC (2005) The central role of vascular extracellular matrix and basement membrane remodeling in metabolic syndrome and type 2 diabetes: the matrix preloaded. Cardiovasc Diabetol 4. https://doi.org/10.1186/1475-2840-4-9

201. Mateus Gonçalves L, Pereira E, Werneck de Castro JP, Bernal-Mizrachi E, Almaça J (2020) Islet pericytes convert into profibrotic myofibroblasts in a mouse model of islet vascular fibrosis. Diabetologia 63(8):1564–1575. https://doi.org/10.1007/S00125-020-05168-7

202. Hayden MR, Karuparthi PR, Habibi J, et al (2007) Ultrastructural Islet Study of Early Fibrosis in the Ren2 Rat Model of Hypertension. Emerging Role of the Islet Pancreatic Pericyte-Stellate Cell. JOP 8(6):725–738

203. Kilimnik G, Zhao B, Jo J, et al (2011) Altered Islet Composition and Disproportionate Loss of Large Islets in Patients with Type 2 Diabetes. PLoS One 6(11):e27445. https://doi.org/10.1371/journal.pone.0027445

204. Williamson JR, Rowold E, Hoffman P, Kilo C (1976) Influence of fixation and morphometric technics on capillary basement membrane thickening prevalence data in diabetes. Diabetes 25(7):604–613. https://doi.org/10.2337/DIAB.25.7.604

205. Capillary Basement Membrane - an overview | ScienceDirect Topics. https://www.sciencedirect.com/topics/immunology-and-microbiology/capillary-basement-membrane

206. Tsilibary EC (2003) Microvascular basement membranes in diabetes mellitus. J Pathol 200(4):537–546. https://doi.org/10.1002/PATH.1439

207. Song WW, Ergul A (2006) Type-2 diabetes-induced changes in vascular extracellular matrix gene expression: Relation to vessel size. Cardiovasc Diabetol 5:3. https://doi.org/10.1186/1475-2840-5-3

208. Sun A, Yang H, Sun J, et al (2025) Treatment of T2DM-related inflammation and vascular injury by regulating cellular crosstalk in the islet microenvironment. Front Endocrinol (Lausanne) 16:1551853. https://doi.org/10.3389/FENDO.2025.1551853

209. Hayes KL (2019) Pericytes in Type 2 Diabetes. Adv Exp Med Biol 1147:265–278. https://doi.org/10.1007/978-3-030-16908-4_12

210. Brownlee M (2005) The pathobiology of diabetic complications: a unifying mechanism. Diabetes 54(6):1615–1625. https://doi.org/10.2337/DIABETES.54.6.1615

211. Giacco F, Brownlee M (2010) Oxidative stress and diabetic complications. Circ Res 107(9):1058. https://doi.org/10.1161/CIRCRESAHA.110.223545

212. Hayden MR, Yang Y, Habibi J, Bagree S V., Sowers JR (2010) Pericytopathy: Oxidative Stress and Impaired Cellular Longevity in the Pancreas and Skeletal Muscle in Metabolic Syndrome and Type 2 Diabetes. Oxid Med Cell Longev 3(5):290. https://doi.org/10.4161/OXIM.3.5.13653

213. Mizutani M, Kern TS, Lorenzi M (1996) Accelerated death of retinal microvascular cells in human and experimental diabetic retinopathy. Journal of Clinical Investigation 97(12):2883. https://doi.org/10.1172/JCI118746

214. Hammes HP, Lin J, Renner O, et al (2002) Pericytes and the pathogenesis of diabetic retinopathy. Diabetes 51(10):3107–3112. https://doi.org/10.2337/DIABETES.51.10.3107

215. Giannini C, Dyck PJ (1995) Basement membrane reduplication and pericyte degeneration precede development of diabetic polyneuropathy and are associated with its severity. Ann Neurol 37(4):498–504. https://doi.org/10.1002/ANA.410370412

216. Shimizu F, Sano Y, Haruki H, Kanda T (2011) Advanced glycation end-products induce basement membrane hypertrophy in endoneurial microvessels and disrupt the blood-nerve barrier by stimulating the release of TGF-β and vascular endothelial growth factor (VEGF) by pericytes. Diabetologia 54(6):1517–1526. https://doi.org/10.1007/S00125-011-2107-7

217. Tilton RG, Hoffmann PL, Kilo C, Williamson JR (1981) Pericyte degeneration and basement membrane thickening in skeletal muscle capillaries of human diabetics. Diabetes 30(4):326–334. https://doi.org/10.2337/DIAB.30.4.326

218. Rickelt S, Hynes RO (2018) Antibodies and methods for immunohistochemistry of extracellular matrix proteins. Matrix Biology 71–72:10–27. https://doi.org/10.1016/J.MATBIO.2018.04.011

219. Engelbrecht LK, Twigger A-J, Ganz HM, et al (2021) A strategy to address dissociation-induced compositional and transcriptional bias for single-cell analysis of the human mammary gland. bioRxiv 2021.02.11.430721. https://doi.org/10.1101/2021.02.11.430721

220. Mattei D, Ivanov A, van Oostrum M, et al (2020) Enzymatic Dissociation Induces Transcriptional and Proteotype Bias in Brain Cell Populations. Int J Mol Sci 21(21):7944. https://doi.org/10.3390/IJMS21217944

221. Truong DD, Lamhamedi-Cherradi SE, Porter RW, et al (2023) Dissociation protocols used for sarcoma tissues bias the transcriptome observed in single-cell and single-nucleus RNA sequencing. BMC Cancer 2023 23:1 23(1):488-. https://doi.org/10.1186/S12885-023-10977-1

Chapter 2 The Spatial Extracellular Matrix Expression Landscape of the Human Adult Pancreas Across Health and Disease

2.1 Introduction

The pancreatic islet microenvironment is maintained through coordinated interactions among endocrine cells, vascular cells, stromal populations, and the surrounding ECM [1, 2]. As discussed in Chapter 1, the basement membrane is a specialized ECM that provides structural support while also regulating β cell polarity, survival, insulin secretion, and vascular integrity [3–6]. Human islets contain two major basement membrane compartments: the peri-islet basement membrane, which separates endocrine tissue from the surrounding exocrine pancreas, and the vascular basement membrane, which surrounds the intra-islet capillary network [7]. Together, these matrices establish the structural and signaling framework required for normal endocrine function.

Despite the recognized importance of basement membrane biology, the cellular mechanisms responsible for assembling and maintaining the adult human islet matrix remain incompletely understood. The prevailing model, derived largely from developmental studies in mice, has emphasized endothelial cells as the principal source of the vascular basement membrane[4]. In this model, mouse endothelial cells are thought to produce the collagen IV, laminins, and other matrix components that surround islet capillaries. However, increasing evidence suggests that this endothelial-centered view may not fully explain basement membrane organization in the adult human pancreas. Pericytes, fibroblasts, and other vascular-associated stromal

populations are now recognized as active regulators of vascular homeostasis rather than passive support cells [8]. In addition to controlling capillary stability, blood flow, and endothelial maturation, these populations express numerous ECM and basement membrane -associated genes, including collagens, laminins, proteoglycans, and glycoproteins [8, 9]. Studies in the brain, retina, kidney, and lung have shown that pericytes contribute directly to vascular matrix deposition, and recent transcriptomic analyses of the mouse pancreas have similarly identified robust basement membrane gene expression in pancreatic pericyte cells [8, 10–14]. Whether these observations extend to the adult human pancreas remains unresolved.

Addressing this question has been technically challenging because vascular-supportive cell populations are closely intermingled within intact tissue [15]. Endothelial cells, pericytes, and fibroblasts reside within microns of one another and may express overlapping marker and ECM genes, making it difficult to assign secreted matrix proteins to their cellular source [16]. Conventional histology preserves tissue architecture but cannot determine which neighboring cell synthesized a deposited ECM protein [17]. Conversely, single-cell RNA sequencing provides transcriptional resolution but requires tissue dissociation, removing the spatial information needed to distinguish endocrine-associated from exocrine-associated vascular cells [8, 18, 19]. As a result, the spatial organization and cellular origins of the human pancreatic basement membrane have remained largely unknown.

An additional unanswered question is how the endocrine vascular niche is remodeled in type 2 diabetes [20]. Diabetic islets exhibit fibrosis, vascular dysfunction, and basement membrane abnormalities, but the specific vascular-supportive

populations that undergo transcriptional remodeling, and whether these changes differ between endocrine and exocrine compartments, remain poorly defined [20–22]. Because the endocrine niche is composed of multiple interacting stromal and vascular populations, understanding disease-associated remodeling requires methods that preserve both transcriptional identity and spatial organization within intact tissue.

Recent advances in spatial transcriptomics provide an opportunity to overcome these limitations. Multiplexed Error-Robust Fluorescence *In-Situ* Hybridization (MERFISH) enables highly multiplexed RNA imaging at single-cell resolution while preserving native tissue architecture [23]. When integrated with whole-transcriptome single-cell RNA sequencing, MERFISH combines broad molecular profiling with precise anatomical localization, allowing ECM-producing cells to be identified directly within their physiological microenvironment. In this chapter, I use this integrated approach to construct a cellular and spatial atlas of the ECM landscape in the adult human pancreas. These analyses define the cellular sources of vascular basement membrane-associated genes, distinguish endocrine and exocrine vascular-supportive niches, identify specialized stromal populations at the islet boundary, and determine how these compartments are remodeled in type 2 diabetes.

2.2 Results

2.2.1: Mesenchymal cells are the Primary Source of Vascular Basement Membrane Gene Expression in the Healthy Adult Human Pancreas.

The human islet vascular niche is organized around a specialized capillary network that supports rapid nutrient sensing, hormone release, and endocrine cell survival. A defining feature of this niche is the vascular basement membrane, which

forms the structural and signaling interface between endothelial cells, pericytes, and adjacent endocrine cells.

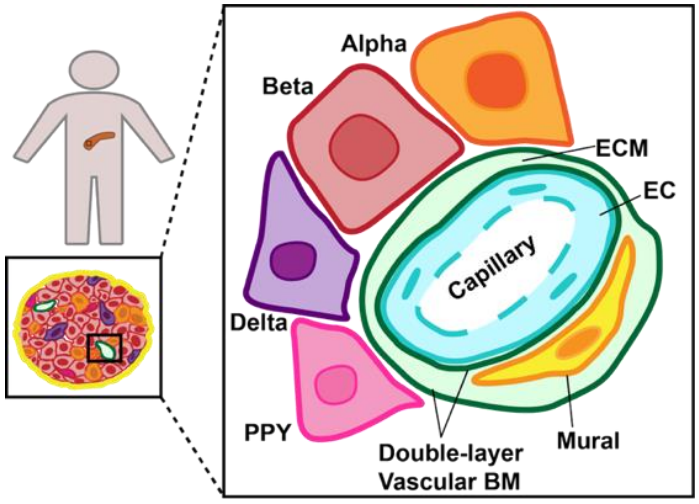

Figure 2-1: Schematic of the pancreatic vascular niche depicting the specialized architecture of the islet microvasculature.

Fenestrated endothelial cells (cyan) are encircled by perivascular mural cells (yellow) and sequestered within a distinct, double-layered vascular basement membrane (BM; green). Endocrine cells (red, beta cell; orange, alpha cell; purple, delta cell; pink, PPY cell) are in close physical contact with the islet vascular BM.

Previous studies in the mouse have indicated a central role for the vascular compartment in forming the islet basement membrane. As the vascular basement membrane in human islets differs in its uniquely bilayered structure (**Fig. 2-1**), we set out to better understand the cellular sources and composition of human islet vascular basement membrane. We first reasoned that the major cellular contributors to the human pancreatic basement membrane should be detectable at the transcript level across dissociated pancreatic cell populations. Although deposited matrix proteins cannot be assigned to their cellular source by histology alone, scRNA-seq provides an initial way to compare ECM and basement membrane gene expression across endocrine, epithelial, endothelial, immune, and mesenchymal compartments.

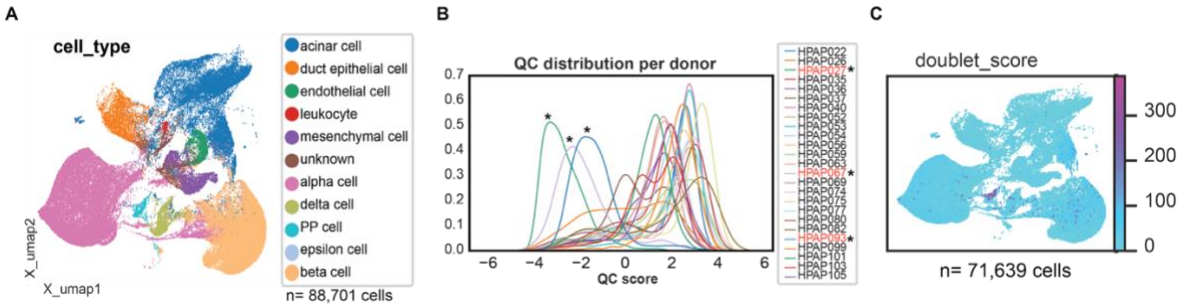

Figure 2-2: Quality control and doublet filtering of the integrated human pancreas scRNA-seq dataset.

(**A**) UMAP visualization of all cells following initial preprocessing and cell type annotation.
(**B**) Distribution of quality control (QC) scores across individual donors. Donors failing QC thresholds (asterisks) were excluded from downstream analyses.
(**C**) UMAP colored by doublet score following doublet detection. Cells with high predicted doublet scores were removed prior to downstream analyses.

To gain an unbiased understanding of the gross composition and basement membrane gene expression patterns across cell types in the human pancreas, we first re-integrated publicly available scRNA-seq data from PancDB, restricting our analysis to non-diabetic adult donors (n = 25 donors; n = 88,701 cells) (**Fig. 2-2A**) [24, 25]. Three samples were flagged because of low-quality RNA (see Methods; **Fig. 2-2B**) and additional quality control and doublet filtering highlighted which cells and donors needed to be filtered out for a cleaner, better resolved dataset for downstream analysis (**Fig. 2-2C**).

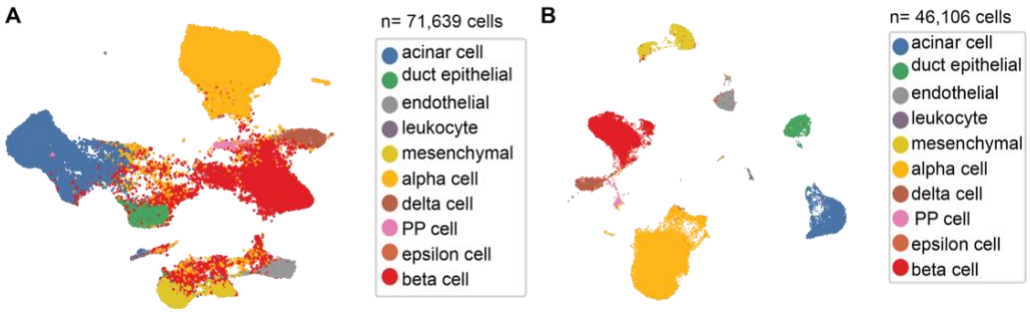

Figure 2-3: CONCORD integrated UMAP of PancDB dataset before and after donor filtering.

(A) Cells are colored by major cell type, including acinar, duct epithelial, endothelial, leukocyte, mesenchymal, alpha, beta, delta, PP, and epsilon cells. CONCORD UMAP of unfiltered PancDB dataset containing 71,639 cells across 25 donors.
(B) CONCORD UMAP of filtered PancDB dataset containing 46,106 cells after quality control and cell filtering across 22 donors.

Donor filtering and batch alignment with CONCORD, a recently reported tool for data integration, dimensionality reduction, and denoising that preserves biological features better than other reported methods, co-embedded the filtered PancDB dataset into well-resolved clusters representing all major pancreatic cell populations (n = 22 donors, n = 46,106 cells; **Fig. 2-3A-B**).

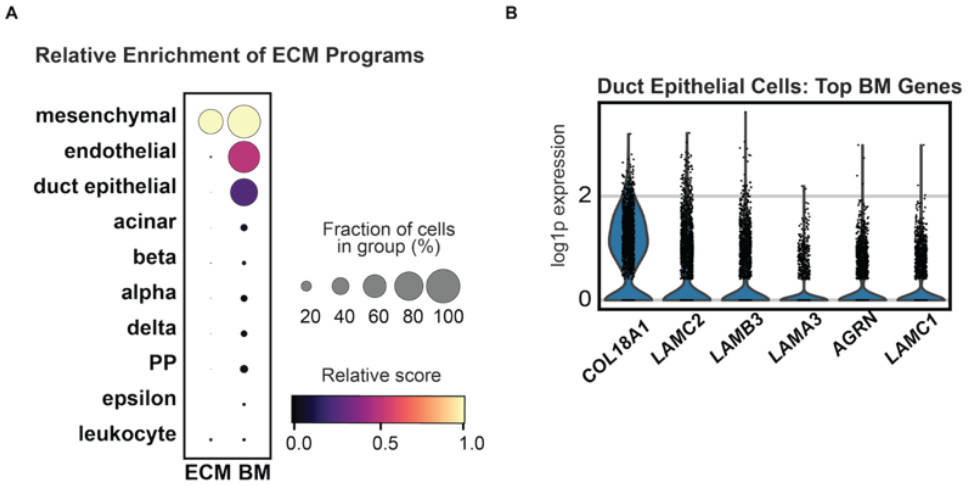

Figure 2-4: Basement membrane gene expression across pancreatic cell types.

(**A**) Dot plot showing relative ECM and BM gene program enrichment across major pancreatic cell types. Dot size represents the fraction of cells expressing the gene set, and color indicates the relative enrichment score.
(**B**) Violin plots showing the expression of the top BM-associated genes in duct epithelial cells. Expression values are shown as log1p-normalized expression.

To assess basement membrane and ECM gene expression across pancreatic cell types, we calculated gene set scores (**Fig. 2-4A**) using the Naba Basement Membrane and Naba Core Matrisome gene sets obtained from Molecular Signature Database (MsigDB) [26–31]. To distinguish broader ECM programs from basement membrane-associated genes, genes present in the basement membrane set were excluded from the Core Matrisome set prior to scoring. Surprisingly, this analysis revealed that mesenchymal cells (relative mean score = 1), rather than ECs (0.508), exhibited the highest relative enrichment of basement membrane scores compared to

other cells. In contrast, endocrine cells exhibited substantially lower ECM and basement membrane gene program enrichment, consistent with previous reports in the mouse (**Fig. 2-4A**). Although ductal cells showed a positive basement membrane signal (0.280), this enrichment was restricted to a subset of cells expressing modest levels of basement membrane -associated genes, most notably *COL18A1* and laminin subunits (**Fig. 2-4B**).

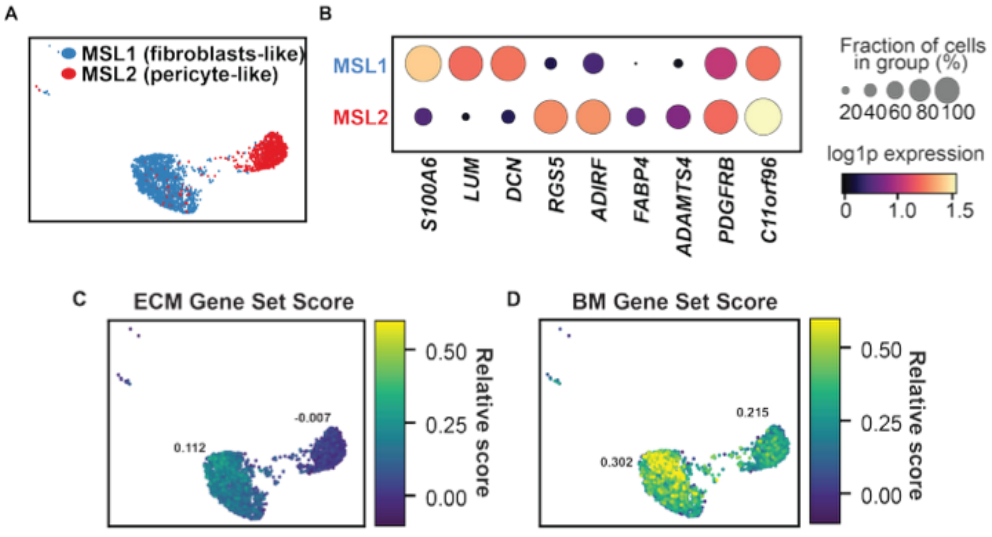

Figure 2-5: Identification of mesenchymal subpopulations and extracellular matrix programs.

(**A**) UMAP of mesenchymal cells showing the two major subpopulations identified by unsupervised clustering: fibroblast-like (MSL1) and pericyte-like (MSL2).
(**B**) Dot plot showing expression of representative marker genes used to distinguish MSL1 and MSL2 populations. Dot size represents the fraction of cells expressing each gene, and color indicates average log1p expression.
(**C**) UMAP colored by ECM gene set score.
(**D**) UMAP colored by basement membrane gene set score.

Given the enrichment of basement membrane gene expression within the mesenchymal population, we next examined heterogeneity within this compartment. Unsupervised sub-clustering revealed two transcriptionally distinct populations (**Fig. 2-5A**). The first population, mesenchymal subtype-1 (MSL1), expressed fibroblast-associated genes, including *S100A6* and *LUM*, indicative of a fibroblast-like identity. The

second population, mesenchymal subtype-2 (MSL2), was enriched for mural cell genes, such as *RGS5*, *PDGFRB*, and *C11orf96*, consistent with a pericyte-like identity (**Fig. 2-5B**). Although both populations expressed ECM genes, MSL2 showed preferential enrichment of basement membrane programs, with a higher mean basement membrane gene set score (0.215) than ECM score (-0.007). MSL1 cells also exhibited elevated basement membrane-associated gene expression but showed concurrent enrichment of broader ECM programs, with basement membrane and ECM scores of 0.302 and 0.112, respectively (**Figs. 2-5C, 2-5D**).

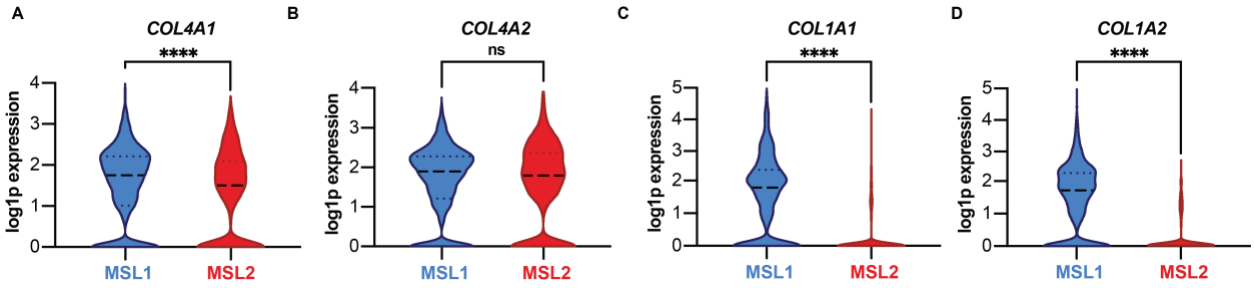

Figure 2-6: Differential expression of basement membrane and fibrillar collagen genes between mesenchymal subpopulations.

(**A–D**) Violin plots comparing expression of *COL4A1*, *COL4A2*, *COL1A1*, and *COL1A2* between fibroblast-like (MSL1) and pericyte-like (MSL2) mesenchymal populations. Statistical significance is indicated above each comparison (****, $P < 0.0001$; ns, not significant).

To further resolve the differences in basement membrane gene expression between MSL1 and MSL2 populations, we compared the expression of core basement membrane genes (*COL4A1*, *COL4A2*) and interstitial collagens (*COL1A1*, *COL1A2*) (**Fig. 2-6A).** Fibroblast-like MSL1 cells displayed significantly higher expression of *COL4A1* (p = 0.001) (**Fig. 2-6B**), while the two populations expressed indistinguishable levels of *COL4A2*. Interstitial collagens *COL1A1* and *COL1A2* were significantly enriched in fibroblast-like MSL1 cells and largely absent in MSL2 (p = 0.001) (**Figs. 2-6C, 2-6D**). These results indicate that MSL1 fibroblast-like cells express a mixed ECM

program containing both basement membrane-associated and fibrillar collagen genes, whereas MSL2 pericyte-like cells lack the fibrillar collagen program characteristic of fibroblast-like cells.

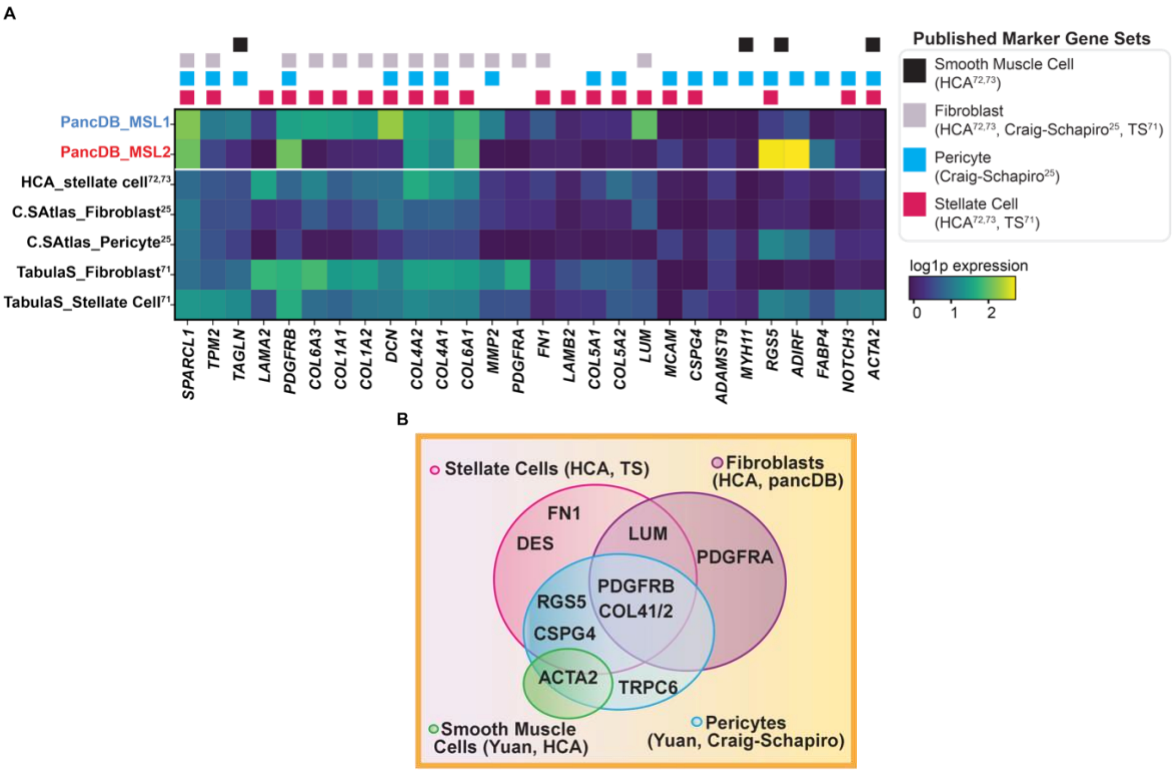

Figure 2-7: Cross-dataset comparison of pancreatic mesenchymal cell populations.

(**A**) Heatmap comparing expression of representative marker genes across mesenchymal cell populations identified in PancDB and previously published human pancreas single-cell RNA-seq datasets. Marker gene categories are indicated above the heatmap.
(**B**) Venn diagram illustrating shared and unique marker genes among fibroblast, pericyte, and smooth muscle cell populations compiled from published human pancreas datasets.

To more precisely classify the MSL1 and MSL2 populations, we compared their transcriptional profiles against established mesenchymal-type signatures from Tabula Sapiens [32], the Craig-Schapiro dataset [19], and the Human Cell Atlas [18, 33](**Fig. 2-7A**). This analysis revealed two reoccurring obstacles in defining pancreatic mesenchymal identity through transcriptomics alone. First, the marker genes historically used to distinguish fibroblasts, stellate cells, smooth muscle cells (SMCs), and pericytes

overlap substantially (**Fig. 2-7B**). Genes such as *PDGFRB*, *ADIRF*, and *CSPG4,* for example, are broadly expressed across multiple clusters rather than being restricted to pericytes as frequently assumed. Second, this marker promiscuity is reflected in the inconsistent labeling of transcriptionally similar populations across datasets. For instance, cells annotated as "pericytes" in one study share expression profiles with cells called “stellate cells” in another, and stellate cells and fibroblasts are often indistinguishable by gene expression alone. These inconsistencies reflect that pancreatic mesenchymal populations may share developmental origins and exhibit functional plasticity, producing transcriptional overlap that confounds annotation [34, 35]. Taken together, resolving pancreatic mesenchymal populations into defined cell types like pericytes or fibroblasts requires additional spatial information alongside transcriptional profiling.

2.2.2: Pre-MERSCOPE Workflow Development and Validation

To definitively resolve the identity of the basement membrane-producing cells in the islet as either pericytes or fibroblasts, we turned to spatial transcriptomics. Specifically, we aimed to define pericytes based on: (1) expression of a mural gene program (*PDGFRB*, *CSPG4*, *RGS5*) and (2) physical proximity to ECs. This strategy additionally enabled us to build a framework to understand how basement membrane gene programs are spatially organized within the endothelial and perivascular compartments of the pancreatic vasculature. We achieved this by performing MERFISH spatial genomics on adult human pancreas tissue sections from seven non-diabetic individuals using the Vizgen MERSCOPE platform [36]. Donor demographic and clinical information are summarized in **Table 2-2**.

A

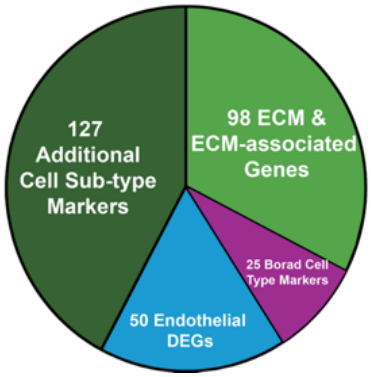

B

1. ECM Genes	2. Canonical Cell Type Marker Genes	3. Subpopulation Cell TypeGenes
Sufficinet Probe Binding Sites on RNA-sequence	Sufficinet Probe Binding Sites on RNA-sequence	Sufficinet Probe Binding Sites on RNA-sequence
FPKM Levels	FPKM Levels	FPKM Levels
Human Proteomics ECM	Human Cell Atlas	Human Cell Atlas
Human Protein Atlas	Cell x Gene	Cell x Gene
Mouse islet ECM RNA-seq		Craig-Shapiro EC Atlas

Figure 2-8: Design and gene selection strategy for the custom MERSCOPE panel.

(**A**) Composition of the 300-gene MERSCOPE panel, including extracellular matrix (ECM) and ECM-associated genes, endothelial differentially expressed genes, broad cell type markers, and additional cell subtype markers.
(**B**) Criteria used for gene selection within each category, including transcript abundance, probe design suitability, and validation using published human transcriptomic, proteomic, and cell atlas datasets.

We then prepared a targeted 300-gene panel designed to annotate all major pancreatic cell types and interrogate the expression of ECM genes. Gene selection was informed by manual curation of publicly available human pancreatic RNA-sequencing datasets [24], human pancreatic proteomic studies [17, 37, 38], the CellxGene platform [39], and the Human Protein Atlas (see Methods, **Fig 2-8A**) [40]. The final probe panel included canonical markers for endocrine, exocrine, immune, endothelial, and mesenchymal populations, as well as 98 ECM-associated genes enriched for basement membrane and interstitial ECM components that are expressed within the pancreas (**Fig. 2-8B**).

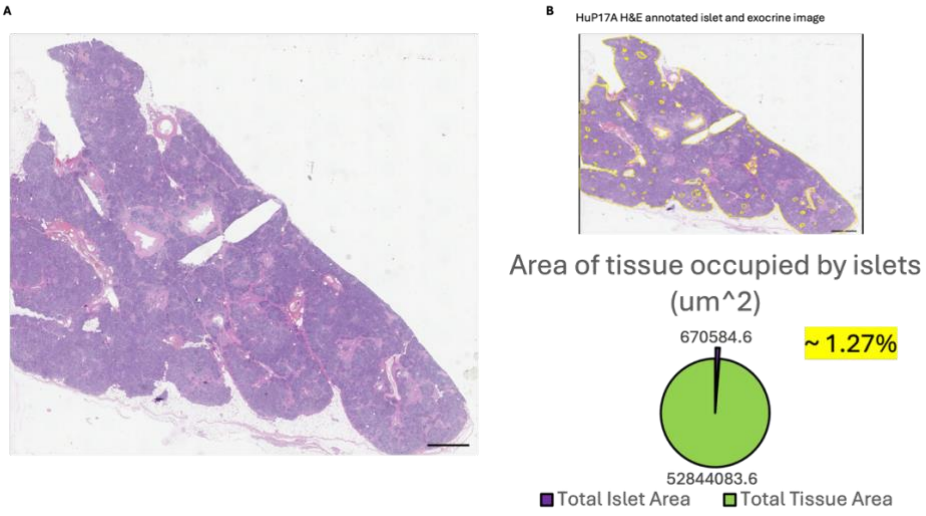

Figure 2-9: H&E Staining of human pancreatic FFPE tissue section.

(**A**) Representative image of H&E staining of FFPE tissue section to ensure enough endocrine-associated tissue is present in the donor pancreas tissue piece provided. Scale bar = 100 µm.
(**B**) Quantification of hand-curated islet regions using QuPath.

Because the MERSCOPE imaging area is constrained to roughly 1 cm^2 per tissue section, maximizing islet content within that limited field was essential to ensure adequate downstream analysis of the endocrine vascular niche. We therefore performed a series of pre-MERSCOPE screening steps on extra tissue sections to select donors and tissue with sufficient islet density and RNA quality prior to committing samples to the MERSCOPE platform. We first performed hematoxylin and eosin (H&E) staining on serial sections from each candidate donor block to visualize tissue morphology and assess overall tissue quality (**Fig. 2-9A**). Using these H&E images, we manually quantified the fraction of islet versus non-islet (exocrine) tissue area across candidate regions to identify areas with islet density sufficient to support robust downstream spatial analysis within the limited MERSCOPE imaging window (**Fig. 2-9B**). This step allowed us to prioritize both donors and specific tissue regions for

imaging, rather than selecting regions arbitrarily and risking an imaging area dominated by exocrine tissue.

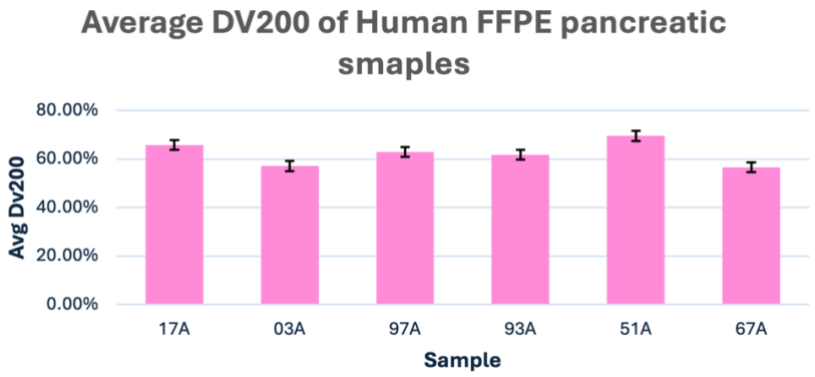

Figure 2-10: DV200 Quantification of FFPE human pancreas samples.

Average DV200 values measured for representative FFPE human pancreatic tissue blocks used for spatial transcriptomic profiling. DV200 represents the percentage of RNA fragments greater than 200 nucleotides in length and was used as a metric of RNA integrity during sample selection. Error bars represent the standard deviation of technical replicates.

In parallel, we assessed RNA integrity for each candidate donor using DV200 analysis, since RNA quality is a critical determinant of transcript detection efficiency in FFPE-based *in situ* hybridization. DV200 values, representing the percentage of RNA fragments longer than 200 nucleotides, were determined for each donor block using the Agilent 4200 TapeStation RNA ScreenTape assay (see Methods). Donors were required to meet a minimum DV200 threshold to be considered eligible for MERFISH processing (**Fig. 2-10**), and donors falling below this threshold were excluded prior to tissue sectioning for the MERSCOPE run.

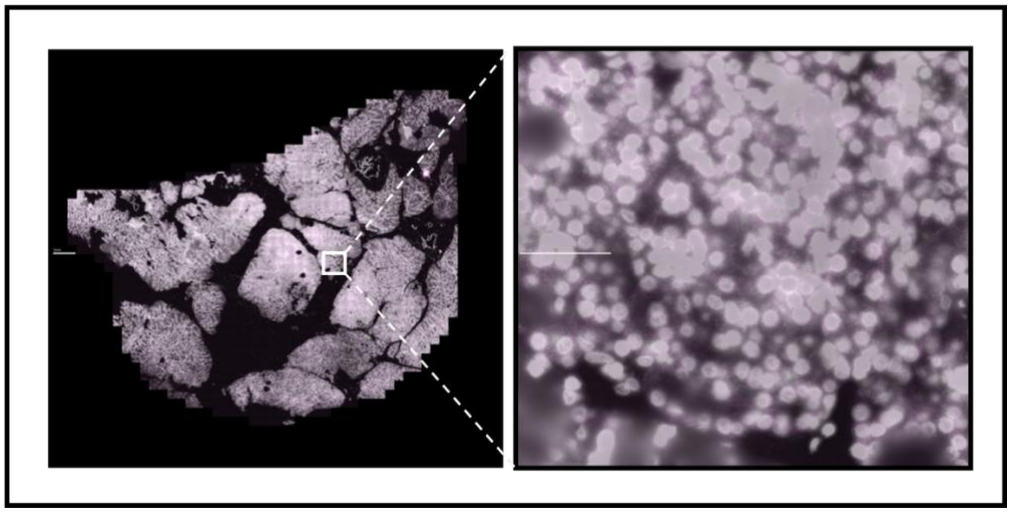

Figure 2-11: Sample verification MERSCOPE run imaging results.

Image result of MERSCOPE sample verification run done using two housekeeping genes to ensure RNA quality is sufficient for full gene panel run. Zoom insert shows RNA hybridization on top of cell nuclei. Scale bar = 1mm, 100 μm.

Finally, we did sample verification runs on the selected donor blocks and regions to confirm that the tissue ultimately mounted for MERSCOPE processing retained the islet content and morphology identified during initial screening (**Fig. 2-11**). This was done using the MERSCOPE sample verification kit, which uses two human-specific housekeeping genes to assess RNA integrity directly in the tissue of interest. Together, these pre-MERSCOPE screening steps ensured that the tissue regions selected for spatial transcriptomic profiling contained sufficient islet content and RNA quality to support robust downstream analysis of the pancreatic vascular niche.

2.2.3 Spatial Transcriptomics Identifies and Maps Pericyte, Endothelial, and Fibroblast Populations within the Human Pancreas

Having done all the necessary pre-workup for MERSCOPE, we now felt confident in applying the costly customized 300-gene panel to sequential adult human pancreas tissue sections. Using the custom gene panel allowed us to map millions of transcripts onto their native tissue location.

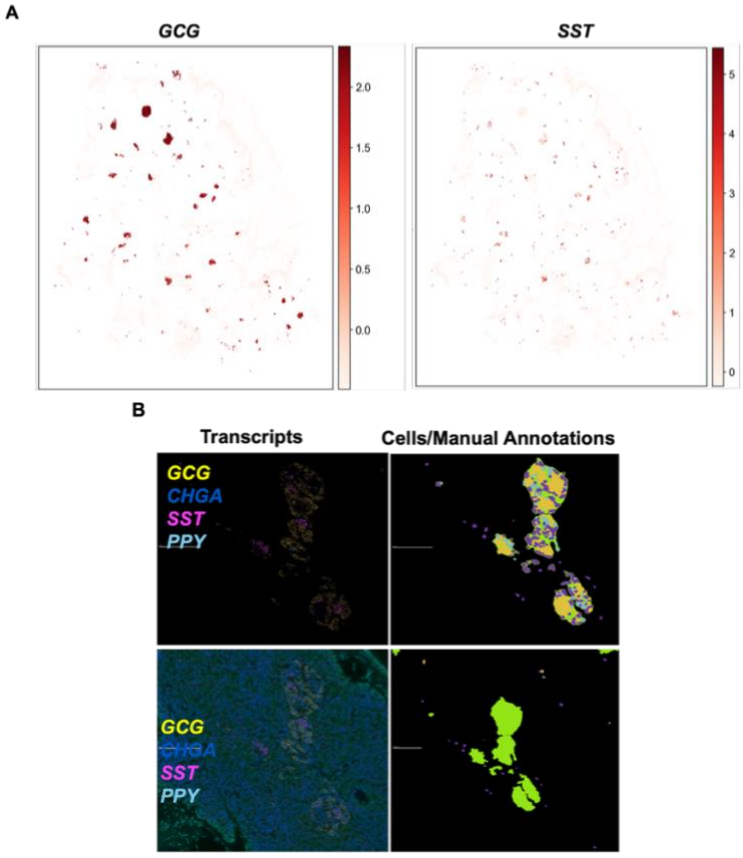

Figure 2-12: Snapshot of manual segmentation of pancreatic islets in MERSCOPE spatial transcriptomic data.

(**A**) Representative whole-section spatial maps showing the expression of the endocrine marker genes *GCG* and *NEUROD1*, which were used together with tissue morphology to identify endocrine regions within the pancreas.
(**B**) Spatial localization of canonical endocrine transcripts used to identify islets, including *GCG* (yellow), *CHGA* (blue), *SST* (magenta), and *PPY* (cyan). Cell segmentation with manually annotated cell identities overlaid. Corresponding tissue image (cell stain) with transcript localization. Final manually delineated islet boundaries (green), which were used for all subsequent compartment-specific spatial analyses. Scale bars = 250 µm.

As an initial step, whole-tissue spatial maps for every sample were reconstructed using computational analysis to visually inspect and ensure expected transcript localization patterns **(Fig. 2-12A**). This was the first step to be able to manually annotate individual islets based on tissue morphology together with the localized expression of canonical endocrine marker genes (**Fig. 2-12B**). This established a high-confidence spatial framework that enabled subsequent analyses of cell-type localization, vascular

organization, and extracellular matrix architecture within the endocrine and exocrine compartments.

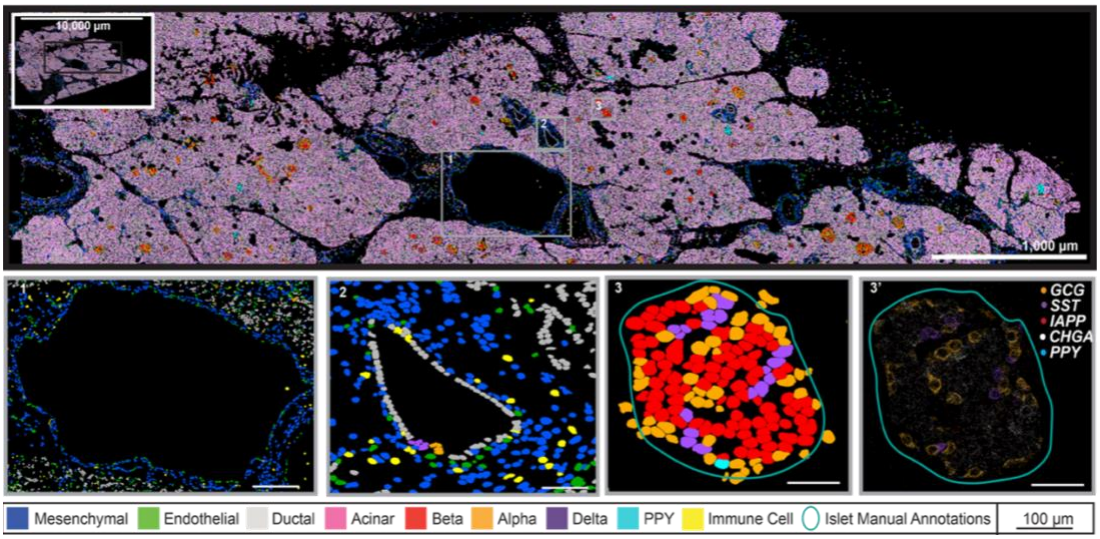

Figure 2-13: Overview of MERFISH spatial transcriptomic profiling and cell annotation of the adult human pancreas.

(**Top**) Whole-tissue MERFISH image showing spatially resolved cell type annotations across a representative human pancreatic tissue section. The inset indicates the region shown at higher magnification below. Colors denote annotated cell types. Scale bars = 10,000 µm (inset), 1,000 µm (main image).
(**Bottom**) Representative high-magnification views illustrating the spatial annotation workflow. (1) MERFISH transcript detection. (2) Cell segmentation and assignment of transcripts to individual cells. (3) Cell type annotation overlaid with manually defined islet boundaries. (3′) Expression of endocrine hormone markers (*GCG*, *SST*, *IAPP*, *CHGA*, and *PPY*) used to guide manual islet annotation.

Whole-section spatial maps confirmed that both islets and the surrounding exocrine tissue were well preserved and displayed the expected histological architecture (**Fig. 2-13**; representative sample shown) [24]. Mapping annotated cell identities back to their spatial coordinates revealed the full diversity of the pancreatic cellular landscape, including endocrine, exocrine, vascular, and immune populations (**Fig. 2-13,** top). To enable compartment-specific analysis, we manually segmented 2,386 islet boundaries based on cell morphology and the localized enrichment of canonical endocrine transcripts (*GCG*, *CHGA*, *SST*, *PPY*, *IAPP*) [24]. Higher

magnification of selected regions further validated the precise spatial organization of vascular and ductal networks, providing a high-confidence dataset for investigating the vascular niches present in the adult pancreas (**Fig. 2-13,** bottom).

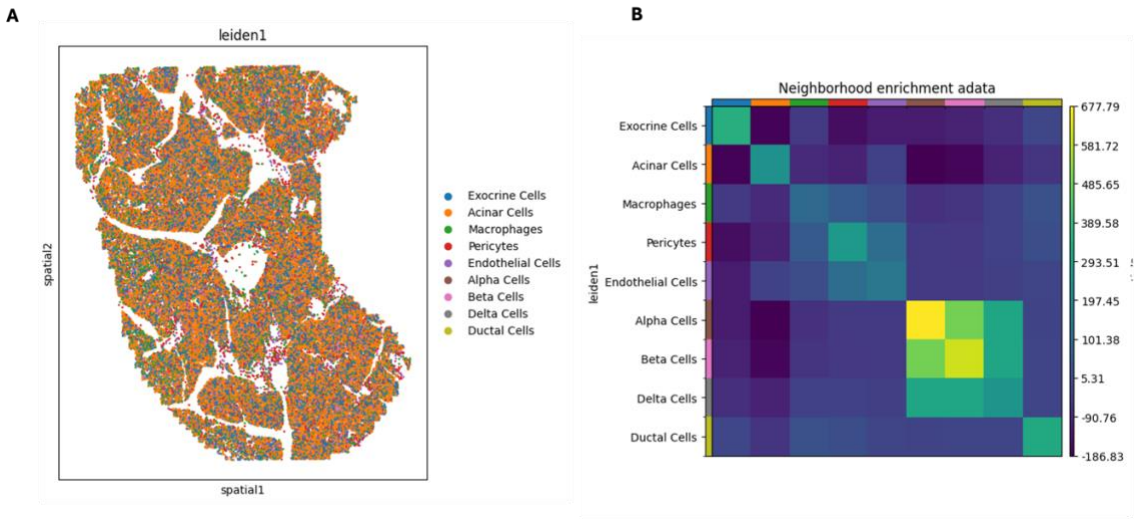

Figure 2-14: Spatial mapping and neighborhood enrichment validate pancreatic cell type annotations.

(A) Spatial projection of annotated cell clusters onto a representative whole-pancreas tissue section. Major pancreatic cell populations, including exocrine cells, acinar cells, endothelial cells, pericytes, macrophages, ductal cells, and endocrine cell types (α, β, and δ cells), localize to their expected anatomical compartments, confirming the accuracy of cell type annotation and providing a validated framework for downstream spatial analyses of the pancreatic vascular niche.
(B) Neighborhood enrichment analysis of annotated pancreatic cell populations demonstrating statistically enriched spatial associations between neighboring cell types.

Spatial mapping of the annotated cell identities back onto the reconstructed tissue sections demonstrated that the computational pipeline accurately resolved the major pancreatic cell populations, including endocrine, exocrine, vascular, immune, and ductal cell populations (**Fig. 2-14A**). Consistent with known pancreatic organization, endocrine cell types co-localized within islets, whereas exocrine acinar cells occupied the surrounding parenchyma and vascular-associated populations were distributed throughout the tissue. Neighborhood enrichment analysis further confirmed these expected spatial relationships, revealing strong enrichment of interactions among

endocrine cell populations within islets and distinct associations between endothelial cells and pericytes within the vascular compartment (**Fig. 2-14B**). Together, these findings validated the accuracy of the spatial cell annotations and established a high-confidence framework for subsequent analyses of vascular niche organization and extracellular matrix architecture in the adult human pancreas.

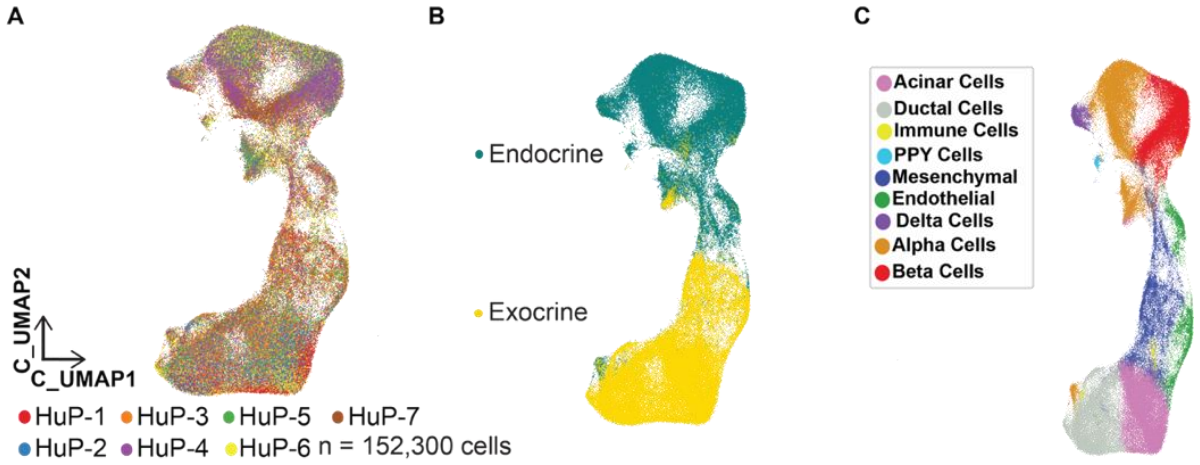

Figure 2-15: Integration and annotation of the MERFISH spatial transcriptomic dataset.

(**A**) UMAP of integrated MERFISH datasets colored by donor, demonstrating successful integration across all pancreatic tissue samples.
(**B**) UMAP colored by tissue compartment, showing separation of endocrine and exocrine cells.
(**C**) UMAP colored by annotated major pancreatic cell types, including acinar, ductal, immune, PPY, mesenchymal, endothelial, delta, alpha, and beta cells.

To generate a unified representation across donors, we next integrated all spatial datasets using CONCORD (**Fig. 2-15A**). From 3,270,093 segmented cells, we retained all islet cells and down-sampled exocrine cells to a similar magnitude, producing a final embedding of 152,300 cells across two major clusters: endocrine-annotated (teal, n = 75,985) and exocrine-annotated (yellow, n = 76,315) (**Figs. 2-15B, 2-15C**).

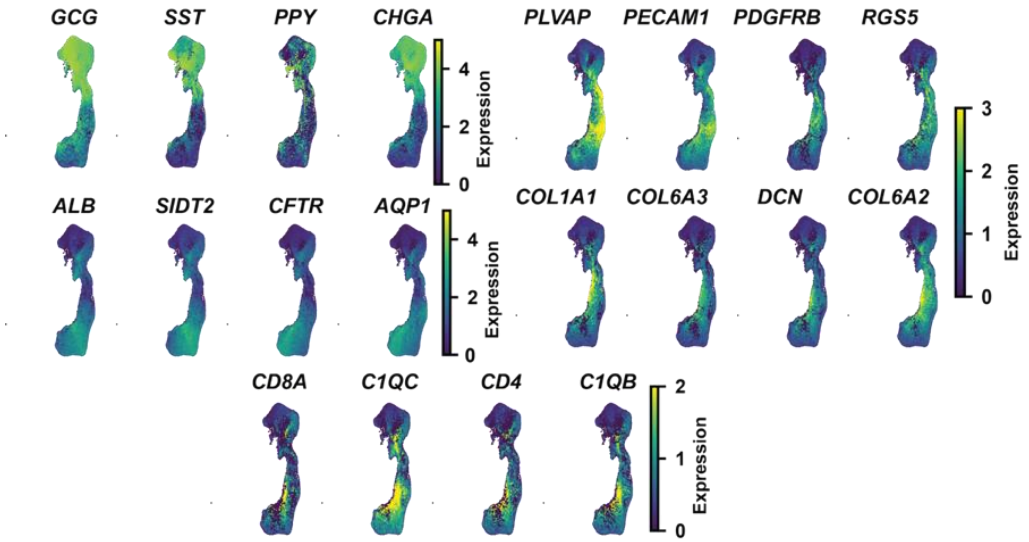

Figure 2-16: Expression of representative marker genes across the integrated MERFISH dataset.

Representative feature plots showing the spatial expression of canonical marker genes used to identify major pancreatic cell populations. Endocrine markers (*GCG*, *SST*, *PPY*, *CHGA*), endothelial markers (*PLVAP, PECAM1*), pericyte markers (*PDGFRB*, *RGS5*), ductal markers (*ALB*, *SIDT2*, *CFTR*, *AQP1*), mesenchymal markers (*COL1A1*, *COL6A3*, *DCN*, *COL6A2*), and immune cell markers (*CD8A*, *C1QC*, *CD4*, *C1QB*) are shown. Color scale indicates normalized gene expression.

Major pancreatic cell types formed resolved clusters, with expected gene expression patterns, including endocrine cells expressing *CHGA* and *GCG*, immune cells expressing *CD8A*, and ductal cells expressing *KRT19* (**Fig. 2-16**) [24].

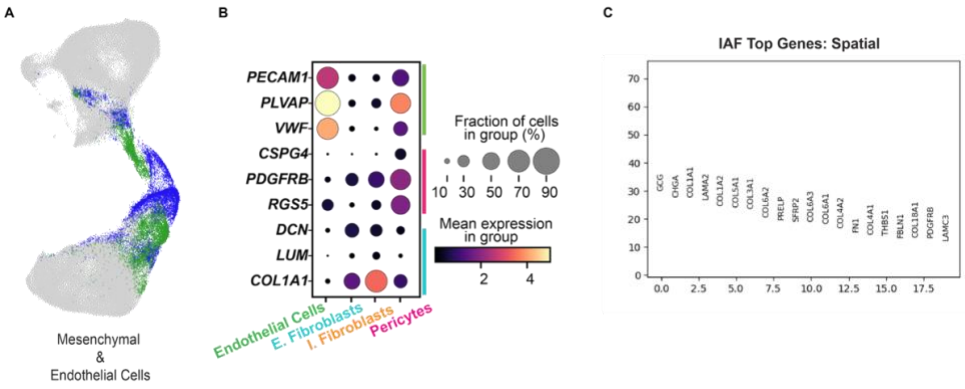

Figure 2-17: Identification and characterization of vascular-associated mesenchymal cell populations in the MERFISH dataset.

(A) UMAP highlighting endothelial and mesenchymal cell populations.
(B) Dot plot showing expression of representative marker genes used to annotate endothelial cells, exocrine fibroblasts (E. fibroblasts), islet-associated fibroblasts (I. fibroblasts), and pericytes.
(C) Bar plot showing the top marker genes enriched in islet-associated fibroblasts (IAFs) identified from the spatial transcriptomic dataset.

To further refine vascular-associated populations, we restricted downstream analysis to the mesenchymal and endothelial populations (**Fig. 2-17A**). Unsupervised clustering identified multiple transcriptionally distinct mesenchymal and vascular populations, which were annotated using differential gene expression (DGE) analysis together with analysis of canonical lineage marker gene expression (**Fig. 2-17B**). ECs were identified by expression of *PECAM1*, *VWF*, and *PLVAP*, whereas pericytes were defined by enrichment of *RGS5*, *PDGFRB*, and *CSPG4* together with additional vascular-associated transcriptional features[18, 19, 24]. Fibroblast populations were characterized by expression of *DCN* and *LUM[19, 32]*. Unsupervised clustering revealed two transcriptionally distinct fibroblast populations. One population comprised most fibroblasts and was localized predominately throughout the exocrine pancreas. In contrast, a second fibroblast cluster retained canonical fibroblast markers while exhibiting enrichment of ECM genes, including *COL1A1*, *LAMA2*, *COL1A2*, *COL5A1*, and *COL3A1* (**Fig. 2-17C**). This population also showed detectable endocrine transcripts (*GCG*, *CHGA*), likely reflecting transcript diffusion or contamination from neighboring endocrine cells due to its close spatial association with islets. Together, these features suggested the presence of a specialized fibroblast population associated with the islet microenvironment, which we designated islet-associated fibroblasts, whereas the broader fibroblast population was designated exocrine-associated fibroblasts (**Fig. 2-17B**).

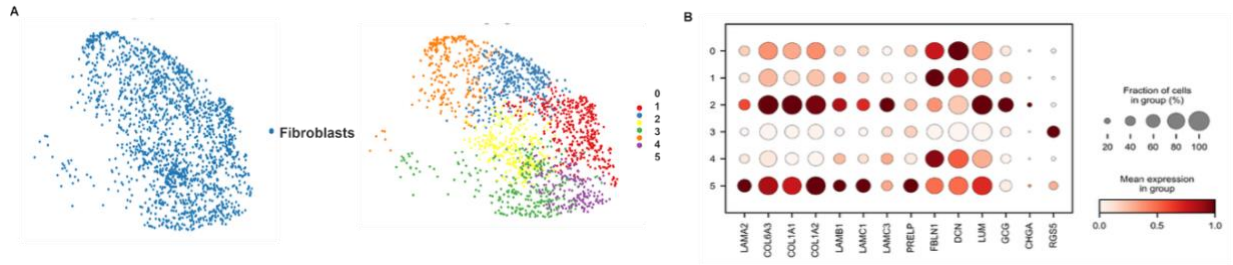

Figure 2-18: Subclustering of fibroblast populations in the PancDB dataset.

(**A**) UMAP visualization of fibroblast cells following unsupervised subclustering, showing six transcriptionally distinct fibroblast subclusters.
(**B**) Dot plot showing expression of representative extracellular matrix, fibroblast, endothelial, endocrine, and pericyte-associated genes across fibroblast subclusters. Dot size represents the fraction of cells expressing each gene, and color indicates mean expression within each subcluster.

To validate this population, we initially compared fibroblast populations against the PancDB human pancreas scRNA-seq atlas, which lacks predefined spatial annotations and is free from contamination artifacts unique to spatial transcriptomic data such as transcript diffusion and segmentation errors (**Fig. 2-18A**). Sub-clustering of the MSL1 (fibroblast-like) population described in Figure 1 identified a fibroblast subset characterized by enrichment of *COL1A1*, *COL1A2*, *COL3A1*, *SPARC*, *COL4A1*, *COL5A2*, *COL5A*1, and *LGALS1* (**Fig. 2-18B**). Notably, this ECM-rich signature distinguished the population from other fibroblast subsets in PancDB and closely matched the transcriptional profile of the spatially identified islet-associated fibroblasts.

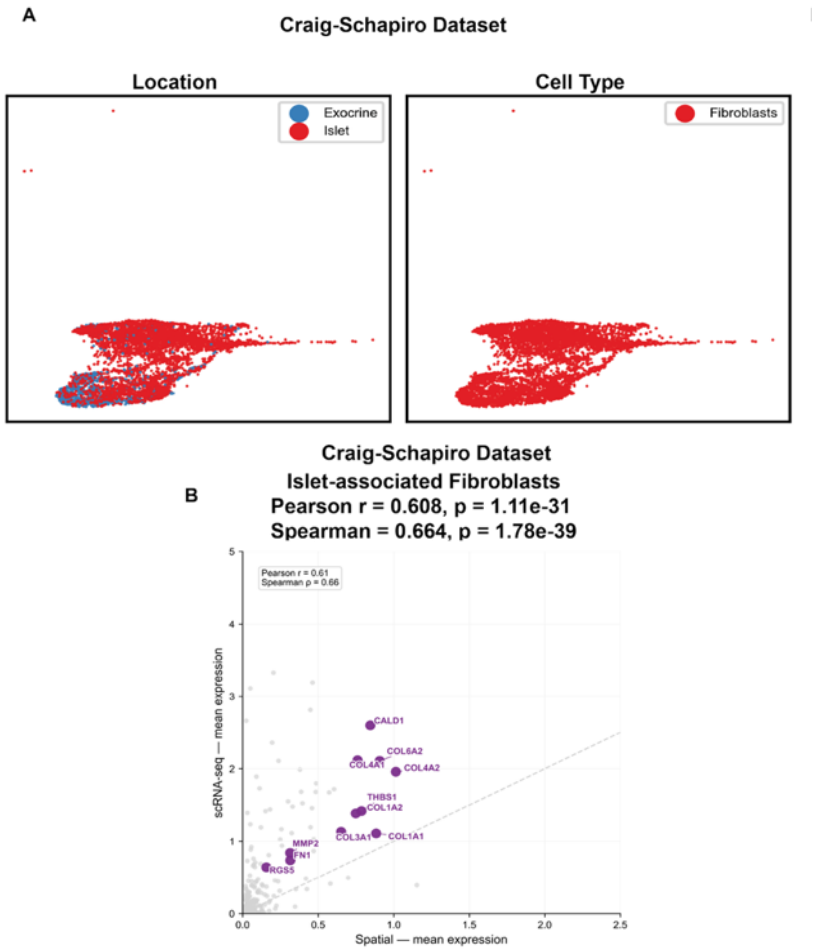

Figure 2-19: Validation of islet-associated fibroblast identity using the Craig-Schapiro dataset.

(**A**) UMAP visualization of fibroblasts from the Craig-Schapiro human pancreas dataset, colored by tissue location and cell type annotation. Fibroblasts are present in both exocrine and islet-associated regions. (**B**) Correlation analysis comparing mean gene expression between spatially identified islet-associated fibroblasts and Craig-Schapiro islet-associated fibroblasts. Purple points indicate representative shared marker and ECM-associated genes. Pearson and Spearman correlation coefficients are shown.

To further validate the identity of the islet-associated fibroblast population, we compared average gene expression profiles with the anatomically annotated Craig-Schapiro reference dataset using Pearson and Spearman correlation analyses (**Fig. 2-19A**). The spatially defined islet-associated fibroblasts exhibited a strong positive correlation with the reference islet fibroblast population (Pearson r = 0.608, $p < 0.001$; Spearman ρ = 0.664, $p < 0.001$), demonstrating substantial agreement between the two datasets (**Fig. 2-19B**). Canonical extracellular matrix genes, including *COL1A1*,

COL1A2, *COL3A1*, *COL4A1*, *COL4A2*, *COL6A2*, *THBS1*, and *CALD1*, showed consistent expression in both datasets and contributed strongly to the observed correlation. Together, these findings confirmed that the spatially identified fibroblast population corresponds closely to previously described islet-associated fibroblasts and supported its use for downstream analyses of extracellular matrix organization within the pancreatic vascular niche.

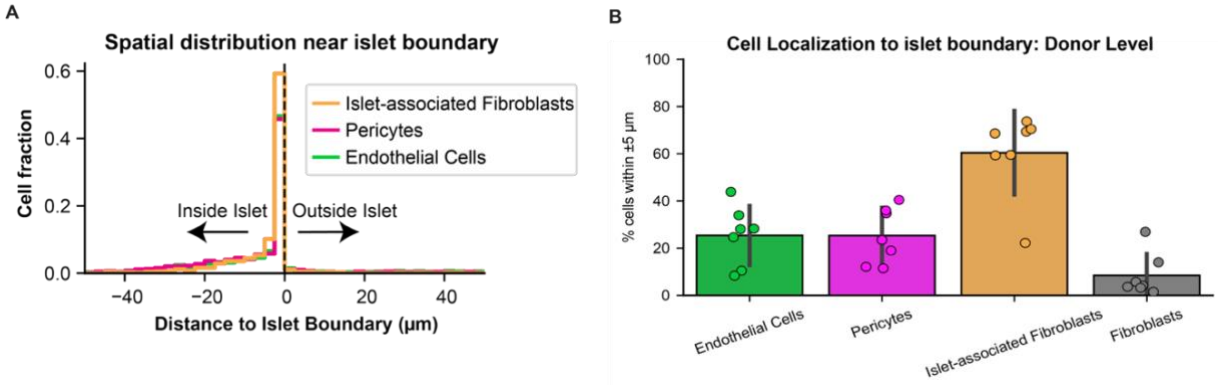

Figure 2-20: Islet-associated fibroblasts are enriched at the islet boundary.

(A) Spatial distribution of endothelial cells, pericytes, and islet-associated fibroblasts relative to the manually annotated islet boundary. Negative distances indicate cells located inside the islet, and positive distances indicate cells located outside the islet.
(B) Donor-level quantification of the percentage of each vascular-associated cell population located within ± 5 µm of the islet boundary. Bars represent mean values across donors, with individual donor values shown as points.

To validate these classifications spatially, we next quantified cell localization relative to the islet boundary at both the single-cell and donor levels. Spatial distribution analysis demonstrated that islet-associated fibroblasts formed a distinct population concentrated at the endocrine–exocrine interface, with a pronounced peak centered on the islet boundary (**Fig. 2-20A**). In contrast, endothelial cells and pericytes exhibited broader distributions extending both within the islet and into the surrounding exocrine tissue, consistent with their incorporation into the continuous pancreatic vascular network. Donor-level quantification confirmed these observations, revealing that

approximately 67% of islet-associated fibroblasts were located within ±5 μm of the islet boundary, compared with only ~25% of endothelial cells and pericytes and <10% of the broader fibroblast population (**Fig. 2-20B**). This boundary-restricted localization was consistently observed across donors despite inter-donor variability, supporting the classification of islet-associated fibroblasts as a spatially distinct stromal population enriched at the endocrine–exocrine interface.

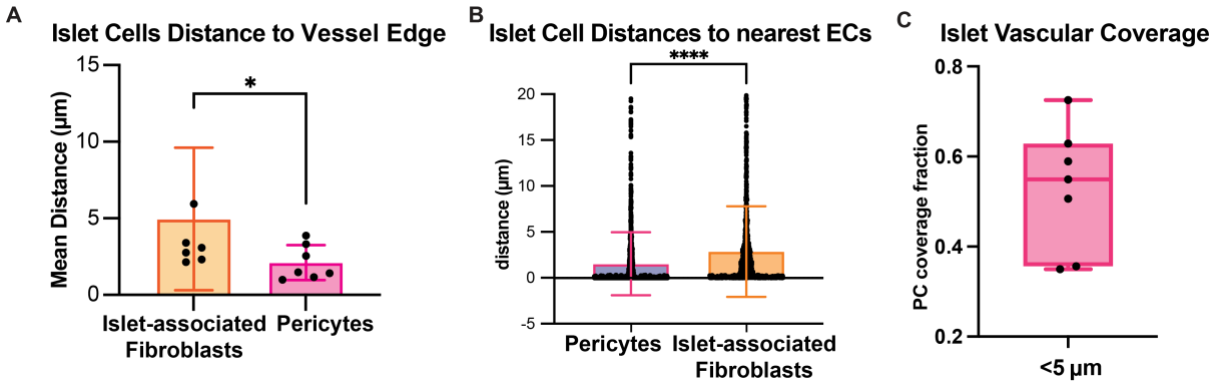

Figure 2-21: Spatial association of pericytes and islet-associated fibroblasts with the islet vasculature.

(A) Donor-level quantification of mean distance from islet associated fibroblasts and pericytes to the nearest vessel edge within islets.
(B) Single-cell distance distribution showing distances from pericytes and islet-associated fibroblasts to the nearest endothelial cells. Pericytes are highly enriched near endothelial cells, consistent with their perivascular localization.
(C) Quantification of islet vascular coverage, shown as the fraction of pericytes located within 5 μm of endothelial cells across donors. Bars or box plots summarize donor-level values, with individual donor values shown as points. Statistical significance is indicated above comparisons (*, $P < 0.05$; ****, $P < 0.0001$).

We further validated these annotations by quantifying the spatial relationship of vascular-associated cell populations to the islet microvasculature. Distances were calculated from the boundary of each cell to the nearest EC mask edge, which served as a proxy for the vascular lumen. Both pericytes and islet-associated fibroblasts were in proximity to the vasculature, consistent with their classification as vascular-associated cell populations (**Fig. 2-21A**). However, pericytes resided significantly closer to

endothelial cells than islet-associated fibroblasts (mean distance, p = 0.0156), reflecting their established role as mural cells directly opposed to the endothelial basement membrane. Analysis at single-cell resolution further confirmed this relationship, with pericytes exhibiting significantly shorter distances to their nearest endothelial cell compared with islet-associated fibroblasts (p < 0.0001; **Fig. 2-21B**). Consistent with these findings, donor-level quantification demonstrated that the majority of pericytes (approximately 55–60%) were positioned within 5 μm of the vasculature (**Fig. 2-21C**), confirming their intimate association with the pancreatic capillary network. Together, these spatial analyses further validated the identity of both vascular-associated populations while distinguishing pericytes as cells immediately associated with endothelial structures and islet-associated fibroblasts as a neighboring stromal population occupying the perivascular niche.

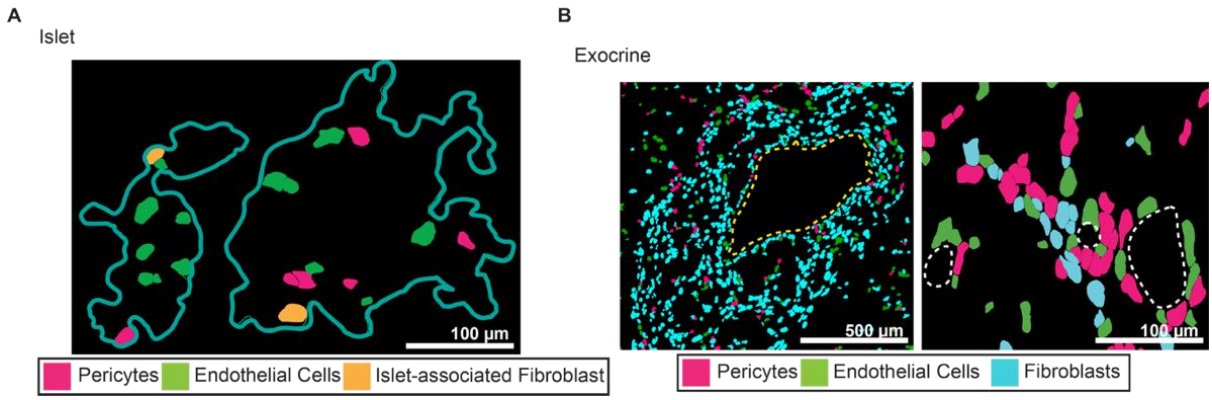

Figure 2-22: *In situ* validation of vascular-associated populations by representative MERSCOPE fields of view.

(**A**) Within islets (teal outline), pericytes (magenta) are tightly associated with ECs (green) along vascular structures, while peri-islet fibroblasts (peach) localize to the islet periphery.
(**B**) In exocrine regions, fibroblast (cyan) populations are more broadly distributed between vascular structures (white dotted outline) composed of ECs and pericytes and enriched around ductal regions (yellow dotted outline). Scale bar = 100 μm.

In situ, we confirmed that within islets, the cells annotated as pericytes were tightly associated with ECs along vascular structures, whereas islet-associated

fibroblasts were enriched at the islet periphery (**Fig. 2-22A**). In exocrine regions, exocrine-associated fibroblasts were predominantly organized within the interstitial stroma, sequestered between periductal bands (yellow dotted lines) and vessel-surrounding stroma (**Fig. 2-22B**). Notably, exocrine-associated fibroblasts remain spatially excluded from the immediate perivascular niche, which is predominately occupied by pericytes in direct contact with the endothelium (white dotted outlines). Together, these analyses confirm that the mesenchymal population annotated as pericytes by scRNA-seq corresponds to bona fide vascular-associated cells *in situ* and occupies the immediate perivascular niche within islets. Importantly, accurate annotation of these populations was only possible through the integration of manual islet annotation and spatial single-cell transcriptomics.

2.2.4: Distinct features of ECM Gene Expression Programs in the Endocrine versus Exocrine Vascular Compartments.

Having validated the identity, spatial localization, and vascular associations of endothelial and mural cell populations within the human pancreas, we next sought to characterize the ECM of the pancreatic vascular niche. We reasoned that the distinct anatomical positions occupied by endothelial cells, pericytes, and islet-associated fibroblasts would be reflected in specialized basement membrane and ECM transcriptional programs.

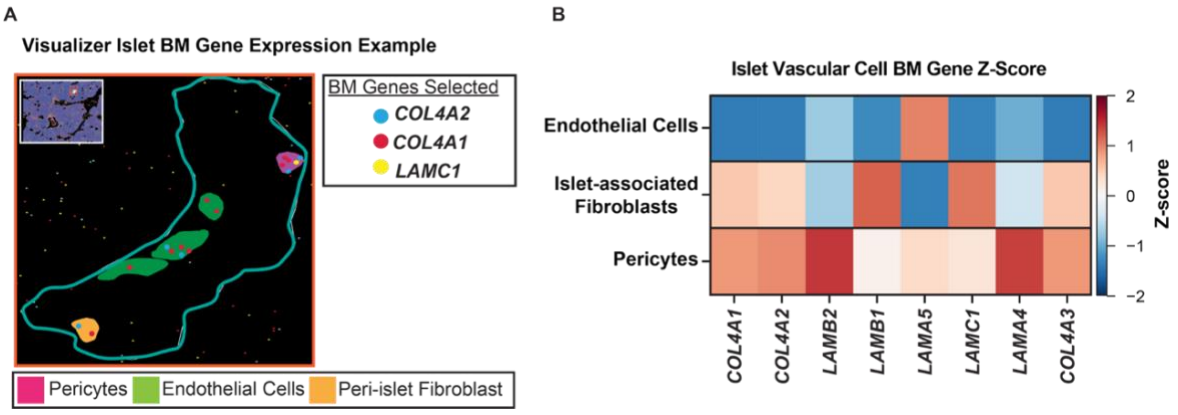

Figure 2-23: Spatial organization and cell-type enrichment of islet basement membrane genes.

(**A**) Representative MERSCOPE spatial transcriptomic image showing localization of BM genes surrounding islet vascular structures. Expression of *COL4A1*, *COL4A2*, and *LAMC1* is enriched in vascular-associated stromal cells adjacent to endocrine tissue.
(**B**) Heatmap showing z-score normalized expression of curated BM genes across ECs, islet-associated fibroblasts, and pericytes within the islet vascular niche. Positive z-scores indicate relative enrichment within a given population, whereas negative values indicate comparatively lower expression relative to the other populations.

Spatial mapping of *COL4A1*, *COL4A2*, and *LAMC1* transcripts revealed localization along islet vascular structures, with signal detected proximal to vascular-associated cells rather than uniformly distributed across the tissue (**Fig. 2-23A**). To quantify these patterns, we examined the expression of a curated set of islet vascular basement membrane genes (*COL4A1*, *COL4A2*, *COL4A3*, *LAMB2*, *LAMB1*, *LAMA5*, *LAMC1*, *LAMA4*) that have been reported to be present at the protein level either in the intra-islet vascular basement membrane, peri-islet basement membrane, or both (**Fig. 2-23B**) [7, 41]. Pericytes displayed the strongest relative enrichment of these core basement membrane components, particularly collagen IV (*COL4A1*, *COL4A2*), together with the laminin subunits *LAMA4* and *LAMB2*. In contrast, ECs exhibited comparatively weaker basement membrane -associated transcriptional signatures within the islet vascular niche, with selective enrichment of *LAMA5*. Islet-associated

fibroblasts demonstrated enrichment of a distinct set of laminin subunits, including *LAMB1* and *LAMC1*.

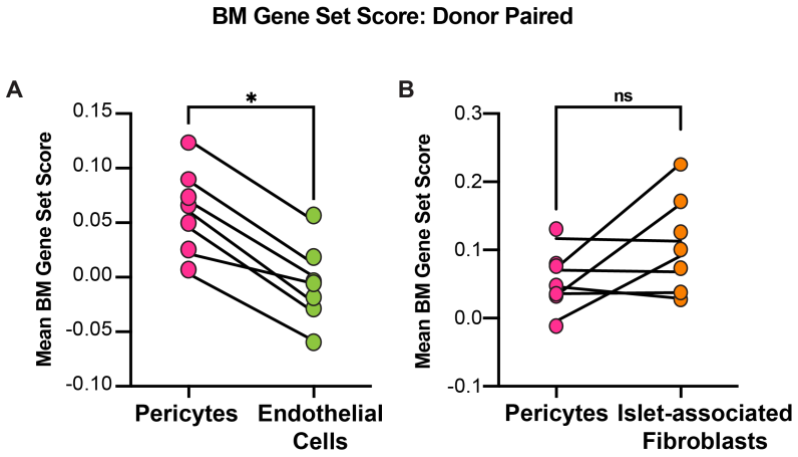

Figure 2-24: Comparison of basement membrane gene-set scores across donor-paired cell populations.

Statistical significance was assessed via the Mann-Whitney U test.
(**A**) Pericytes have significantly higher BM scores compared to ECs (median 0.015 vs -0.048; p = 0.0156).
(**B**) No significant difference exists between pericyte and islet-associated fibroblasts scores (median 0.056 vs 0.039; p = 0.468).

To determine whether these basement membrane transcriptional differences were consistently maintained across donors rather than driven by cell abundance or sampling effects, we performed donor-paired comparisons. basement membrane gene set scores were calculated separately within each donor, allowing direct comparison of matched cell types within each tissue section. Across all seven donors, ECs consistently showed significant lower basement membrane scores than pericytes (n = 7 donors; median score = 0.015 vs -0.048; p = 0.01; **Fig. 2-24A**). In contrast, islet-associated fibroblasts had comparable basement membrane scores to pericytes (p = 0.58; **Fig. 2-24B).**

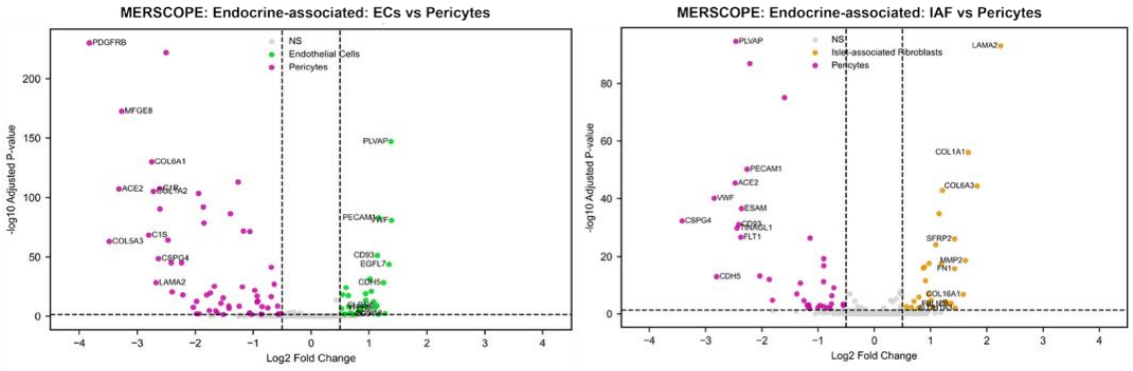

Figure 2-25: Endocrine vascular cell differential expression.

(**A**) Differential expression analysis results in volcano plot comparing endocrine-associated endothelial cells and pericytes.
(**B**) Differential expression analysis results in volcano plot comparing endocrine-associated islet associated fibroblasts (IAF) and pericytes.

Differential expression (DE) analysis was next performed to further characterize the transcriptional programs distinguishing ECs, pericytes, and islet-associated fibroblasts within the endocrine compartment (**Fig. 2-25**). Comparison of ECs and pericytes revealed distinct but complementary vascular expression programs. ECs were enriched for canonical endothelial genes, including *PLVAP*, *PECAM1*, *CD93*, *EGFL7*, and *CDH5*, consistent with their specialized role in forming the vascular lining (**Fig. 2-25A**). In contrast, pericytes preferentially expressed mural cell markers such as *PDGFRB*, *CSPG4*, *RGS5*, *MFGE8*, and *COL6A1*, confirming their identity as vascular support cells closely associated with the endothelial basement membrane. Comparison of islet-associated fibroblasts and pericytes further demonstrated that these populations occupy transcriptionally distinct stromal states (**Fig. 2-25B**). Islet-associated fibroblasts exhibited enrichment of extracellular matrix genes, including *COL1A1*, *COL6A1*, *COL6A3*, *LAMA2*, *SFRP2*, and *FN1*, consistent with a matrix-producing phenotype. Conversely, pericytes retained higher expression of vascular-associated genes,

including *PLVAP*, *PECAM1*, *ACE2*, *FLT1*, *VWF*, and *CSPG4*, reflecting their close association with the pancreatic microvasculature.

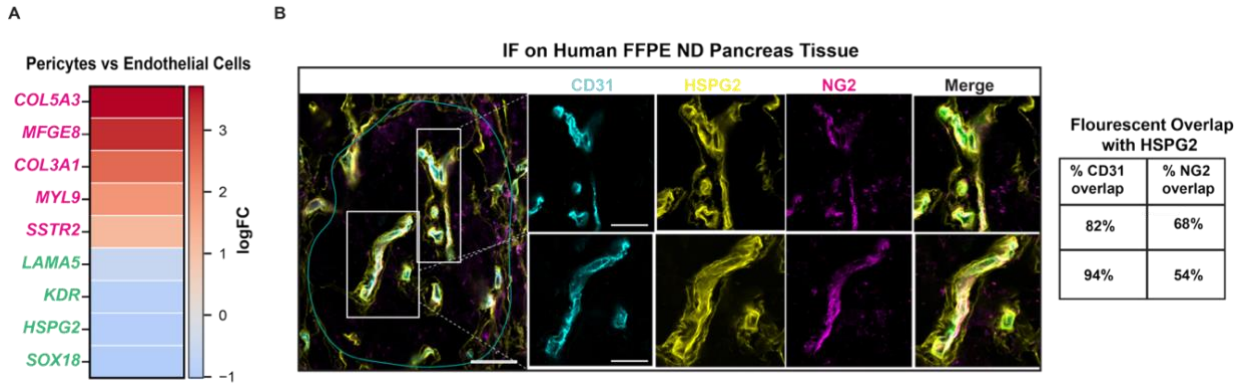

Figure 2-26: Immunofluorescence image showing the vasculature within a representative ND human islet.

(**A**) Differential gene expression heatmap comparing pericytes and endothelial cells within the endocrine vascular compartment. Genes enriched in pericytes are shown in magenta, and genes enriched in endothelial cells are shown in green.
(**B**) IF of ND human pancreatic tissue stained for CD31 (endothelial; cyan), HSPG2 (BM; yellow), and NG2 (pericyte; magenta). Quantitative channel colocalization analysis performed using ImageJ Coloc2 demonstrating stronger spatial association between endothelial and BM-associated HSPG2 signals within the intra-islet vasculature. 63x; scale bars = 40 μm for large image and 5 μm for higher-magnification images.

To further prioritize candidates for experimental validation, we summarized the most differentially expressed genes distinguishing endothelial cells and pericytes using a heatmap (**Fig. 2-26A**). This analysis highlighted distinct transcriptional programs between the two vascular-associated populations, with pericytes showing increased expression of mural cell markers including *COL3A1*, *MFGE8*, *MYL9*, and *SSTR2*, whereas ECs were enriched for canonical endothelial and basement membrane-associated genes including *KDR*, *SOX18*, *HSPG2*, and *LAMA5*. The prominent enrichment of HSPG2 and LAMA5, both key structural components of the vascular basement membrane, identified these genes as strong candidates for orthogonal validation. Because spatial transcriptomics measures mRNA abundance rather than

protein localization, we next sought to determine whether these transcriptional differences were reflected at the protein level within intact islets. We therefore performed immunofluorescence (IF) staining to validate the cellular localization of HSPG2 relative to endothelial cells and pericytes *in situ*. IF staining confirmed strong spatial association of HSPG2 with CD31+ endothelial structures relative to adjacent pericytes (NG2+) within islets (**Fig. 2-26B**).

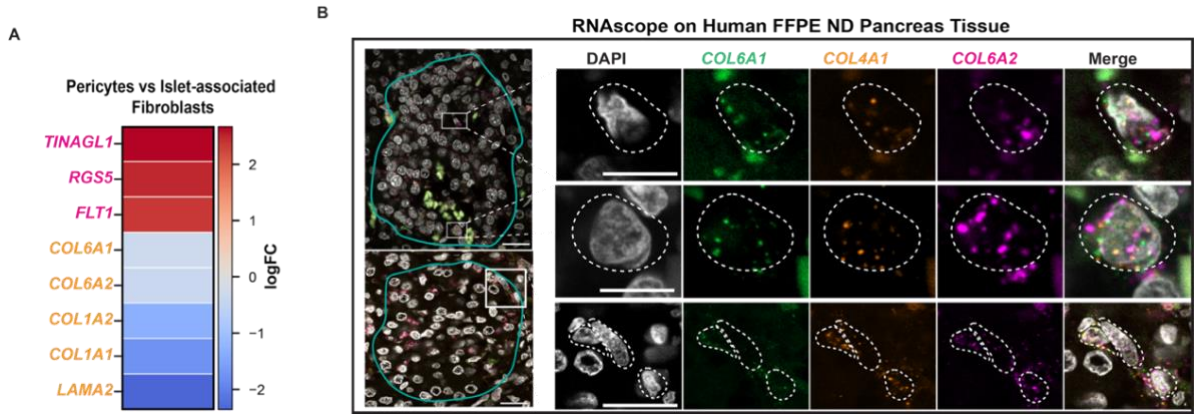

Figure 2-27: Immunofluorescence RNAscope image showing the vasculature within a representative ND human islet.

(**A**) Differential gene expression heatmap comparing pericytes and islet-associated fibroblasts within the endocrine vascular compartment. Genes enriched in pericytes are shown in magenta, and genes enriched in islet-associated fibroblasts are shown in orange.
(**B**) Multiplexed RNA *in situ* hybridization image of ND human pancreatic tissue, showing expression of *COL6A1* (green), *COL4A1* (orange), and *COL6A2* (magenta) transcripts; nuclei are stained with DAPI in white. Representative positive cells (outlined in dashed while lines) were selected for inspection at higher magnification to verify presence of ECM-expressing cells. 63x; scale bars: 40 μm (top), 20 μm (bottom) in large image and 5 μm in higher-magnification insets.

In contrast, islet-associated fibroblasts showed enrichment of a broader ECM program defined by interstitial and fibrillar collagens including *COL6A1*, *COL1A1*, and *COL1A2* (**Fig. 2-27A**), reflecting a matrix-producing phenotype distinct from the vascular basement membrane. To validate the spatial distribution of these ECM-producing cells within intact pancreatic tissue, we next performed multiplexed RNA *in situ* hybridization targeting representative basement membrane and interstitial matrix

genes. Multiplexed RNA *in situ* hybridization analysis further identified *COL4A1+*, *COL6A1+*, *COL6A2+* cells along the islet boundary and occasionally within the intra-islet interior (**Fig. 2-27B**); however, we could not exclude the possibility that these interior cells were artifacts of 2D segmentation or sectioning.

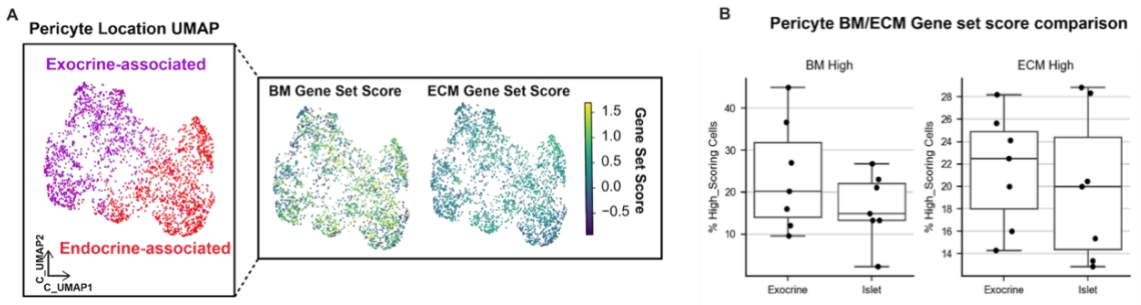

Figure 2-28: Pericyte BM and ECM programs are maintained across endocrine and exocrine compartments.

(**A**) UMAP of pericytes colored by endocrine- or exocrine-associated location, with BM and ECM gene set scores projected onto the same embedding.
(**B**) Donor-level comparison of the percentage of BM-high and ECM-high pericytes in exocrine and islet compartments. Box plots show donor-level distributions with individual donors shown as points.

Lastly, to investigate whether pericyte transcriptional programs were conserved between the endocrine and exocrine compartments, we subsetted pericytes by location (**Fig. 2-28A**, left). Qualitative projection of gene set scores onto the subsetted UMAP suggested that basement membrane and ECM transcriptional activity was broadly consistent across both compartments, with gene set scores distributed relatively uniformly across the UMAP (**Fig. 2-28A**, right). To better resolve potential differences, we performed donor-paired analysis. This revealed no significant difference in basement membrane or ECM gene set scores in islet-associated pericytes relative to their exocrine counterparts (**Fig. 2-28B**).

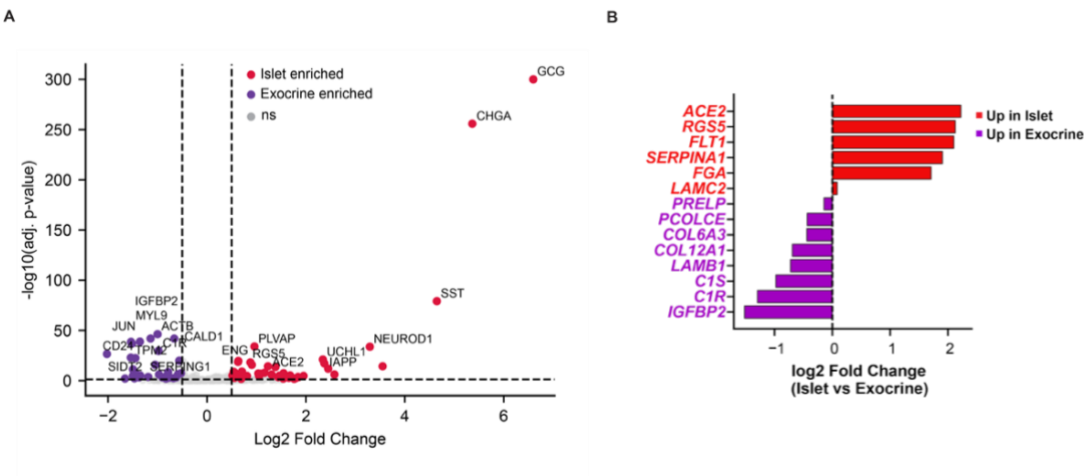

Figure 2-29: Endocrine and exocrine pericytes display compartment-specific transcriptional programs.

(**A**) Volcano plot showing differentially expressed genes between endocrine-associated and exocrine-associated pericytes in the MERFISH dataset. Red points indicate genes enriched in endocrine-associated pericytes, purple points indicate genes enriched in exocrine-associated pericytes, and gray points indicate non-significant genes.
(**B**) Bar plot showing selected differentially expressed genes ranked by log2 fold change between endocrine- and exocrine-associated pericytes.

DE analysis did, however, identify significant niche-specific tuning of broader ECM-related gene programs (**Fig. 2-29A**). Exocrine-associated pericytes were enriched for genes linked to interstitial matrix remodeling and inflammatory signaling, including *IGFBP2*, *C1R*, *C1S*, *COL12A1, COL6A1* [12, 42]. In contrast, islet pericytes exhibited enrichment of *ACE2*, *RGS5*, *FLT1*, *SERPINA1*, *FGA* and *LAMC2* (**Fig. 2-29B**). These findings indicate that while pancreatic pericytes maintain a conserved core cell identity and vascular maintenance program, they also undergo substantial niche-dependent specialization.

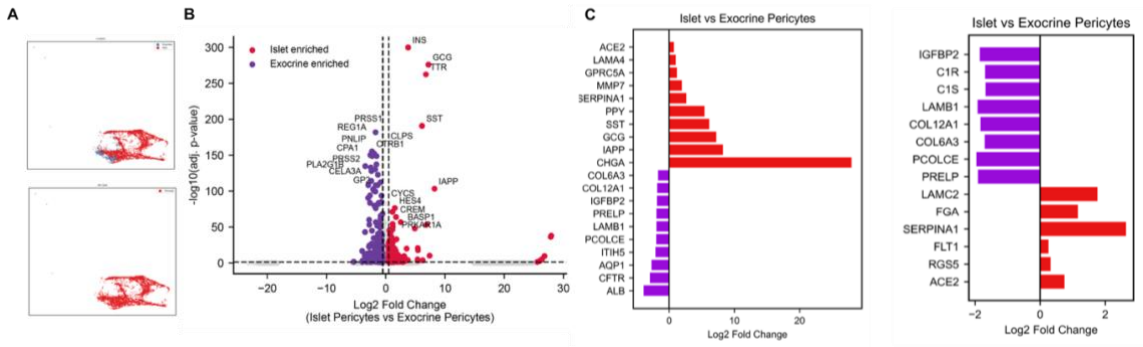

Figure 2-30: Differential gene expression between islet and exocrine pericytes in the Craig-Schapiro dataset.

(**A**) UMAP plots showing pericytes classified by compartment, with islet-enriched pericytes shown in red and exocrine-enriched pericytes shown in blue.
(**B**) Volcano plot comparing gene expression between islet and exocrine pericytes. Red points indicate genes enriched in islet pericytes, and purple points indicate genes enriched in exocrine pericytes.
(**C**) Bar plots showing selected genes differentially expressed between islet and exocrine pericytes. Positive log2 fold-change values indicate enrichment in islet pericytes, while negative values indicate enrichment in exocrine pericytes.

Importantly, these niche-associated transcriptional programs were independently supported using the anatomically annotated Craig-Schapiro single-cell reference dataset, providing orthogonal validation of the spatial transcriptomic findings (**Fig. 2-30**). Cells annotated as islet- and exocrine-associated pericytes occupied distinct transcriptional states that segregated according to their anatomical compartment (**Fig. 2-30A**). Differential expression analysis identified endocrine-enriched genes, including canonical islet hormones (*CHGA*, *GCG*, *SST*, *IAPP*, and *PPY*), together with vascular-associated genes such as *ACE2* and *LAMA4*, whereas exocrine-associated pericytes preferentially expressed extracellular matrix and complement-related genes including *IGFBP2*, *C1R*, *C1S*, *COL6A3*, *COL12A1*, and *LAMC2* (**Fig. 2-30B**). Direct comparison of the most differentially expressed genes further demonstrated enrichment of vascular-associated markers, including *FLT1*, *RGS5*, *FGA*, and *SERPINA1*, in islet pericytes, while exocrine pericytes exhibited increased expression of matrix-remodeling and structural ECM genes (**Fig. 2-30C**). Together, these independent analyses demonstrate

that pericytes adopt anatomically distinct transcriptional programs that are conserved across complementary single-cell and spatial transcriptomic datasets, supporting the existence of specialized vascular niches within the adult human pancreas.

2.2.5: Pericyte and Fibroblast Transcriptional Remodeling in the Type 2 Diabetes PancDB Dataset

Having established the cellular organization of the healthy pancreatic vascular niche, we next leveraged the CONCORD-reintegrated PancDB atlas to include type 2 diabetic donors. This integrated reference enabled systematic comparison of endothelial cells, pericytes, and fibroblast populations across health and disease, allowing us to identify diabetes-associated changes in transcriptional state and ECM remodeling. Using the same quality control and filtering parameters outlined in the initial PancDB non-diabetic dataset, low-quality cells and donors were identified for removal to have a clean dataset for downstream analysis.

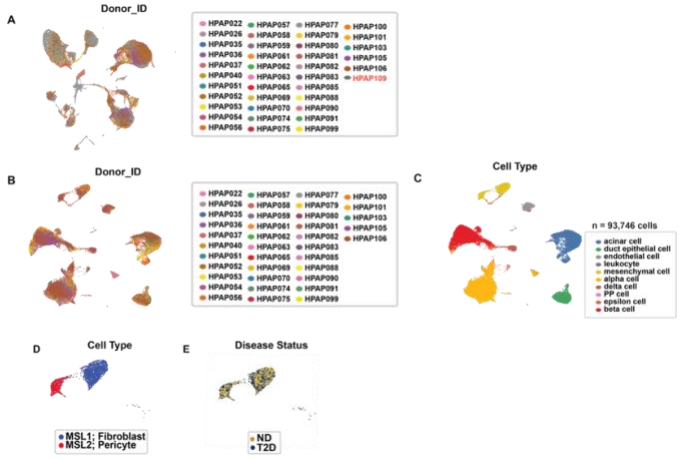

Figure 2-31: Quality control and annotation of the CONCORD re-integrated PancDB atlas.

(**A**) UMAP of the initial integrated PancDB dataset colored by donor identity.
(**B**) UMAP of the filtered dataset after removal of the low-quality donor HPAP109, colored by donor identity.
(**C**) UMAP of the filtered dataset colored by major pancreatic cell type.
(**D**) Subset of mesenchymal stromal populations annotated as MSL1/fibroblast and MSL2/pericyte.
(**E**) MSL1 and MSL2 populations colored by disease status.

After cell filtering and CONCORD re-integration, donor HPAP109 did not embed cleanly with the remaining donors, suggesting that its transcriptional profile was driven more by sample quality than biological variation (**Fig. 2-31A**). Therefore, HPAP109 was excluded prior to downstream comparisons, and the final re-integrated PancDB dataset included only donors that passed quality control (**Figs. 2-31B, 2-31C**). This dataset was then subset for mesenchymal cells and used to map MSL1 (fibroblast) and MSL2 (pericyte) populations across non-diabetic and type 2 diabetic donors (**Figs. 2-31D, 2-31E**).

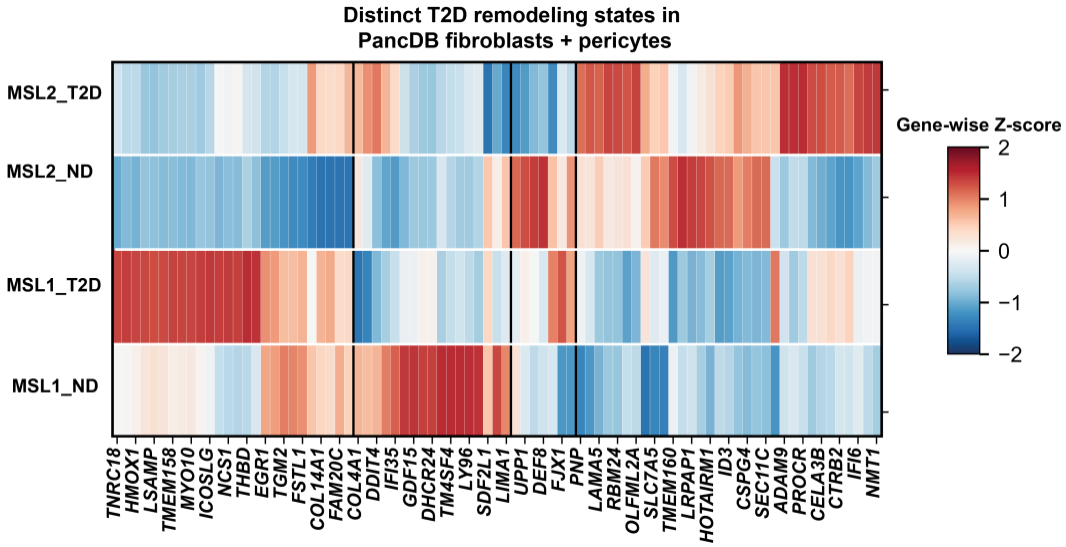

Figure 2-32: Type 2 diabetes-associated remodeling programs in MSL1 and MSL2 mesenchymal populations.

Heatmap showing scaled expression of differentially expressed genes across MSL1 and MSL2 populations from control and type 2 diabetic donors in the PancDB reference atlas.

To characterize how these populations respond transcriptionally to disease, we first performed pseudobulk DE analysis comparing type 2 diabetic and non-diabetic samples within each vascular-associated population (**Fig. 2-32**). Unsupervised clustering of the resulting differentially expressed genes resolved four largely non-overlapping gene modules, each defined by a distinct combination of cell identity (MSL1 vs MSL2) and disease state, indicating that fibroblast-like and pericyte-like

mesenchymal populations undergo largely independent, rather than convergent, transcriptional remodeling in type 2 diabetes. The first gene module, comprising *TNRC18, HMOX1, LSAMP, TMEM158, MYO10, ICOSLG, NCS1, THBD, EGR1, TGM2, FSTL1,* and *FAM20C* was selectively upregulated in the type 2 diabetic MSL1 population relative to all other groups, including non-diabetic MSL1 cells, indicating a fibroblast-specific transcriptional response to the diabetic environment that is largely absent from the non-diabetic fibroblast state and from either pericyte condition. A second module including *COL14A1*, *DDIT4, IFI35, GDF15, DHCR24, TM4SF4, LY96, SDF2L1,* and *LIMA1* was enriched in non-diabetic MSL1 cells. A smaller, third module comprising *UPP1, DEF8,* and *FJX1* showed a distinct pattern, with the strongest enrichment appearing in non-diabetic MSL2 cells rather than in the type 2 diabetic group, suggesting that this small gene set marks a baseline pericyte identity feature that is attenuated with disease rather than induced by it.

The largest and most striking module, spanning *PNP, LAMA5, RBM24, OLFML2A, SLC7A5, TMEM160, LRPAP1, HOTAIRM1, ID3, CSPG4, SEC11C, PROCR, ADAM9, CELA3B, CTRB2, IFI6,* and *NMT1*, was selectively upregulated in type 2 diabetic MSL2 cells and comparatively low across non-diabetic MSL2 and MSL1 cells, and type 2 diabetic MSL1 cells. Notably, this module includes *LAMA5*, a basement membrane laminin subunit, together with several genes linked to vascular and stress-response biology (*PROCR, ADAM9, IFI6*), suggesting that the type 2 diabetes-associated pericyte transcriptional shift extends beyond the contractile and inflammatory

genes already discussed to include additional matrix and vascular-regulatory components.

Together, this pattern indicates that MSL1 and MSL2 populations mount largely distinct, non-redundant transcriptional programs in response to type 2 diabetes, with disease-associated gene sets that are, for the most part, unique to each cell type rather than shared across the mesenchymal compartment.

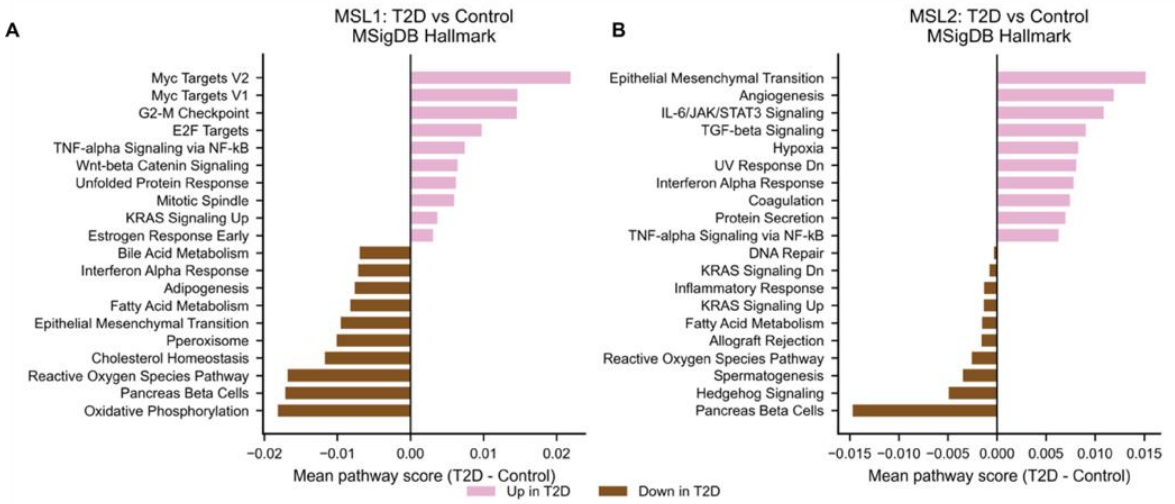

Figure 2-33: Diabetes-associated pathway score changes in MSL1 and MSL2 populations.

(**A**) Bar plots showing mean pathway score differences between type 2 diabetic and ND control cells in MSL1 populations. Positive pink values indicate pathways increased in T2D, while negative brown values indicate pathways decreased pathway.
(**B**) Bar plots showing mean pathway score differences between type 2 diabetic and ND control cells in MSL2 populations. Positive pink values indicate pathways increased in T2D, while negative brown values indicate pathways decreased pathway.

To interpret the biological significance of these gene-level changes, we ranked the resulting DEG lists by signed statistical significance and applied gene set enrichment analysis (GSEA) against the MSigDB Hallmark collection [30]. MSL1 showed enrichment for proliferative and stress-response programs in type 2 diabetes, with Myc Targets V1/V2, G2-M Checkpoint, E2F Targets, and the unfolded protein response among the most upregulated pathways, while oxidative phosphorylation, the

pancreas beta cell gene set, and the reactive oxygen species pathway were the most strongly downregulated (**Fig. 2-33A**). MSL2 showed a distinct pattern, with epithelial-mesenchymal transition, angiogenesis, IL-6/JAK/STAT3 signaling, and TGF-beta signaling among the most upregulated pathways in type 2 diabetes, while the pancreas beta cell gene set was again the most strongly downregulated pathway (**Fig. 2-33B**).

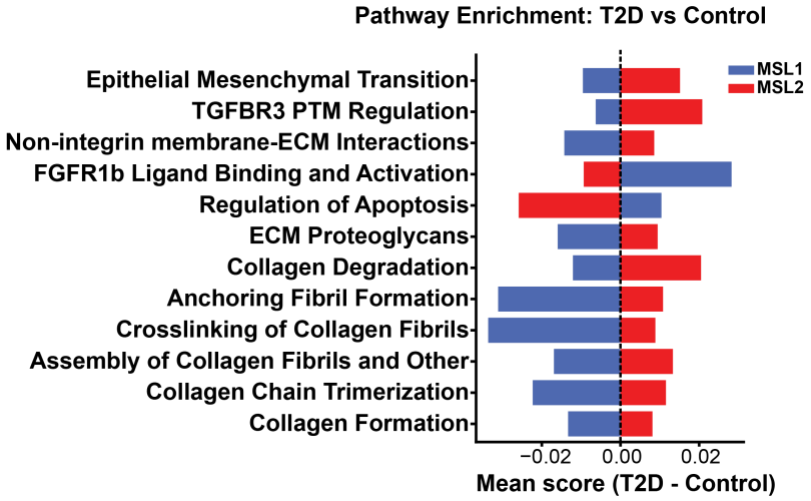

Figure 2-34: Gene set enrichment analysis comparing PancDB T2D and non-diabetic fibroblasts and pericyte populations.

Differentially expressed genes were ranked by log fold change and analyzed using curated Reactome, GO, and ECM-associated pathways. T2D-associated populations exhibited enrichment of collagen organization, ECM proteoglycan, collagen fibril assembly, and TGFβ-related pathways, consistent with matrix remodeling and fibrotic activation.

Reactome analysis shows that fibroblast-associated populations exhibited reduced enrichment of collagen formation, matrix crosslinking, and fibril assembly pathways, whereas pericyte-associated populations showed increased enrichment of these same pathways, suggestive of a less differentiated pericyte state and a shift towards a more fibrotic phenotype **(Fig. 2-34**) [43].

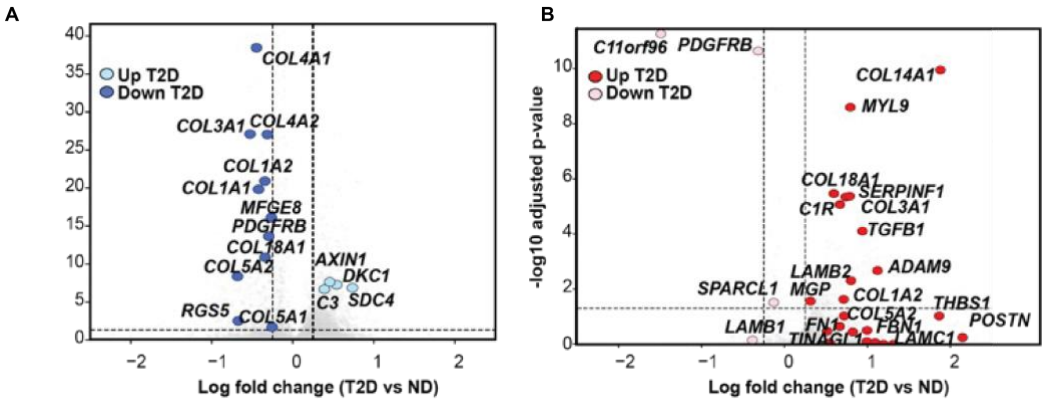

Figure 2-35: Differential gene expression and ECM/ basement membrane changes in T2D mesenchymal populations.

(**A**) Blue, Spatial gene subset volcano plots showing significant ECM and basement membrane gene changes in MSL1 between T2D and ND conditions. Positive log fold-change values indicate increased expression in T2D, while negative values indicate decreased expression in T2D.
(**B**) Red, Spatial gene subset volcano plots showing significant ECM and basement membrane gene changes in MSL2 between T2D and ND conditions. Positive log fold-change values indicate increased expression in T2D, while negative values indicate decreased expression in T2D.

To further characterize these transcriptional changes, we performed DGE analysis between non-diabetic and type 2 diabetic populations to include only genes in the spatial transcriptomic panel. Fibroblast-associated populations exhibited reduced expression of several basement membrane -associated collagens, including *COL4A1* and *COL4A2* (**Fig. 2-35A**). In contrast, pericyte populations exhibited increased expression of contractile, fibrillar ECM and angiogenic-related genes including *MYL9*, *COL1A2*, *COL14A1*, and *SERPINF1*, together with reduced expression of *PDGFRB*, a receptor critical for pericyte survival and perivascular retention (**Fig. 2-35B**) [44–48].

2.2.6 Type 2 Diabetes MERSCOPE Analysis Reveals Altered Vascular Composition and Spatial Remodeling in Type 2 Diabetic Islets

Having established these transcriptional signatures through pseudobulk DE and pathway enrichment using droplet data, we next asked whether these disease-associated changes could also be resolved at single-cell resolution while preserving

their native spatial context. We therefore performed MERSCOPE spatial transcriptomic profiling on pancreatic sections from type 2 diabetic donors, generating single-cell-resolution expression data using the same custom 300-gene panel applied to the non-diabetic cohort.

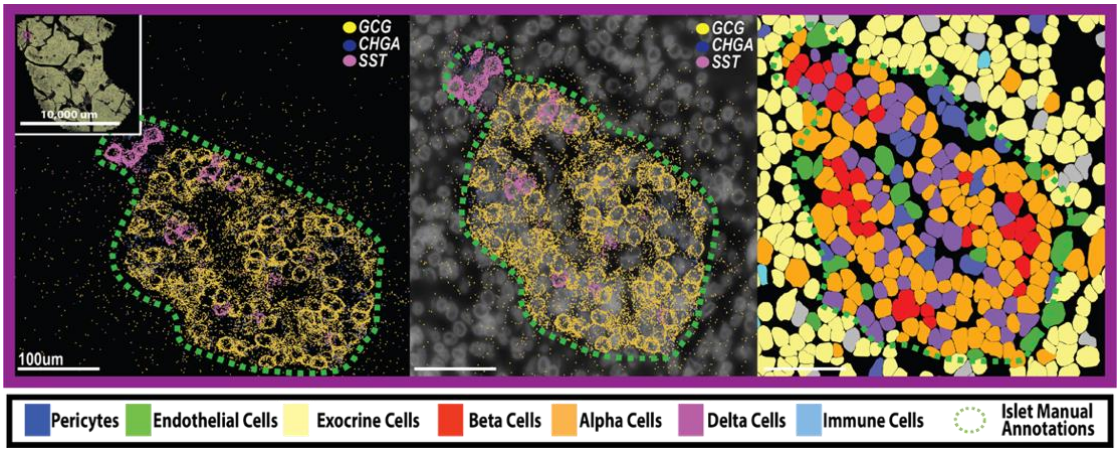

Figure 2-36: Spatial distribution of endothelial cells and pericytes in the adult human pancreas.

Representative MERSCOPE image showing an annotated human islet. Endocrine marker transcripts are shown for *GCG*, *CHGA*, and SST, with the manually annotated islet boundary outlined in green. The corresponding cell segmentation map shows assigned major cell types. Scale bars = 10,000, 100 µm.

This enabled direct comparison of cell type composition, spatial organization, and gene expression between healthy and diabetic pancreas while preserving the anatomical relationships between endocrine, exocrine, vascular, and stromal compartments. Reconstruction of whole-tissue sections revealed that major pancreatic cell populations could be readily identified and mapped back to their native spatial locations within the tissue (**Fig. 2-36**; representative sample shown).

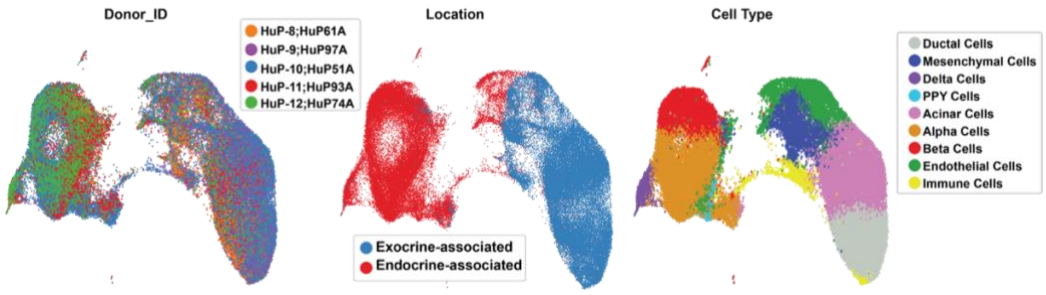

Figure 2-37: Integrated spatial vascular cell annotations across T2D MERSCOPE samples.

CONCORD integrated UMAP visualizations of T2D spatial transcriptomics cells colored by sample ID, tissue compartment, and major cell type.

CONCORD integration of type 2 diabetes sample datasets demonstrated preservation of the major pancreatic cell types across endocrine and exocrine-associated regions (**Fig. 2-37**).

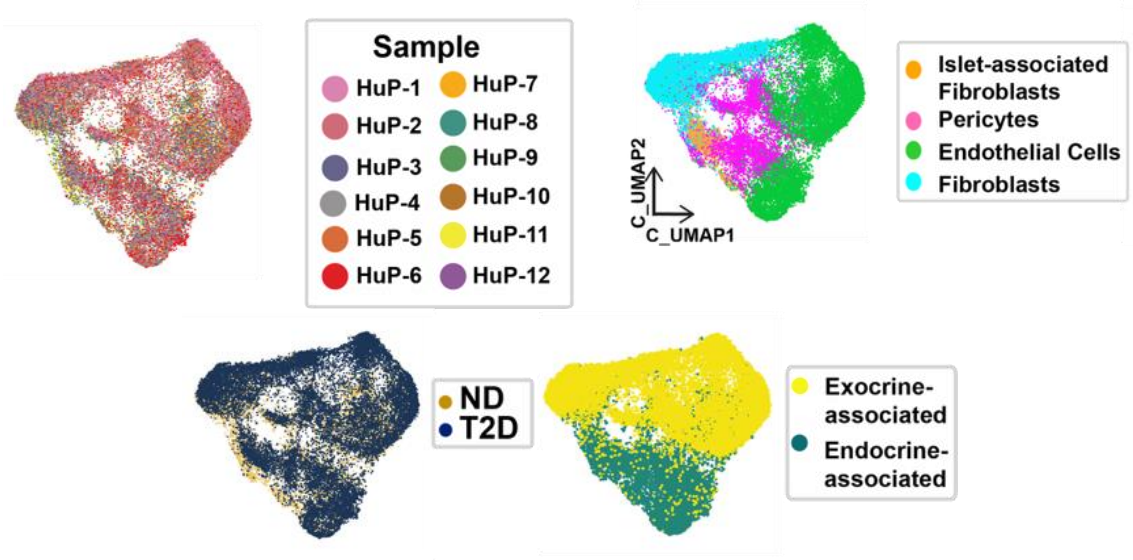

Figure 2-38: Integrated spatial vascular cell annotations across ND and T2D MERSCOPE samples.

(**Top**) UMAP visualizations of CONCORD integrated ND and T2D spatial transcriptomics cells colored by sample ID and vascular cell annotation.
(**Bottom**) UMAP visualizations of CONCORD integrated ND and T2D spatial transcriptomics cells colored by disease status and tissue compartment.

We next sought to determine how vascular-associated cell types are compositionally, transcriptionally, and spatially remodeled in type 2 diabetes. To resolve these changes

at higher resolution than the broad cell type annotations allowed, mesenchymal and endothelial cells were subset from a non-diabetes and type 2 diabetes integrated dataset. From this integrated dataset, cells were reclustered and annotated allowing canonical cell markers described previously in the non-diabetic vascular cell analysis (**Fig. 2-38**).

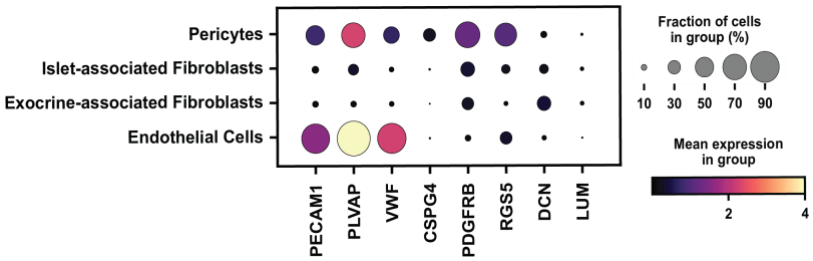

Figure 2-39: T2D MERSCOPE vascular-associated population marker gene expression.

Dot plot showing expression of known EC (*PECAM1*, *PLVAP*, *VWF*), pericyte (*PDGFRB*, *CSPG4*, *RGS5*), or fibroblasts (*DCN, LUM*) markers confirms cell identities.

Using this targeted analysis again resolved pancreatic pericytes, islet-associated fibroblasts, exocrine-associated fibroblasts, and endothelial cells across type 2 diabetic samples, each expressing canonical markers consistent with their non-diabetic counterparts (**Fig. 2-39**).

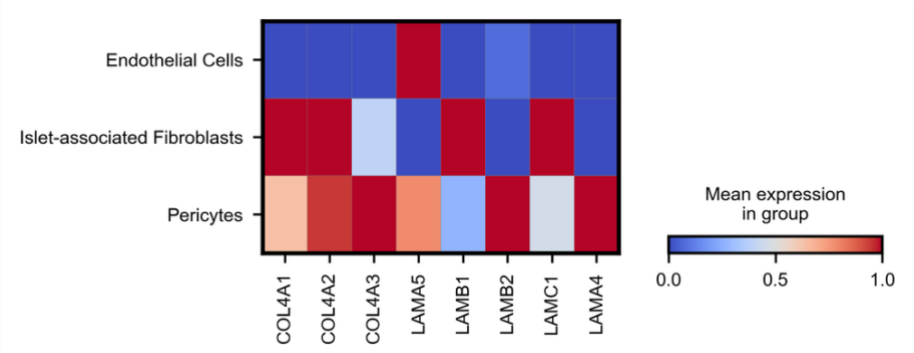

Figure 2-40: Heatmap of BM genes across T2D vascular-associated populations.

Heatmap showing mean expression of selected basement membrane genes in endothelial cells, islet-associated fibroblasts, and pericytes.

Basement membrane gene expression across islet-specific populations was broadly similar to that observed in non-diabetic tissue, except for islet-associated fibroblasts, which showed increased expression of *COL4A1/COL4A2* in type 2 diabetes (**Fig. 2-40**). Compositional analysis revealed a significant shift in the type 2 diabetes islet vascular niche, characterized by expansion of islet-associated fibroblasts and a corresponding reduction in pericytes.

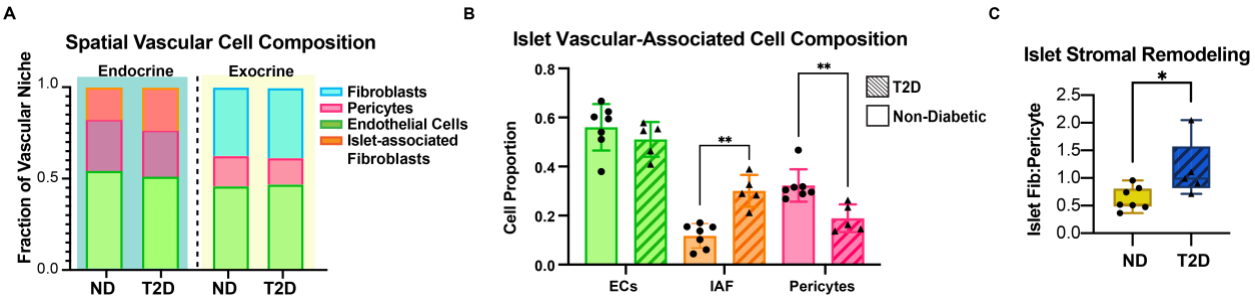

Figure 2-41: Spatial vascular cell composition and islet stromal remodeling in T2D.

(**A**) Stacked bar plots showing the fraction of vascular-associated cell types in endocrine and exocrine compartments from ND and T2D samples.
(**B**) Donor-level quantification of islet vascular-associated cell composition, including endothelial cells, islet-associated fibroblasts, and pericytes.
(**C**) Ratio of islet-associated fibroblasts to pericytes in ND and T2D samples, showing increased islet stromal remodeling in T2D. Data points represent individual donors. *p < 0.05; **p < 0.01.

These changes were significant at the donor level, whereas the composition of the exocrine vascular compartment remained largely unchanged (**Figs. 2-41A, 2-41B**). To further assess changes within the endocrine niche, we directly compared islet-associated fibroblasts and pericytes and observed a significant increase in the islet fibroblast-to-pericyte ratio in type 2 diabetes islets relative to non-diabetic controls (**Fig. 2-41C**).

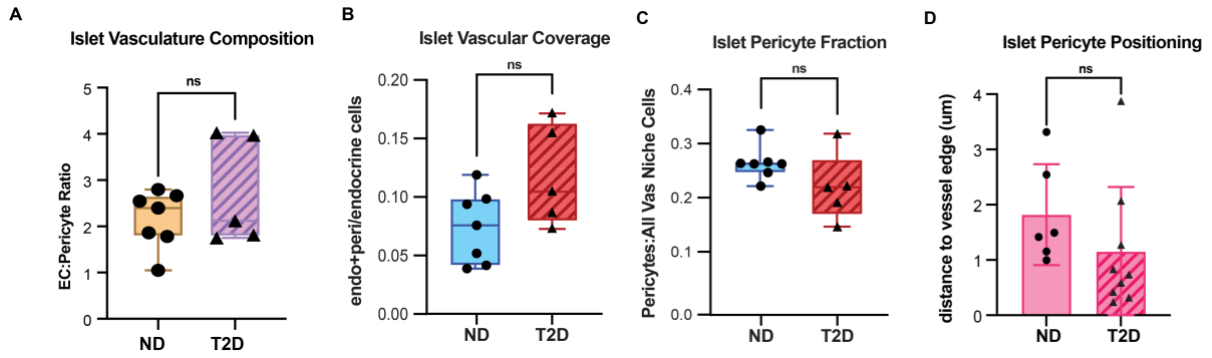

Figure 2-42: Islet vascular composition and pericyte positioning in T2D.

(**A**) Ratio of endothelial cells to pericytes in ND and T2D islets. ns, not significant.
(**B**) Islet vascular coverage, quantified as the fraction of endothelial and pericyte cells among endocrine cells. ns, not significant.
(**C**) Fraction of pericytes among all vascular niche cells in ND and T2D islets. ns, not significant.
(**D**) Distance of islet pericytes to the nearest vessel edge in ND and T2D samples. Data points represent individual donors. ns, not significant.

In contrast, the endothelial-to-pericyte ratio, the combined vascular-to-endocrine cell ratio, and the relative contribution of pericytes to the total vascular compartment were not significantly altered between non-diabetes and type 2 diabetes islets (**Fig. 2-42**).

Table 2-1: Gene programs derived from differential expression analysis between ND and T2D PancDB.

Includes Contractile, ECM Remodeling, Vascular BM, Interstitial ECM, Cell Stress/Inflammatory programs. Representative genes contributing to each transcriptional program are shown. (*) Asterisks represent genes significantly differentially expressed in T2D.

Gene Programs Dysregulated in T2D

Contractile	*MYL9*, CALD1, TPM2, MGP**
ECM Remodeling	*THBS1, ADAM9*, TGFB1*, HES1*, FBN1*, SDC4*, TINAGL1, MMP2*
Vascular BM	*COL4A1*, COL4A2*, LAMB2*, LAMC1, COL18A1*, HSPG2*
Interstitial ECM	*COL14A1*, COL1A2*, COL1A1*, COL3A1* COL5A1*, COL5A2*, COL6A3, POSTN*
Cell Stress/ Inflammatory	*SERPINF1*, C1R*, JUN*, CTSB*, FOS*, C3**

To better define vascular niche remodeling at the gene program level, we curated five transcriptional modules from genes differentially expressed between type 2 diabetes and non-diabetes vascular-associated populations in the PancDB dataset. To

enable direct evaluation in the spatial dataset, only genes represented within the MERFISH panel were included and were assigned to modules based on Reactome and Gene Ontology annotations, and established markers of pericytes, fibroblast, and ECM programs [43, 49, 50]. This process generated five transcriptional modules: Contractile, ECM Remodeling, Vascular Basement Membrane, Interstitial ECM, and Cell Stress/Inflammatory (**Table 2-1**).

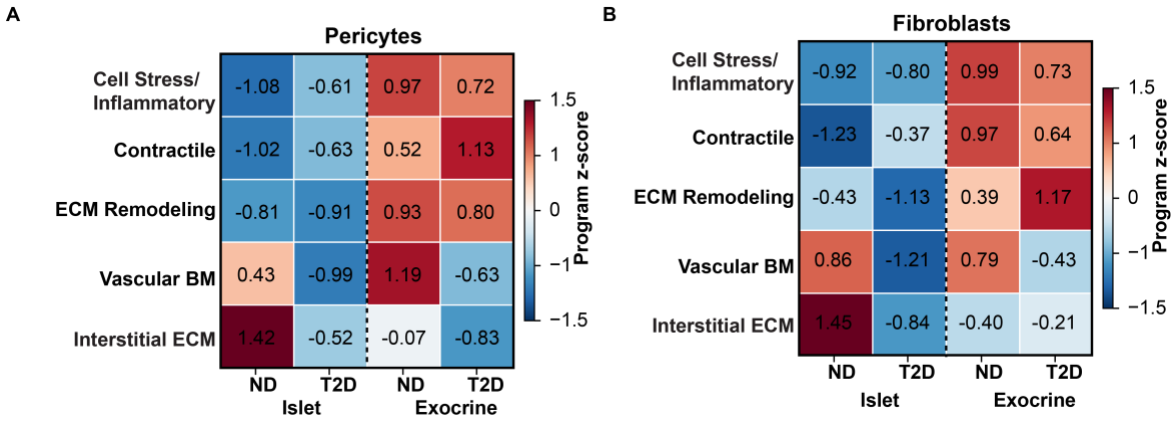

Figure 2-43: Heatmap showing z-score normalized enrichment of transcriptional programs.

(**A**) Heatmap plotted across spatial pericyte populations stratified by disease state and anatomical location. Program scores were calculated independently for each condition and subsequently scaled by z-score across groups to visualize relative enrichment patterns.
(**B**) Heatmap plotted across spatial fibroblast populations stratified by disease state and anatomical location. Program scores were calculated independently for each condition and subsequently scaled by z-score across groups to visualize relative enrichment patterns.

Within type 2 diabetes islet pericytes, stress/inflammatory and contractile program scores were increased relative to non-diabetic controls, whereas vascular basement membrane, interstitial ECM, and ECM-remodeling module scores were reduced (**Fig. 2-43A**). Exocrine pericytes similarly exhibited increased contractile program scores together with reduced vascular basement membrane interstitial ECM, and ECM-remodeling signatures. In contrast to islet pericytes, however, stress/inflammatory signaling was increased in type 2 diabetes exocrine pericytes

relative to non-diabetic controls. We next examined islet-associated fibroblasts in type 2 diabetes and observed broad reductions across most transcriptional modules, accompanied by increased contractile and stress/inflammatory program scores, mirroring the pattern observed in islet pericytes. Exocrine fibroblasts displayed a similar overall profile but additionally showed increased ECM-remodeling and interstitial ECM program scores. (**Fig. 2-43B**).

To validate the upregulation of interstitial collagens identified by spatial transcriptomics, we performed COL1A2 immunofluorescence staining in non-diabetes and type 2 diabetes pancreatic sections (**Fig. 2-44).**

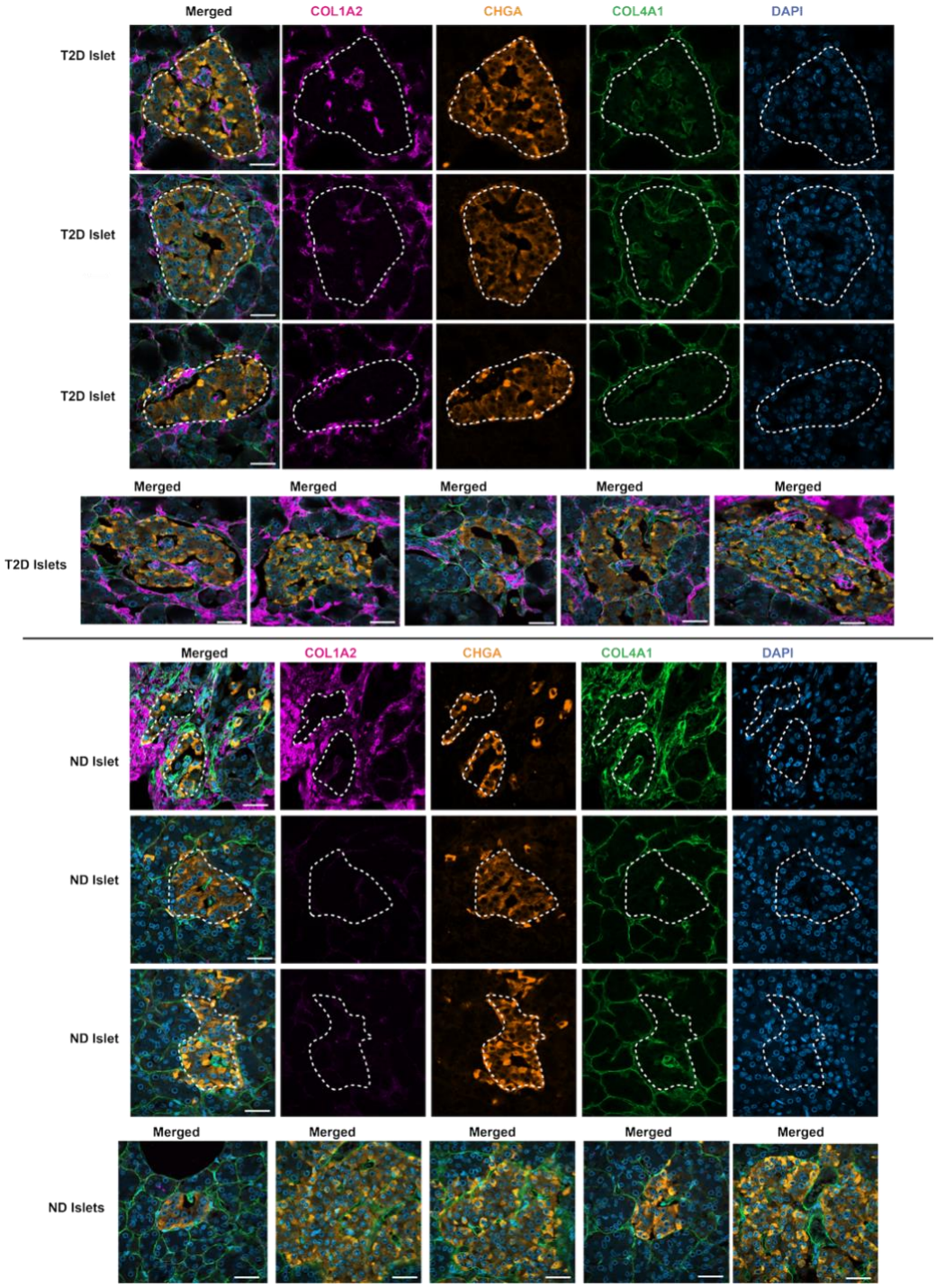

Figure 2-44: IF validation of increased intra-islet COL1A2 protein expression in type 2 diabetic human islets.

Additional representative images of immunofluorescence staining for COL1A2 (magenta), CHGA (orange), COL4A1 (green), and DAPI (blue) in ND and T2D human pancreatic islets. Dashed lines indicate CHGA-defined islet boundaries used for quantification. Bottom rows show additional representative merged images from each condition. All images were acquired using identical staining, imaging, and acquisition settings. Scale bars = 40 μm.

Consistent with MERFISH analyses, COL1A2 fluorescence intensity within chromogranin A (CHGA)-defined islet regions was increased in type 2 diabetes islets compared with non-diabetic controls (**Figs. 2-45A, 2-45B**). Together, these findings support coordinated remodeling of the islet vascular niche in type 2 diabetes through both ECM accumulation and altered vascular transcriptional states.

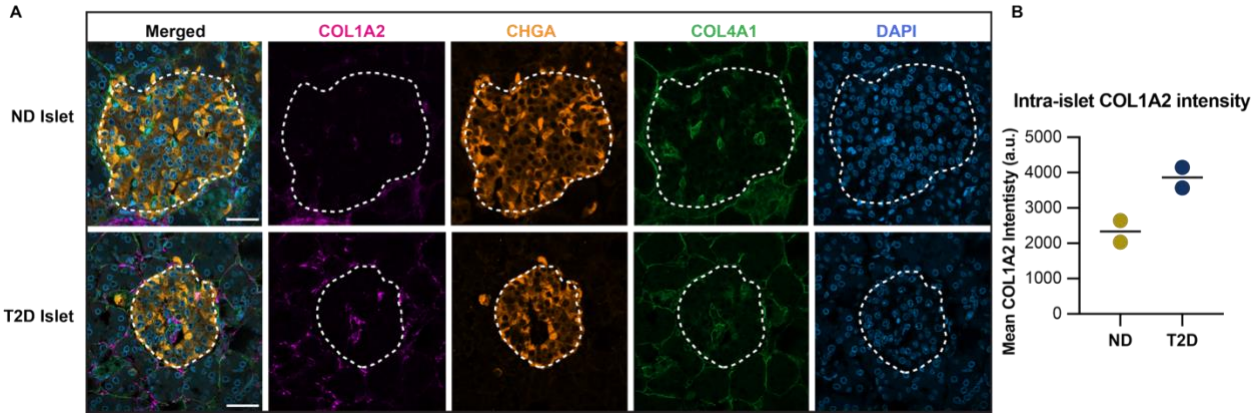

Figure 2-45: Immunofluorescence of ND and T2D pancreatic tissue sections.

(**A**) Representative immunofluorescence images of COL1A2, CHGA, COL4A1, and DAPI staining in ND and T2D human pancreatic islets. Dashed lines indicate CHGA-defined islet boundaries used for quantification. Images were acquired at 63x magnification. Scale bar = 40 μm.
(**B**) Mean COL1A2 fluorescence intensity (arbitrary units, a.u.) was quantified within CHGA-defined islet regions. Each point represents the mean COL1A2 fluorescence intensity of an individual donor; 30 islets were analyzed from 2 ND and 2 T2D donors. COL1A2 fluorescence intensity appeared higher in islets from T2D donors than in ND controls.

2.3 Discussion

In this study, we combined donor-resolved MERFISH spatial transcriptomics with computational integration of public human pancreas single-cell RNA-sequencing datasets to build a high-resolution atlas of ECM gene expression in the adult human pancreas. Profiling matrix-producing cells within their native tissue architecture, and validating each observation across independent datasets, allowed us to resolve several open questions about the cellular organization of the pancreatic vascular niche and its remodeling in type 2 diabetes.

The central conclusion is that the human islet basement membrane is built and maintained not by endothelial cells alone but through coordinated contributions from several vascular-associated populations, and that this multicellular niche is selectively remodeled in metabolic disease. Four findings support this conclusion. First, pericytes, not endothelial cells, are the predominant transcriptional source of vascular basement membrane genes, including *COL4A1*, *COL4A2*, *LAMA4*, and *LAMB2*, while endothelial cells contribute the complementary components *HSPG2* and *LAMA5*. Second, a transcriptionally and spatially distinct islet-associated fibroblast population predominately occupies the endocrine boundary and expresses a peri-islet matrix program enriched for *LAMB1* and *LAMC1*. Third, pericytes retain a conserved mural cell identity while specializing their matrix and signaling programs according to whether they reside in the endocrine or exocrine compartment. Fourth, type 2 diabetes remodels the endocrine vascular niche at both the compositional and transcriptional level, shifting the fibroblast-to-pericyte balance and reducing basement membrane programs while increasing contractile, stress, and inflammatory signatures.

These results address the knowledge gaps outlined in Chapter 1 and motivate a revised, cooperative model of basement membrane assembly, developed below.

2.3.1 A Revised Model of Human Vascular Basement Membrane Assembly

For more than two decades, islet basement membrane biology has centered on endothelial cells as the principal architects of the vascular matrix [6]. This view originated in mouse developmental studies, where disrupting β cell VEGFA signaling to endothelial cells prevented formation of intra-islet basement membranes [4]. Because the surrounding peri-islet and acinar basement membrane was unaffected, endothelial

cells were assumed to be the dominant, and perhaps sole, source of islet basement membrane.

Those studies were not designed to apportion matrix synthesis among neighboring stromal populations in mature human tissue. Endothelial cells, pericytes, and fibroblasts occupy an exceptionally compact niche, residing within microns of one another and sharing a common matrix [51]. Conventional histology can localize a matrix protein but cannot identify the cell that produced it, and dissociation-based sequencing recovers transcriptional identity at the cost of the spatial context needed to distinguish endocrine- from exocrine-associated cells [17, 52]. Integrating single-cell profiling with spatial transcriptomics, as done here, was designed to overcome that limitation.

Our data support a model in which the mature human vascular basement membrane is assembled through the coordinated output of several specialized populations rather than a single dominant producer. Endothelial cells remain essential but act primarily as providers of specific components, while regulating permeability, angiocrine signaling, and barrier function [19, 53]. Pericytes supply most of the structural collagen IV transcript together with the vascular laminins, positioning them as the principal organizers of the scaffold immediately surrounding the capillary wall. At the endocrine boundary, islet-associated fibroblasts contribute the complementary laminins *LAMB1* and *LAMC1* that define the peri-islet basement membrane [41]. The combined output of these three populations accounts for the double-layer architecture that distinguishes the adult human islet.

Cooperative basement membrane assembly of this kind is increasingly recognized across vascularized organs [6, 54]. In the central nervous system, pericytes

contribute to basement membrane production and are required for blood-brain barrier integrity through coordinated signaling with endothelial cells and astrocytes [55]. In the kidney, multiple vascular-associated populations supply distinct components of the glomerular basement membrane, and in the retina, pericyte dysfunction is a central driver of diabetic microvascular disease affecting both matrix organization and vascular stability [47, 56, 57]. Comparable contributions from mural and stromal cells to matrix deposition have been described in the lung and other highly vascularized tissues [13, 58]. The adult human pancreas appears to follow the same principle.

This model has implications beyond matrix composition. Because the basement membrane governs growth factor presentation, integrin signaling, endothelial maturation, and endocrine cell polarity, identifying the cellular source of each component clarifies how the endocrine microenvironment is established and maintained [51, 59]. It also implies that pathological remodeling of any single vascular-supportive population, pericyte or islet-associated fibroblast, can alter the shared matrix and affect neighboring cells well beyond its own lineage.

2.3.2 Pericytes as Specialized Basement Membrane-Producing Cells

The strongest single line of evidence for this cooperative model is the behavior of pericytes. Across both the integrated single-cell atlas and the spatial data, pericytes showed high transcriptional enrichment of canonical basement membrane components, particularly the network-forming collagen IV genes *COL4A1* and *COL4A2* [19, 24]. Collagen IV differs from the fibrillar collagens in assembling into two-dimensional networks rather than fibers, providing the scaffold on which laminins, nidogens, and heparan sulfate proteoglycans are subsequently organized [60]. Because collagen IV

polymerization is among the earliest steps in basement membrane assembly, strong collagen IV expression by islet pericytes suggests that these cells may play an important role in organizing and stabilizing the vascular basement membrane[61]. The finding that pericytes, rather than endothelial cells, dominate collagen IV expression may position them as active organizers of the vascular basement membrane, rather than passive mural support cells.

This functional role for pericytes would also fit their anatomical position. As mural cells embedded within the vascular basement membrane on the abluminal surface of capillaries, pericytes share a matrix with the endothelium and sit at the interface between the vessel and surrounding tissue [62]. Unlike interstitial fibroblasts or luminal-facing endothelial cells, pericytes are positioned along the abluminal vascular surface, where their collagen IV expression could directly contribute to basement membrane organization, local matrix remodeling, and vascular stability [63].

Pericyte identity and retention depend on platelet-derived growth factor signaling through the PDGF-B/PDGFRβ axis [64]. Loss of either *PDGFB* or *PDGFRB* produces pericyte deficiency, vascular instability, microaneurysm, and embryonic lethality [65]. The pathway remains active in the adult, where continued signaling sustains mural cell identity and vascular quiescence and supports the reciprocal endothelial-pericyte communication that maintains the shared basement membrane [64]. This dependence becomes directly relevant to the diabetic remodeling discussed below, where *PDGFRB* expression is reduced in diabetic pericytes, as discussed below.

The conclusion that pericytes are major matrix expressors is strengthened by its reproducibility across experimental datasets. Basement membrane enrichment was first

detected in the re-integrated PancDB single-cell atlas, confirmed with spatial resolution by MERFISH, and recovered independently in the Craig-Schapiro human pancreas atlas. Agreement across platforms and donor cohorts argues that the signal reflects genuine biology rather than a platform-specific artifact.

Positioning pericytes as central organizers of the vascular matrix has consequences for how the endocrine niche is understood. Because the basement membrane regulates endothelial differentiation, growth factor availability, vascular permeability, and β cell polarity, changes in pericyte function can influence the islet through several routes at once [5, 7, 66]. Preserving pericyte identity and matrix-producing capacity may therefore be as important to endocrine integrity as preserving the endocrine cells themselves, a point the diabetic remodeling data suggest directly [5].

2.3.3 Islet-Associated Fibroblasts Define a Specialized Endocrine Stromal Niche

The second pillar of the model is a fibroblast population dedicated to the endocrine compartment. Fibroblasts have long been treated as a relatively uniform source of interstitial matrix, but our combined single-cell and spatial analysis identified a transcriptionally distinct subset enriched along the islet boundary that expresses a peri-islet matrix program rather than a generic interstitial one, extending the principle of fibroblast specialization into the endocrine niche [19, 67, 68].

This specialization fits a broader reappraisal of fibroblast biology. Single-cell studies across many tissues have shown that fibroblast identity is dictated largely by anatomical location and local signals rather than a single conserved program: subepithelial fibroblasts in the intestine supply Wnt ligands and matrix that maintain

epithelial stem cells, papillary and reticular fibroblasts impose distinct properties on the dermis, and compartment-specific fibroblasts have been described around alveoli, portal tracts, and nephrons [69–72]. Boundary-associated fibroblasts therefore appear to represent a recurring stromal organizational strategy across tissues, and the pancreas may follow this broader pattern through the presence of islet-associated fibroblasts at the endocrine-exocrine interface [73–76].

The islet-associated population fits this pattern closely. Roughly two-thirds of these cells localized within five microns of the islet boundary across non-diabetic donors, placing them directly against the peri-islet basement membrane [67, 77–79]. Their transcriptional profile matched this position: alongside canonical fibroblast markers, they preferentially expressed *LAMB1* and *LAMC1*, laminin subunits previously localized to the human peri-islet basement membrane [7, 41]. Because laminins are among the earliest proteins incorporated during matrix assembly and show strongly tissue-specific distributions, selective enrichment of these subunits suggests that islet-associated fibroblasts build a basement membrane distinct from the vascular one produced by pericytes and endothelial cells [80, 81].

This assignment offers a cellular explanation for a long-standing morphological observation. Ultrastructural studies established that human islets are surrounded by a double-layer basement membrane comprising distinct peri-islet and vascular compartments, but the cellular origin of each layer remained uncertain [7, 41, 82]. Our data support a division of labor in which pericytes specialize in structural vascular collagens, endothelial cells add complementary laminins and proteoglycans, and islet-associated fibroblasts supply peri-islet laminins, a partitioning that accounts for the

molecular diversity of the endocrine matrix despite the close physical proximity of the cells that build it.

An alternative interpretation is that this population reflects activated pancreatic stellate cells, which are reported to deposit matrix following injury and share several markers with fibroblasts, including *PDGFRB, COL1A1, COL1A2, DCN, and LUM* [83, 84]. This overlap is precisely why stromal annotation is inconsistent across pancreas atlases, where similar populations are variously labeled fibroblasts, stellate cells, mesenchymal cells, or pericytes. Spatial transcriptomics contributes information that transcription alone cannot: the highly reproducible localization of this population at the endocrine boundary supports its designation as a specialized endocrine-associated fibroblast, regardless of the label applied in earlier dissociation-based datasets.

The strategic location of these cells suggests functions beyond matrix deposition. Fibroblasts communicate with epithelial, endothelial, immune, and mural neighbors through secreted factors and matrix-bound signals, and a population stationed at the islet boundary is well placed to influence immune trafficking into islets, endocrine polarity, and vascular maturation [85]. Their coordinated remodeling in type 2 diabetes, discussed below, reinforces their status as integral components of the endocrine niche rather than incidental interstitial cells.

2.3.4 Endocrine Versus Exocrine Vascular Niche Specialization

The pancreas houses two compartments with fundamentally different jobs. The exocrine pancreas secretes digestive enzymes into a ductal network, while the endocrine pancreas is a densely vascularized tissue that senses circulating nutrients and releases hormones directly into the blood. These distinct demands are reflected in

the vasculature. Although endothelial cells and pericytes retain a conserved vascular-supportive identity throughout the organ, their matrix and signaling programs are tuned to local tissue context, indicating that the pancreatic vasculature is organized into distinct endocrine and exocrine niches rather than a uniform capillary bed [86–89]

These functional demands are reflected transcriptionally. Endocrine- and exocrine-associated pericytes exhibited similar basement membrane scores, yet differential expression revealed clear niche-dependent tuning of broader programs: endocrine pericytes favored vascular-regulatory genes including *ACE2*, *FLT1*, *RGS5*, *LAMC2*, *SERPINA1*, and *FGA*, while exocrine pericytes favored interstitial-remodeling and inflammatory genes including *C1R*, *C1S*, *COL12A1*, *COL6A1*, and *IGFBP2* [45, 90–93]. These differences were reproduced in the anatomically resolved Craig-Schapiro dataset, arguing that they are conserved features of human pancreatic vascular organization rather than technical artifacts [19].

The pattern itself is informative since basement membrane integrity is essential to vascular stability everywhere, so its preservation across both compartments is expected, whereas matrix-remodeling, inflammatory, and vascular-regulatory programs are free to track local cues [5, 94]. Pericytes thus appear to maintain a conserved vascular-maintenance program onto which regional specialization is superimposed, mirroring the way endothelial cells preserve a core identity while diversifying across organs [95]. Local signals likely responsible for this tuning, including endocrine hormones, β cell-derived VEGFA, and the metabolic and mechanical environment of pulsatile islet blood flow, plausibly shape pericyte identity throughout adult life [54, 96, 97].

Endocrine specialization is not confined to pericytes. Exocrine-associated fibroblasts expressed interstitial ECM-rich programs, elevated fibrillar collagen and matrix-remodeling gene expression. This compartment-restricted distribution suggests that exocrine fibroblasts primarily support the broader stromal architecture of the exocrine pancreas rather than the peri-islet niche.

2.3.5 Type 2 Diabetes Remodels the Endocrine Vascular Niche

A central result of this work is that type 2 diabetes remodels the endocrine vascular niche, and that this remodeling extends well beyond the endocrine cells themselves. Increased metabolic demand and peripheral insulin resistance has long defined the disease, but the surrounding vascular and stromal microenvironment also changes substantially, in both cellular composition and transcriptional state [21, 98]. The coordinated nature of these changes across pericytes and islet-associated fibroblasts indicates that the niche behaves as an integrated unit whose homeostasis is progressively disrupted. One of the most informative transcriptional changes in diabetic pericytes was reduced expression of *PDGFRB*. Given the central role of PDGF-B/PDGFRβ signaling in mural cell survival and retention described above, lower PDGFRB is widely regarded as a marker of pericyte dysfunction, and disrupted endothelial-pericyte communication underlies pericyte loss, microaneurysm, and capillary loss in diabetic retinopathy, with parallel abnormalities reported in diabetic nephropathy and the diabetic brain [99]. The same signaling vulnerability appears to operate in the human pancreas.

Reduced PDGFRB occurred alongside increased contractile genes, including *MYL9*, and stress-responsive genes such as *JUN*, *FOS*, and *CTSB*, a combination

suggesting a shift from a homeostatic vascular-supportive state toward an activated, dysfunctional phenotype [100–102]. Increased pericyte contractility has been reported under chronic hyperglycemia and inflammation and can impair capillary perfusion [96, 103, 104]. Because β cells depend on rapid, precisely regulated blood flow for glucose sensing and insulin delivery, even modest changes in pericyte contractility may carry physiological weight. The stress signature was more pronounced in endocrine than exocrine pericytes, implying that the endocrine microenvironment exposes vascular cells to metabolic or inflammatory pressure.

The accompanying reduction in basement membrane and broader matrix programs may seem at odds with the matrix thickening classically seen in diabetic microvascular disease, but the two observations are reconcilable [105, 106]. Histological thickening is the cumulative product of years of altered synthesis, reduced turnover, and increased crosslinking, whereas transcriptomic profiling captures the instantaneous state of living cells [107, 108]. Reduced matrix gene expression may therefore reflect impaired maintenance of the normal program rather than reduced matrix abundance, a discordance also reported in other fibrotic tissues where long-lived proteins persist as their transcripts decline [109–111].

Diabetic pericytes also increased expression of *COL18A1*, the basement membrane collagen that yields the anti-angiogenic fragment endostatin [112]. Although we did not measure collagen XVIII processing, increased *COL18A1* raises the possibility that pancreatic pericytes participate in angiostatic remodeling that could further limit the capacity of endocrine capillaries to adapt to metabolic stress.

Remodeling was not confined to pericytes. Islet-associated fibroblasts showed changes that closely paralleled their pericyte neighbors, with reduced basement membrane programs and increased contractile and stress signatures, indicating that diabetes drives convergent adaptation across the vascular-supportive populations that share the matrix. The composition of the niche changed as well: islet-associated fibroblasts expanded relative to pericytes, raising the islet fibroblast-to-pericyte ratio. Fibroblast expansion is a common feature of chronic fibrotic and metabolic tissue remodeling, and whether it reflects proliferation, altered survival, or phenotypic conversion of resident cells, it is likely to alter matrix organization and tissue mechanics within the endocrine niche [113].

A consistent theme was the compartmental selectivity of the diabetes-associated stromal response. Although endocrine and exocrine compartments are both exposed to systemic hyperglycemia, islet-associated pericytes and fibroblasts showed substantially stronger induction of stress-, inflammatory-, and contractility-related transcriptional programs than their exocrine counterparts. This compartment-specific vulnerability may help explain why endocrine dysfunction can develop even when the surrounding exocrine architecture remains relatively preserved.

The picture that emerges is not isolated β cell failure but coordinated, multicellular remodeling of the endocrine vascular niche, in which altered endothelial-pericyte communication, impaired matrix maintenance, increased contractility, inflammatory activation, and a shifted stromal balance combine to destabilize the environment on which endocrine function depends.

2.3.6 Implications for Regenerative Medicine and Disease Modeling

The findings presented here reframe a central problem in the field of cell replacement therapy for patients with diabetes. Human pluripotent stem cells now reliably yield glucose-responsive β cells, yet these cells often fall short of the functional maturity, stability, and vascular integration of native islets [114]. Increasing evidence attributes this gap not only to incomplete endocrine maturation but to the absence of the specialized matrix and vascular-supportive niche that surrounds β cells *in vivo* [59, 114]. Defining the cellular sources of that matrix is a prerequisite for rebuilding it.

Most strategies for vascularizing engineered islets have focused on endothelial cells, on the assumption that they construct the vascular basement membrane [115, 116]. Our data indicate that this is insufficient: endothelial cells contribute *LAMA5* and *HSPG2*, but pericytes supply most collagen IV and islet-associated fibroblasts add peri-islet laminins, so faithful reconstruction of the endocrine matrix will require the multicellular interactions that generate native basement membrane architecture rather than endothelial vascularization alone. For stem cell-derived islet organoids, this argues for including pancreatic pericytes or equivalent mural cells in engineered vascular networks.

The islet-associated fibroblast widens the set of stromal cells worth incorporating. Fibroblasts are often excluded from engineered tissues because of their association with fibrosis, but the boundary population identified here is transcriptionally distinct from conventional interstitial fibroblasts and is enriched for peri-islet laminins, suggesting it could help recreate the matrix that separates endocrine from exocrine tissue [115]. More broadly, defining the components made by each population provides a blueprint for

tissue-specific matrices and hydrogels that better mimic the human pancreas than generic collagen scaffolds or commercial basement membrane extracts [117–120].

The same logic applies to clinical islet transplantation, where enzymatic isolation strips away the native matrix along with its pericytes and stromal cells, and revascularization rarely restores the original basement membrane [121, 122]. Preserving or co-transplanting vascular-supportive populations may improve graft integration and survival [123, 124]. Finally, because diabetic remodeling involves the whole niche rather than β cells alone, microphysiological models that incorporate endothelial cells, pericytes, specialized fibroblasts, and tissue-specific matrix are likely to model disease progression more faithfully and to provide better platforms for testing interventions [125].

2.4 Strengths of the Study

Several features strengthen confidence in these conclusions. Previously, our understanding of islet basement membrane biology was derived largely from rodent models, despite important species differences in islet architecture, vascular organization, and matrix composition. By focusing specifically on adult human pancreatic tissue, this study addresses a major gap in our understanding of the human islet microenvironment. The double-layer vascular basement membrane of human islets has no direct murine equivalent, so the use of human tissue from both non-diabetic and type 2 diabetic donors makes the findings directly relevant to human physiology and disease.

The work also pairs complementary technologies with a replication-aware design. Dissociation-based single-cell sequencing supplies transcriptional breadth but loses spatial context, while MERFISH preserves architecture across a focused gene set. By integrating the two, the strengths of each technology were used, enabling accurate annotation of vascular populations within intact tissue. Wherever possible, comparisons have used donor-paired, pseudo-bulk testing rather than treating individual cells as independent replicates, which guards against the influence of uneven cell numbers and supports the biological reproducibility of the differences observed.

Spatial resolution is particularly important for matrix biology. Because matrix proteins are secreted, conventional immunostaining cannot reliably identify the cells in which they were synthesized. In contrast, MERFISH permits visualization of matrix transcripts *in situ*, and manual segmentation of more than two thousand islets allowed direct comparison of endocrine and exocrine niches that tissue dissociation cannot provide.

The major conclusions also rest on extensive orthogonal validation. Populations identified by MERFISH were supported by the PancDB reference atlas, by the anatomically resolved Craig-Schapiro dataset, and by immunofluorescence and RNA *in situ* hybridization for selected genes. By combining transcriptional enrichment, spatial organization, neighborhood analysis, differential expression, pathway enrichment, and disease-associated remodeling in a single framework, the study offers one of the more comprehensive accounts to date of vascular-associated matrix programs in the human pancreas.

2.5 Limitations

Several limitations qualify the interpretation of these findings, many of them inherent to studies of adult human pancreas rather than specific to this work. Although these limitations do not alter the central conclusion that multiple vascular and stromal populations cooperate to maintain the endocrine niche and are altered in type 2 diabetes, they limit the extent to which the findings can be generalized beyond the donors, cell populations, genes, and experimental methods examined in this study.

The first is the modest number of donors. High-quality adult pancreatic tissue suitable for spatial transcriptomics is difficult to obtain because RNA integrity depends on tightly controlled procurement, ischemic time, and fixation, and well-characterized type 2 diabetic tissue is scarcer still [126, 127]. The cohort here is comparable to many spatial studies of the human pancreas, and we mitigated the constraint of tissue availability by designing analyses around donor-level replication and by validating findings against two external reference atlases [128, 129]. Even so, larger cohorts will be needed to capture variation associated with age, sex, ethnicity, disease duration, glycemic control, and medical history.

A second limitation is the use of formalin-fixed, paraffin-embedded tissue [130, 131]. Fixation fragments RNA and reduces transcript recovery, an effect that is relevant for the large, low-abundance transcripts typical of matrix genes, so some components may be underrepresented despite ongoing expression. The same preservation, however, retains the native architecture that is essential for assigning matrix-producing cells to anatomical locations, which for secreted proteins matters more than maximal

transcript recovery, and modern probe chemistry has substantially improved detection from archival tissue.

The MERFISH panel was also targeted, rather than transcriptome wide [132]. A predefined panel cannot discover unanticipated transcripts, but it offers sensitivity and quantitative accuracy, and the 300-gene panel was designed to capture all major pancreatic populations together with ninety-eight curated matrix genes. It therefore covered the basement membrane and vascular-supportive programs central to the questions posed here, even though additional matrix regulators certainly remain to be identified.

Matrix biology also poses an interpretive challenge unique to transcriptomics [16, 133]. Because matrix proteins are secreted, assembled extracellularly, and generally long-lived, the cell nearest a given protein need not be the one that made it, and transcript abundance does not directly report protein secretion, assembly, or stability. Expression data therefore index the capacity for matrix synthesis at the time of collection rather than the deposited matrix itself.

For the same reason, key features of matrix assembly lie beyond RNA measurement. Collagen crosslinking, laminin polymerization, proteolytic processing, and matrix stiffness are set post-transcriptionally and cannot be inferred from expression [134]. Integrating spatial proteomics, quantitative immunohistochemistry, second harmonic generation imaging, and biomechanical measurements will be needed to connect the transcriptional programs described here to matrix composition and function [135].

A further consideration is transcript assignment in densely vascularized regions, where endothelial cells and pericytes are separated only by a shared basement membrane. Despite the resolution of MERFISH, segmentation can occasionally misassign transcripts across these boundaries. We limited this by combining transcriptional identity with anatomical location, validating vascular populations through neighborhood and proximity analyses, and reproducing the major observations in dissociation-based data not subject to diffusion or segmentation artifacts. The convergence of these approaches argues that the cell type-specific programs are genuine.

Finally, the study is cross-sectional and observational [136]. Single time points from donors with established phenotypes cannot establish whether vascular remodeling precedes, accompanies, or follows β cell dysfunction, and transcriptomic data alone cannot prove that the changes observed alter vascular function. Reduced PDGFRB, increased contractile programs, and altered matrix expression are consistent with impaired endothelial-pericyte communication, but direct measures of perfusion, permeability, contractility, and matrix mechanics, together with targeted perturbation of islet-associated fibroblasts, lie beyond what is feasible in fixed human tissue and define clear objectives for future work.

2.6 Future Directions

These findings open several lines of investigation. They establish the major transcriptional cellular sources of basement membrane programs in the adult human pancreas but leave open the developmental origins, functional interactions, and

dynamic remodeling of these populations, questions that will require emerging spatial, molecular, and functional tools applied to intact human tissue.

A priority is functional validation, as transcriptomic association cannot establish causality. Systems that permit selective manipulation, including human vascular and pancreas organoids and defined co-culture systems, would allow direct tests of how pericytes and islet-associated fibroblasts contribute to basement membrane deposition, endothelial maturation, β cell polarity, and insulin secretion [137]. Targeted perturbation of individual matrix genes identified here, including *COL4A1*, *COL4A2*, *LAMB1*, *LAMC1*, and *LAMA5*, would help resolve the roles of specific components [138].

The diabetic remodeling described here similarly invites functional follow-up. The coordinated loss of basement membrane programs with gains in contractile and inflammatory signaling suggests a phenotypic transition whose consequences for capillary contractility, permeability, and blood flow could be tested directly with live imaging and perfusable microvascular systems, and the consequences of reduced PDGFRβ signaling could be probed by asking whether restoring pericyte identity preserves vascular integrity.

Another priority is to define the developmental origins and lineage relationships of the vascular-supportive populations [139]. Fibroblasts, mural cells, smooth muscle, and stellate cells share transcriptional features and may derive from common mesenchymal progenitors, so it remains unclear whether islet-associated fibroblasts are a stable lineage, a fibroblast subset, or a regulated state. Genetic lineage tracing is largely confined to animal models, but approaches based on somatic mutations,

mitochondrial variants, and epigenomic profiling may allow stromal ontogeny to be reconstructed directly in human tissue [140].

Technological advances will extend the analysis. Higher-plex spatial transcriptomics now measures thousands of transcripts *in situ* and could reveal additional stromal states and the signaling networks linking endothelial cells, pericytes, fibroblasts, immune cells, and endocrine cells without the constraints of a targeted panel. Pairing transcriptomics with spatial proteomics is especially important for matrix biology, since imaging mass cytometry, multiplexed immunofluorescence, and MALDI imaging report protein localization and modification that RNA-based techniques cannot, allowing matrix-producing cells and the proteins they deposit to be visualized together [141, 142].

The mechanical properties of the endocrine matrix also warrant study. The basement membrane regulates stiffness and mechanotransduction as well as biochemistry, and crosslinking and fiber organization influence integrin signaling and endocrine function independently of gene expression [143]. Combining transcriptomics with biomechanical measurement and collagen imaging would show how the programs identified here translate into functional changes during diabetes [144].

The multicellular model also guides regenerative strategies, suggesting that engineered islets may require specialized stromal populations and tissue-specific matrices rather than endothelial cells alone, and the matrix signatures defined here provide a starting point for such designs. Larger cohorts spanning prediabetes to established disease, together with longitudinal models, will be needed to order the events of niche remodeling in time. More broadly, the integrated single-cell and spatial

framework used here applies to any vascularized organ, and its extension to the kidney, liver, lung, retina, and brain may reveal both conserved principles of basement membrane assembly and organ-specific adaptations.

2.7 Conclusions

The ECM is now understood as a dynamic regulator of tissue organization and cell communication rather than a passive scaffold, and in the pancreas the basement membranes surrounding endocrine cells and islet vessels are integral to β cell survival, polarity, and insulin secretion. Despite this importance, the cellular origins of these matrices and their fate in type 2 diabetes had remained unclear.

By integrating donor-resolved MERFISH spatial transcriptomics with human single-cell reference atlases, this chapter characterizes the populations that build and maintain the matrix of the adult human pancreas and shows the endocrine vascular niche to be more complex than the long-standing endothelial-centric model allows. Rather than producing the vascular basement membrane alone, endothelial cells cooperate with pericytes and islet-associated fibroblasts to generate distinct but complementary matrix programs. Pericytes supply the structural collagens, endothelial cells add laminins and proteoglycans, and islet-associated fibroblasts define a peri-islet stromal niche.

These populations are not static. Endocrine- and exocrine-associated pericytes hold a conserved vascular identity while tuning their matrix and signaling programs to local demand, and type 2 diabetes remodels the endocrine niche through coupled changes in cellular composition and transcriptional state. The pathology of the disease

therefore extends beyond β cells to the multicellular microenvironment that sustains them.

Beyond pancreatic biology, these results offer a framework for vascular biology, diabetes pathogenesis, and regenerative medicine, and a basis for engineering vascularized endocrine tissue, improving islet transplantation, and building more faithful disease models. Their central contribution is a change in perspective. The human vascular basement membrane is best understood not as the product of endothelial cells but as the work of endothelial cells, pericytes, and specialized fibroblasts acting together to construct, maintain, and remodel the endocrine vascular niche, a view that more accurately reflects the adult human pancreas and points toward new ways of investigating how matrix biology shapes endocrine health and disease.

2.8 Materials and Methods

2.8.1 Human pancreas sample acquisition

De-identified blocks of formalin fixed, paraffin-embedded (FFPE) pancreatic tissue from 12 unremarkable, cancer-free adult cadaveric donors were purchased from ProteoGeneX (Inglewood, CA; RRID:SCR_013844) or collected by the University of California San Francisco Diabetes Research Center Islet Production Core Facility (RRID:SCR_015106). All donors' families gave informed consent for the use of pancreatic tissue in research. Of these 12 donors, 7 were classified as non-diabetic, and 5 had a documented clinical diagnosis of type 2 diabetes. Disease status was determined from donor clinical metadata provided by the tissue source. One non-diabetic donor was obtained through UCSF Human Islet Core; the remaining donors

were obtained from ProteoGeneX. Available donor demographic and clinical information is provided bellow in **Table 2-2.**

Table 2-2: Donor characteristics of human pancreatic tissue samples included in this study.

Clinical and demographic information for the 12 human pancreatic tissue donors analyzed by spatial transcriptomics. The cohort consisted of seven non-diabetic (ND) donors and five donors with type 2 diabetes (T2D). Reported donor characteristics include sample ID, cluster label, sex, age, tissue source (cohort), ethnicity, tissue preservation method, diagnosis, RNA quality (DV200, %), and body mass index (BMI, kg/m²). Cluster labels correspond to donor identifiers used throughout the spatial transcriptomic analyses.

Sample ID	Cluster Label	Sex	Age	Cohort	Ethnicity	Type	Diagnosis	DV200	BMI
121771A(2)	HuP-4	M	46	ProteoGeneX	Caucasian	FFPE	Non-Diabetic	34.65%	29.4
121753A(1)	HuP-5	F	41	ProteoGeneX	Caucasian	FFPE	Non-Diabetic	65.36%	19.3
121467A(5)	HuP-3	M	70	ProteoGeneX	Caucasian	FFPE	Non-Diabetic	56.55%	29.3
121431A(4)	HuP-6	F	73	ProteoGeneX	Caucasian	FFPE	Non-Diabetic	51.25%	33.1
121320A(4)	HuP-2	M	46	ProteoGeneX	Caucasian	FFPE	Non-Diabetic	65.76%	26.9
121261A(3)	HuP-8	M	69	ProteoGeneX	Caucasian	FFPE	T2D	40.20%	26.8
12997A(1)	HuP-9	F	69	ProteoGeneX	Caucasian	FFPE	T2D	62.93%	31.2
12951A(1)	HuP-10	F	74	ProteoGeneX	Caucasian	FFPE	T2D	69.51%	15.1
12893A(2)	HuP-11	M	71	ProteoGeneX	Caucasian	FFPE	T2D	61.74%	24.7
12774A(1)	HuP-12	F	58	ProteoGeneX	Caucasian	FFPE	T2D	45.21%	32.9
121903A(3)	HuP-1	M	75	ProteoGeneX	Caucasian	FFPE	Non-Diabetic	57.08%	30.2
RHIP156	HuP-7	F	48	UCSF	African Ameri	FFPE	Non-Diabetic	70.50%	24.1

2.8.2 Python analysis

All computational analyses were performed in Visual Studio Code (v.1.124), Python (v3.8-v3.13) using Scanpy (v1.12) [145], Squidpy (v1.6.2) [146], scvi-tools (v0.6)[147], DoubletDetection (v2.5.2), GSEApy (v1.2.1) [148], SciPy (v1.17.1), Shapely (v2.1.2), CONCORD-sc (v1.11.4) [149], Fiji/ImageJ (v2.16) [150], or QuPath (v.0.5.1) [151].

2.8.3 scRNA-seq Quality Control and Filtering

scRNA-seq data (.h5ad) were downloaded from the PancDB website, and further filtering using Scanpy quality control was performed to exclude low-quality cells and technical artifacts. QC score was quantified using a composite score base total counts and number of detected genes; log10-transformed and z-score normalized. The final QC score was defined as: QC score = z (log (10(total_counts + 1))) + z

(log10(n_genes_by_counts + 1)). Higher scores indicate cells with greater transcript detection and gene diversity (higher quality cells). Cells with ‘unknown’ cell label, fewer than 100 detected gene counts, or greater than 20,000 were removed to eliminate empty droplets and potential doublets, respectively. Doublets were identified using DoubletDetection. The expected number of doublets was estimated, and cells were classified as singlets or doublets using the doubletdetection classification framework. Predicted doublets (score of 1) were excluded from further analysis.

2.8.3.1 Refining Adult Non-Diabetic PancDB dataset

Cells were first filtered to retain those with more than 100 and fewer than 20,000 counts, resulting in 75,763 cells. Cells annotated as unknown were removed. DoubletDetection was then applied, and cells with a positive doublet prediction score of 1 were excluded, leaving 71,639 cells for CONCORD integration. After integration, additional low-quality samples were removed, resulting in a final reference dataset of 46,106 cells from 22 donors.

From this dataset, 3,010 mesenchymal cells were subset for further analysis. Because several small clusters were separated from the main mesenchymal populations, we examined doublet scores and found that these cells had relatively higher doublet scores. Therefore, cells with a doublet score greater than 20 were removed before downstream analysis. Unsupervised clustering was then performed at a resolution of 0.1, yielding eight clusters. Clusters 7 and 8 were small, containing 118 and 50 cells, respectively. Differential gene expression analysis using sc.rank_genes_groups showed that cluster 7 was enriched primarily for ribosomal genes, while cluster 8 expressed fibroblast-like genes. Based on these results, cluster 7

was removed. Clusters 0, 1, 4, 5, 6, and 8 were merged and annotated as fibroblast-like MSL1 cells, while clusters 2 and 3 were merged and annotated as pericyte-like MSL2 cells.

2.8.3.2 Refining Adult Non-Diabetic and Type 2 Diabetic PancDB dataset

The combined non-diabetic and T2D PancDB dataset was processed using the same quality control, filtering, doublet removal, and CONCORD integration workflow described for the non-diabetic analysis. HPAP109, along with additional low-quality donors identified during quality control, was excluded prior to downstream analyses. Mesenchymal populations were then subset and classified using the same clustering strategy, marker gene criteria, and differential expression framework applied to the non-diabetic dataset. This approach identified fibroblast-like MSL1 cells and pericyte-like MSL2 cells for subsequent comparison. Downstream analyses were performed within each vascular-associated population to assess differences in cell composition, gene expression programs, and pathway enrichment between non-diabetic and type 2 diabetic samples.

2.8.4 Cross-Reference Validation with External scRNA-seq Datasets

To validate spatially identified stromal and vascular-associated populations, comparisons were performed against external human pancreas scRNA-seq reference datasets, including PancDB and the Craig-Schapiro pancreas dataset. Spatial populations were compared against reference populations using shared genes present across datasets and restricted to genes included within the spatial transcriptomics panel where indicated. For transcriptional concordance analyses, average gene expression profiles were calculated for each annotated spatial and reference population. Pearson

correlation and Spearman correlation metrics were used to quantify cross-platform similarity between matched populations. Gene-level comparisons were performed using normalized mean expression values across shared genes. Differentially expressed genes identified in spatial analyses were additionally cross-referenced against external reference datasets to reduce the likelihood that observed transcriptional differences reflected segmentation artifacts, transcript diffusion, or spatial contamination effects. Where PancDB lacked explicit anatomical annotations, corresponding stromal populations were identified computationally based on transcriptional similarity and marker gene enrichment. Spatially defined islet-associated fibroblasts were subsequently validated against anatomically annotated stromal populations in the Craig-Schapiro dataset.

2.8.4.1 PancDB Dataset

MSL1 fibroblast-like cells from PancDB were subset and re-clustered to further resolve fibroblast heterogeneity. This subset included 1,833 cells and was analyzed using Leiden clustering at a resolution of 0.5, which identified six transcriptionally distinct clusters, each containing more than 100 cells. Differential expression analysis was then performed for each cluster using the Wilcoxon rank-sum test.

Two clusters, clusters 2 and 5, showed increased expression of extracellular matrix and basement membrane-associated genes and closely resembled the spatially identified islet-associated fibroblast population. Representative enriched genes included *COL1A1*, *COL1A2*, *COL3A1*, *COL4A1*, *COL5A1*, *SPARC*, *SERF2*, *LGALS1*, *PRELP*, and other matrix-associated genes. In contrast, cluster 3 expressed canonical pericyte markers, including *RGS5*, *CSPG4*, *MCAM*, and *PDGFRB*. Based on these

transcriptional profiles, clusters 2 and 5 were merged and annotated as IAF-like cells, clusters 0, 1, and 4 were merged and annotated as fibroblasts, and cluster 3 was annotated as pericytes.

Subsequent differential expression analyses showed strong concordance between the PancDB IAF-like population and the spatially identified IAF population, including shared enrichment of fibrillar collagen genes, basement membrane-associated genes, and extracellular matrix remodeling programs. Together, these findings provided independent support for a transcriptionally distinct endocrine niche-associated fibroblast population.

2.8.4.2 Craig-Schapiro Dataset

The anatomically annotated human pancreas scRNA-seq dataset generated by Craig-Schapiro et al. was downloaded from GEO and processed in Scanpy. Major pancreatic cell populations were reconstructed using the published cell annotations. Endothelial cells, pericytes, and fibroblasts were then subset and analyzed independently to cross-reference vascular-associated populations identified in the spatial MERFISH dataset.

To enable direct comparison with the MERFISH data, the Craig-Schapiro reference dataset was restricted to genes included in the custom 300-gene spatial transcriptomics panel. Gene expression values were normalized and log-transformed prior to downstream analysis. For validation of islet vascular populations, endothelial cells, pericytes, and fibroblasts were first restricted to cells annotated as originating from islet tissue. Expression of spatially identified marker genes was then assessed in the corresponding reference populations and visualized using violin plots and feature plots.

To examine compartment-specific transcriptional programs, pericytes were further stratified by anatomical location as either islet-associated or exocrine-associated. Differential expression analysis between islet and exocrine pericytes was performed using the Wilcoxon rank-sum test, and results were visualized using volcano plots. Genes identified as compartment-enriched in the spatial dataset were then examined in the Craig-Schapiro dataset to determine whether similar location-associated expression patterns were observed across platforms.

2.8.5 Integration and Batch Alignments with CONCORD

To correct for donor- and dataset-specific batch effects, data were integrated using the CONCORD framework, incorporating donor/sample identity as a batch variable

2.8.6 Gene Set Scoring

Gene set scores were calculated using Scanpy's score_genes function. For each cell, a score was computed as the average expression of genes within the target gene set minus the average expression of expression-matched control genes. Scores were calculated using the expression matrix stored in adata.X (use_raw=False) and stored in adata.obs for downstream analyses. To ensure separation between matrix programs, genes contained within the basement membrane gene set were excluded from the broader ECM gene set prior to scoring, such that ECM scores reflected non-basement membrane matrix components. For visualization, mean gene set scores were scaled across cell types using Scanpy's standard_scale='var' option.

Table 2-3: Basement membrane and extracellular matrix gene sets used for gene set scoring.

The Naba Basement Membrane (NABA_BM) and Naba Core Matrisome (NABA_CORE_ECM) gene sets obtained from the MSigDB. To distinguish broader ECM programs from BM-associated programs, genes

present in the NABA Basement Membrane gene set were excluded from the NABA Core Matrisome gene set prior to scoring. The resulting spatial BM and spatial ECM gene sets include only genes represented in the custom 300-gene MERFISH panel.

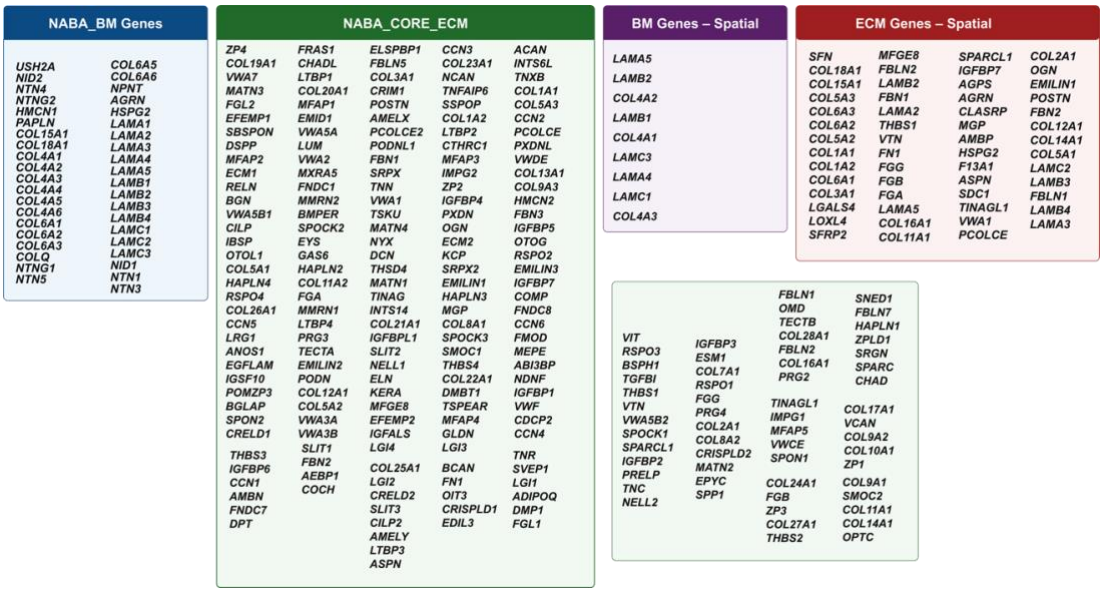

2.8.7 Differential Expression Analysis

Differential gene expression (DGE) analysis was performed using Scanpy's sc.tl.rank_genes_groups with the Wilcoxon rank-sum test. Analyses were conducted on log-transformed expression values (use_raw = False), and p-values were adjusted using the Benjamini-Hochberg procedure to control the false discovery rate.

2.8.8 Hematoxylin and Eosin (H&E) staining

Formalin-fixed paraffin-embedded (FFPE) human pancreatic tissue sections were evaluated by hematoxylin and eosin (H&E) staining to assess tissue integrity, morphology, and islet abundance. Briefly, 5-μm FFPE sections were deparaffinized in xylene, rehydrated through graded ethanol solutions, and stained with hematoxylin followed by eosin using standard histological procedures. Slides were examined by light microscopy to identify well-preserved pancreatic regions containing intact endocrine islets with minimal processing artifacts.

2.8.9 H&E Imaging and Annotation

Following H&E staining, whole-slide images were acquired using a Keyence BZ-X810 digital microscope at 40x resolution using identical acquisition settings across all samples. Individual image tiles were automatically stitched to generate whole-section images and exported for downstream analysis using the QuPath program. Islet and non-islet annotations were exported, and tissue area regions were quantified and plotted. Across all samples, 1 to 2% of the tissue area imaged was occupied by islets, consistent with literature reports.

2.8.10 RNA DV200 Analysis

To assess RNA integrity prior to MERFISH analysis, RNA was extracted from FFPE tissue using the Zymo Quick-RNA FFPE Miniprep kit (Zymo Research, R1008). RNA concentration was measured by NanoDrop spectrophotometry. RNA fragment size distribution and DV200 values were assessed using the Agilent 4200 TapeStation RNA ScreenTape assay according to the manufacturer's protocol. DV200 values represent the percentage of RNA fragments longer than 200 nucleotides.

2.8.11 MERSCOPE Sample Verification

Tissue sections from each donor block were evaluated using the Vizgen MERSCOPE Sample Verification Kit () according to the manufacturer's instructions. This assay employs fluorescent RNA probes targeting two constitutively expressed human housekeeping genes to assess RNA preservation within FFPE tissue sections prior to spatial transcriptomic profiling. Slides were processed using the sample verification workflow and imaged on the MERSCOPE platform to evaluate transcript detection efficiency and tissue morphology.

2.8.12 Gene selection for MERFISH

A custom 300-gene MERFISH panel was designed using the Vizgen MERSCOPE Gene Panel Design Portal (https://portal.vizgen.com). Gene selection was informed by integration of published human single-cell/nucleus RNA-seq datasets, proteomic studies of human pancreas, Human Protein Atlas and the CellxGene tool. Genes were selected based on probe design feasibility (sufficient probe binding sites), expression abundance thresholds (FPKM), and avoidance of optical crowding during imaging. Insulin (*INS*) was excluded due to probe design constraints related to transcript abundance and sequence composition.

The final 300-gene panel included 3 categories. Category 1 genes comprised 98 ECM genes reported to be expressed in the human pancreas and differentially expressed in islets and exocrine tissue at the protein level. Category 2 genes were composed of 25 canonical human endocrine, exocrine, and vascular cell-type markers widely used in the field to annotate known cell types (e.g., *GCG* to mark alpha cells, *PECAM1* to mark endothelial cells, *KRT19* to mark ductal cells). Category 3 genes were reported in recently published literature as being expressed by subpopulations of beta cells and endothelial cells in the pancreas. To serve as a control for nonspecific binding of probes, we included 15 blank barcodes. The full gene is shown in **Table 2-4**.

Table 2-4: Custom MERSCOPE 300 Gene Panel.

Table of the 300 genes used in the MERSCOPE spatial gene panel.

Custom 300-Gene MERFISH Panel

CFTR	PDGFRB	FOS	TH	SERPING1	ACTB	IAPP	SPARCL1	CD86	LRRC40	FGA	PECAM1
CD4	FBN2	COL3A1	AXIN1	DCDC2	COL6A3	NPY	GMCL1	SOX1	JUN	GCK	MSLN
GPRC5A	LGALS3BP	P2RY1	LAMB3	PAX6	FERMT1	SOX9	HHEX	DLK1	EGFL7	FGG	SLC6A2
STYK1	SYP	LAMB2	CD34	AGRN	LAMB4	CD93	UCHL1	CALCA	COL5A1	ITGA6	MRC1
CEACAM1	LIFR	PLPP1	SSTR2	UCN3	ADAM9	COL14A1	SST	TRAK2	TSPAN1	MEIS1	MRTFB
CTSA	WDR11	LGALS4	GHR	SERPINB6	SELENOO	TSPAN8	FCER1G	MAFA	BMPR1A	CAPG	TRPV1
LGALS2	CD81	PLG	ADCY6	SERPINB1	COL2A1	ACE2	GJD2	F3	LRRC8A	SCAF8	ADCYAP1
IL2RB	KDR	CSPG4	SERPINH1	PDX1	COL6A1	PLVAP	RSPH1	PKM	SDC4	PCNT	LAMA3
CHGA	LAMC2	ADAM17	TGFBR2	FBXL18	BEND4	MNX1	CSTB	VWA1	ENG	GCG	PCAT19
MMP2	AGPS	CBX2	PLXNB2	IRX2	TGFBI	LAMA5	S100A1	SFN	GLP1R	FOXA2	C3
CLASRP	CHST10	PDE12	UBAP1	LOXL2	PROM1	RAMP2	CXCL16	SOX18	MAFB	ERLIN1	SELENOW
CD79A	SERPINI2	AQP1	CD300A	IGKC	C1QB	LGALS3	NEUROD1	SYN1	COL16A1	LAMA2	ITPR3
PCOLCE	COL5A3	F2	COL4A2	SH3BP4	ALB	SDC1	IGFBP7	ATF3	CXCR3	COL12A1	CD24
MPO	ICAM1	CD7	TMEM123	CRLF1	CD3E	SERPINF1	FEV	CDH5	IL2RG	ABCC5	TNXB
COL1A1	F13A1	RGS5	KRT19	LAMB1	SERGEF	CRP	FBLN2	CLEC14A	CD52	SIMC1	PAX4
PPY	ANXA3	SLC2A2	CALD1	GRIA2	CTNND1	MTNR1B	NKX6-1	COL18A1	C1QC	PIGL	C11orf96
VTN	AMBP	SERTM1	DUSP10	MCUB	C1R	ANXA1	ITGA2	PRELP	COL5A2	SEPTIN7	HNF1B
IL2	ANLN	TCIM	VIP	SPP1	OCLN	LAMC1	COL1A2	VHL	COL15A1	EMILIN1	CLDN5
CTSC	HPX	NCAM1	NAV1	CCR3	POSTN	IL18BP	DEFB1	SGK3	ASPN	FAT1	GAPDH
MGP	MFGE8	NOS1	POGK	RPL14	DCN	MMP7	HIF1AN	ALDH1A3	OGN	HCFC1	SIDT2
LAMA4	ITGAX	CD19	SLAMF7	COL4A3	LUM	THBS1	COL6A2	MYL9	COL4A1	TNF	IFI27
ISL1	TINAGL1	FBLN1	CCDC186	ITIH5	RAB5B	LOXL4	IRX1	DLG1	AIF1	CTSB	FAP
HES1	SFRP2	CRELD2	DKC1	FOXRED2	TUBB3	ASNSD1	FGB	FTSJ1	MDC 1.00	FN1	HSPG2
NPRL2	ESAM	C1S	COL11A1	MET	TMEM229B	VWF	VAT1L	IL4	PTF1A	PARD6A	SERPINA1
IGFBP2	FLT1	TPM2	GOT1	ITGB2	FBN1	CDH1	DONSON	CD8A	BMI1	LAMC3	TBL1XR1

2.8.13 MERFISH for FFPE tissue samples

A fully detailed, step-by-step guide to the MERFISH sample preparation full protocol is available at https://vizgen.com/resources/fresh-and-fixed-frozen-tissue-sample-preparation. Briefly, FFPE samples from selected donors were sectioned using a microtome (Leica Microtome, HM325) at 4-µm thickness and placed on a MERSCOPE FFPE slide (Vizgen, catalog no. 20400100) in accordance with Vizgen's MERSCOPE User Guide for FFPE samples. The tissue sections were then deparaffinized three times using Deparaffinization Buffer (Vizgen, catalog no. 20300112) at 55 °C for 5 min and washed three times with 100% ethanol. Each wash was for 2 min, followed by 2 min in 90% ethanol and a 2-min 70% ethanol rehydration step. The rehydrated tissue sections were incubated with Decrosslinking Buffer (Vizgen, catalog no. 20300115) at 90 °C for 15 min and cooled at room temperature for 10 min.

The uncrosslinked tissue sections were then incubated with Conditioning Buffer (Vizgen, catalog no. 20300116) at 37 °C for 30 min, and Pre-Anchoring Reaction Buffer (Vizgen, catalog no. 20300113) for 2 h at 37 °C. Following anchoring pretreatment,

tissue slices were stained for cell boundaries using Vizgen's Cell Boundary Kit (catalog no. 10400009) following the user guide. Samples were then washed with Formamide Wash Buffer (Vizgen, catalog no. 20300002) at 37 °C for 30 min and incubated with Anchoring Buffer (Vizgen, catalog no. 20300117) at 37 °C overnight. Following overnight incubation, samples were washed, then gel embedded and cleared. Tissues were cleared using the resistant-clearing protocol for the allowed maximum time (72 h). After tissue clearing, samples were treated with MERSCOPE Photobleacher (Vizgen, catalog no. 10100003) for 4 h, washed with Formamide Wash Buffer at 37 °C for 30 min, and then incubated with MERSCOPE Gene Panel Mix for 48 h at 37 °C.

2.8.14 Cell Segmentation

Automated cell segmentation was performed on nuclear and cell membrane stains using Cellpose v2.0 within the MERSCOPE analysis workflow[152]. Segmentation outputs included cell masks and associated cellular metadata stored in .json files. In addition, stitched mosaic images corresponding to the DAPI, cell boundary, and poly(A) channels were exported as .jpeg files.

2.8.15 Islet Annotations using MERSCOPE Visualizer

Manual islet annotation was performed in MERSCOPE Visualizer (2.1.2593.1). Annotations were selected using four criteria: (1) expression of endocrine-associated transcripts within the candidate region, (2) presence of DAPI signal confirming cellular localization, (3) presence of cells annotated as endocrine populations based on transferred cell labels displayed in the Visualizer overlay, and (4) a minimum of three endocrine cells per annotated islet. Regions meeting all criteria were annotated as islets. Annotated islet geometries and associated metadata, including transcript

coordinates, cell identities, and islet assignments for each cell were exported as .csv files for downstream analyses (Tables S8-S9). A total of 2,387 ND islets and 1,311 T2D islets were annotated.

2.8.16 Spatial Transcriptomics Quality Control and Filtering

Cells with fewer than 10 detected transcripts were removed during quality control. No genes were excluded from the dataset, and all 300 genes included in the MERFISH panel were retained for downstream analyses**.** Raw counts were retained in adata.raw and adata.layers['counts']. For downstream analyses, transcript counts were normalized by total counts per cell using Scanpy's normalize_total function and subsequently log-transformed using log (1 + x).

2.8.17 Spatial Transcriptomics Clustering and Cell-type Annotation

To construct integrated compartment-level datasets, islet-associated cells from all donors were concatenated to generate a combined islet dataset. Exocrine-associated cells from all donors were similarly concatenated to generate a combined exocrine dataset. Because the exocrine compartment contained substantially more cells than the islet compartment, exocrine cells were randomly downsampled (2.8%) to achieve comparable cell numbers between compartments and reduce potential clustering biases driven by unequal sampling. The balanced islet and exocrine datasets were subsequently combined into a single AnnData object for downstream integration and analysis. Spatial datasets were integrated using CONCORD with donor identity specified as the batch variable. A k-nearest neighbor graph was constructed using 15 neighbors and 30 principal components (n_neighbors = 15, n_pcs = 30). Two-dimensional embeddings were generated from the CONCORD latent space and graph-

based clustering was performed using the Leiden algorithm (resolution = 1.0) to identify major cellular populations. Cluster identities were assigned using canonical marker genes and differential expression analysis performed with Scanpy's Wilcoxon rank-sum test implementation (sc.tl.rank_genes_groups).

2.8.17.1 Spatial mesenchymal and endothelial cell refinement

Endothelial and mesenchymal populations were subsetted from the integrated spatial transcriptomic dataset and re-clustered using Leiden clustering to resolve vascular-associated stromal heterogeneity. Initial clustering at a resolution of 0.5 did not adequately separate populations expressing distinct levels of the canonical pericyte marker *RGS5*. Therefore, cells were re-clustered at a higher resolution (resolution = 1.0), resulting in 14 transcriptionally distinct clusters. Cluster identities were assigned based on differential gene expression and canonical marker genes. Clusters were classified as ECs, pericytes, fibroblasts, or a distinct fibroblast population characterized by enrichment of ECM genes, basement membrane-associated genes, and endocrine niche-associated transcriptional programs. This population remained transcriptionally distinct from both pericyte and exocrine fibroblast populations and was therefore annotated as islet-associated fibroblasts (IAFs). To evaluate anatomical localization, annotated cell populations were intersected with manually defined islet regions of interest (ROIs). Approximately 93% of IAFs were located within islet ROIs, whereas approximately 93% of exocrine fibroblasts were located outside of islet ROIs.

2.8.18 Spatial Distance Calculations

Spatial relationships between vascular-associated cell populations were quantified using segmentation-derived cell polygons and Shapely geometric operations.

Cell boundaries generated from MERSCOPE segmentation masks were converted into polygon geometries and indexed using STRtree spatial indexing to enable efficient nearest-neighbor queries. Distances were calculated in microns using the native MERSCOPE coordinate system. For cell-to-cell analyses, the shortest edge-to-edge distance between cell boundaries was computed using polygon geometry. This approach measures the minimum physical separation between neighboring cells and avoids biases introduced by differences in cell size or morphology. Distances between ECs, pericytes, fibroblasts, and endocrine cells were calculated using nearest-neighbor searches across annotated cell populations. For islet boundary analyses, manually annotated islet polygons generated in MERSCOPE Visualizer were used to define endocrine compartment boundaries. The shortest edge-to-edge distance between each cell polygon and the nearest islet boundary polygon was calculated. Cells located within the annotated islet region were assigned negative distance values, whereas cells located outside the islet boundary were assigned positive values.

Distances were summarized at both the cell level and donor level for downstream statistical analyses and visualization of vascular niche organization. To quantify vascular niche organization within pancreatic islets, nearest-neighbor analyses were performed between ECs, pericytes, and endocrine cells using segmentation-derived cell boundaries. Endothelial-pericyte interactions were assessed by calculating the shortest edge-to-edge distance between each endothelial cell and its nearest pericyte. Pericyte coverage was subsequently calculated as the proportion of ECs satisfying this criterion and summarized at the donor level.

2.8.19 Cell Composition Analysis

Vascular-associated cell composition was assessed using annotated endothelial cells, pericytes, fibroblasts, and islet-associated fibroblasts identified from the integrated spatial transcriptomics dataset. For each donor, the total number of cells belonging to each vascular-associated population was quantified and expressed as a proportion of all vascular-associated cells within the analyzed region (islet or exocrine). Cell composition was calculated on a donor-by-donor basis prior to statistical testing. Endothelial-to-pericyte ratios were calculated by dividing the number of islet endothelial cells by the number of islet pericytes identified within each donor. Islet vascularization was calculated as the ratio of endothelial cells plus pericytes to the total number of endocrine cells within each donor. Similarly, the relative abundance of pericytes was calculated as the percentage of pericytes divided by total islet vascular-associated cells. For disease-state comparisons, donor-level composition metrics were compared between non-diabetic and type 2 diabetic samples using Mann-Whitney U tests.

2.8.20 Immunofluorescence (IF) Staining of Human FFPE Pancreatic Tissue

FFPE human pancreatic tissue sections (4–5 μm thick) were baked at 55°C for 15 minutes prior to processing. Sections were deparaffinized in xylene and rehydrated through graded ethanol washes to distilled water. Antigen retrieval was performed using heat-mediated retrieval in citrate buffer pH = 6.0 (Vector Labs, H-3300-250) for 15 minutes and then cooled to RT for another 15 minutes. Tissue sections were permeabilized and blocked in 0.5% PBST with 5% normal donkey serum (Jackson ImmunoResearch Labs Cat# 017-000-121) for 1 hour at RT. Primary antibodies were

incubated overnight at 4 °C in a humidified chamber. Following three 1X PBS washes, sections were incubated with species-specific AlexaFluor-conjugated secondary antibodies at RT for 1 hour. Nuclei were counterstained with DAPI if needed. Slides were mounted using antifade mounting media (Vector Labs, H-1000-10). Fluorescence imaging was performed using a Zeiss LSM800 laser-scanning confocal microscope. For colocalization analysis, images were processed in Fiji/ImageJ and quantified using the Coloc2 plugin [153]. Mean fluorescence intensity was quantified within manually annotated CHGA-defined islet regions in Fiji using identical processing, staining, incubation, and image acquisition settings for all samples. A complete list of antibodies, vendors, catalog numbers, working dilutions, and RRID's is shown below in **Table 2-5**.

Table 2-5: Table of Antibodies used for IF staining.

IF

Primaries

Protein	Host	Vendor	Catalolg Number	Dilution	RRID
HSPG2	Mouse	ThermoFisher	13-4400	1/100	RRID:AB_2533020
CD31	Sheep	RD	AF806	1/200	RRID:AB_355617
Ng2	rabbit	Abcam	ab275024	1/100	RRID:AB_2922401
Collagen 1 A2	rabbit	Abcam	ab308455	1/100	RRID:AB_3678665
Collagen 4 A1	goat	NovusBio	NBP1-26549	1/200	RRID:AB_1853202
CHGA	mouse	NovusBiio	NBP2-34674	1/100	RRID:AB_286438

Secondaries

Channel	Host	Target	Vendor	Cataolog Number	Dilution	RRID
AF 488	donkey	sheep	ThermoFisher	A-11015	1/200	RRID:AB_2534082
AF488	donkey	goat	ThermoFisher	A-11055	1/200	RRID:AB_2534102
AF555	donkey	mouse	ThermoFisher	A-31570	1/200	RRID:AB_2536180
AF647	donkey	rabbit	ThermoFisher	A-31573	1/200	RRID:AB_2536183
DAPI			ThermoFisher	62248	1/1000	RRID:AB_2307445

2.8.21 RNAscope Multiplex Fluorescence Assay on Human FFPE Pancreatic Tissue

RNAscope multiplex fluorescence *in situ* hybridization was performed on FFPE human pancreatic tissue sections using the RNAscope Multiplex Fluorescent Reagent Kit (Advanced Cell Diagnostics, Cat. No. 323100 & 323270) according to the manufacturer's protocol[154]. Target-specific RNAscope probes were hybridized to tissue sections followed by sequential signal amplification steps according to the

manufacturer's instructions. Fluorescent detection was performed using Opal fluorophores (Akoya Biosciences). Nuclei were counterstained with DAPI, and slides were mounted using an antifade mounting medium (Vector Labs, H-1000-10). Fluorescence imaging was performed using a Zeiss LSM800 laser-scanning confocal microscope at either 40x or 63x magnification. Table of probes used is shown below in **Table 2-6**.

Table 2-6: Table of probes used for RNAscope.

RNAscope				
Gene	**Name**	**Vendor**	**Catalog Number**	**Channel**
COL4A1	RNAscope® Probe - Hs-COL4A1-	ACDBio	61881-C2	C2
COL6A2	RNAscope® Probe - Hs-COL6A2-	ACDBio	482611-C3	C3
COL6A1	RNAscope® Probe - Hs-COL6A1-	ACDBio	482461	C1
Opal Dyes	**Vendor**	**Catalog Number**	**Dilution**	
Opal 520	Akoya Biosciences	FP1487001KT	1/1000	
Opal 620	Akoya Biosciences	FP1495001KT	1/1000	
Opal 690	Akoya Biosciences	FP1497001KT	1/1000	

2.8.22 Gene set enrichment analysis

We performed gene set enrichment analysis (GSEA) separately for MSL1 (fibroblast-like) and MSL2 (pericyte-like) populations using GSEApy. Pseudobulk differential expression was first computed by aggregating counts per donor within each mesenchymal subtype, followed by differential testing using a donor-level t-test on log-normalized CPM (counts per million) values. Genes were ranked by their pseudobulk t-statistic, which was chosen as the ranking metric over log-fold change alone to account for cross-donor variance. The ranked gene list was passed to gseapy.prerank with the following parameters: min_size=5, max_size=500, permutation_num=1000, and seed=1. Gene sets were drawn from MSigDB Hallmark (v.2023) and Reactome Pathways 2024 databases. Terms with a false discovery rate (FDR) q-value < 0.25 were

considered significant, consistent with standard GSEA reporting thresholds. Normalized enrichment scores (NES) are reported with direction indicating enrichment in T2D (positive) or ND (negative). Results were visualized using matplotlib.

2.8.23 Identification of Islet-Associated Fibroblasts

A distinct islet-associated fibroblast population was identified in the spatial transcriptomics data that was observed to localize preferentially to the islet boundary and exhibited elevated expression of fibrillar collagen genes (*COL1A1*, *COL1A2*, and *COL3A1*), basement membrane-associated genes (*LAMA2*, *LAMB1*, *LAMC1*, and *LAMC3*), and ECM-remodeling genes including *PRELP*, *FBLN1*, and *COL6A3*. These cells were annotated as islet-associated fibroblasts (IAFs). Independent validation was subsequently performed using the PancDB and Craig-Schapiro human pancreas reference datasets.

2.8.24 Manual gene set curating for Type 2 Diabetes spatial analysis

To characterize T2D-associated transcriptional remodeling in vascular-associated populations, custom gene programs were manually curated using differential expression results from the PancDB human pancreas single-cell RNA-seq reference dataset (Table S14-15). Differential expression analyses comparing type 2 diabetic and non-diabetic pericytes and fibroblasts were used to identify genes consistently associated with disease-related changes in ECM organization, basement membrane maintenance, contractility, stress responses, inflammation, and matrix remodeling. Genes exhibiting significant or strong differential expression, together with genes present in the spatial gene panel and supported by prior literature, were grouped into biologically coherent transcriptional modules. Curated gene sets included basement membrane, interstitial

ECM, ECM remodeling, contractile, and stress/inflammatory programs. Gene program activity was quantified in spatial transcriptomic datasets using Scanpy's score_genes function and gene program scores were subsequently Z-score normalized across cells. These manually curated programs were used to compare healthy and type 2 diabetic tissues and to identify compartment-specific remodeling signatures within endocrine and exocrine vascular niches.

2.8.25 Statistical Analysis:

Statistical analyses were performed in Python using SciPy and in GraphPad Prism (v10.6.1). For donor-level analyses, paired comparisons were assessed using two-sided Wilcoxon matched-pairs signed-rank tests and unpaired comparisons between non-diabetic and type 2 diabetic donors were assessed using two-sided Mann-Whitney U tests. Cell-level comparisons were performed using two-sided Mann-Whitney U tests. Donors were considered the biological replicate for donor-level analyses, whereas individual cells were used as the unit of analysis for cell-level comparisons. Non-parametric statistical tests were selected because they do not require assumptions of normality and are appropriate for the sample sizes used in this study. Data are presented as indicated in the figure legends. P values < 0.05 were considered statistically significant.

2.9 References

1. Tang SC, Jessup CF, Campbell-Thompson M (2018) The Role of Accessory Cells in Islet Homeostasis. Curr Diab Rep 18(11):1–10. https://doi.org/10.1007/S11892-018-1096-Z

2. Da Silva Xavier G (2018) The Cells of the Islets of Langerhans. Journal of Clinical Medicine 2018, Vol 7, 7(3). https://doi.org/10.3390/JCM7030054

3. Yurchenco PD (2011) Basement Membranes: Cell Scaffoldings and Signaling Platforms. Cold Spring Harb Perspect Biol 3(2): a004911. https://doi.org/10.1101/CSHPERSPECT.A004911

4. Nikolova G, Jabs N, Konstantinova I, et al (2006) The Vascular Basement Membrane: A Niche for Insulin Gene Expression and β Cell Proliferation. Dev Cell 10(3):397–405. https://doi.org/10.1016/J.DEVCEL.2006.01.015

5. Kragl M, Lammert E (2010) Basement membrane in pancreatic islet function. Adv Exp Med Biol 654:217–234. https://doi.org/10.1007/978-90-481-3271-3_10

6. Nikolova G, Strilic B, Lammert E (2007) The vascular niche and its basement membrane. Trends Cell Biol 17(1):19–25. https://doi.org/10.1016/J.TCB.2006.11.005

7. Otonkoski T, Banerjee M, Korsgren O, Thornell LE, Virtanen I (2008) Unique basement membrane structure of human pancreatic islets: Implications for β-cell growth and differentiation. Diabetes Obes Metab 10(SUPPL. 4):119–127. https://doi.org/10.1111/J.1463-1326.2008.00955.X

8. Sakhneny L, Epshtein A, Landsman L (2021) Pericytes contribute to the islet basement membranes to promote beta-cell gene expression. Scientific Reports 2021 11:1 11(1):1–10. https://doi.org/10.1038/s41598-021-81774-8

9. Sasson A, Rachi E, Sakhneny L, et al (2016) Islet Pericytes Are Required for β-Cell Maturity. Diabetes 65(10):3008–3014. https://doi.org/10.2337/DB16-0365

10. Santos GSP, Magno LAV, Romano-Silva MA, Mintz A, Birbrair A (2018) Pericyte Plasticity in the Brain. Neurosci Bull 35(3):551. https://doi.org/10.1007/S12264-018-0296-5

11. López-Luppo M, Nacher V, Ramos D, et al (2017) Blood Vessel Basement Membrane Alterations in Human Retinal Microaneurysms During Aging. Invest Ophthalmol Vis Sci 58(2):1116–1131. https://doi.org/10.1167/IOVS.16-19998

12. Hannan RT, Miller AE, Hung RC, Sano C, Peirce SM, Barker TH (2020) Extracellular matrix remodeling associated with bleomycin-induced lung injury supports pericyte-to-myofibroblast transition. Matrix Biol Plus 10:100056. https://doi.org/10.1016/J.MBPLUS.2020.100056

13. He L, Vanlandewijck M, Mäe MA, et al (2018) Data descriptor: Single-cell RNA sequencing of mouse brain and lung vascular and vessel-associated cell types. Sci Data 5. https://doi.org/10.1038/SDATA.2018.160

14. Merl-Pham J, Basak T, Knüppel L, et al (2019) Quantitative proteomic profiling of extracellular matrix and site-specific collagen post-translational modifications in an in vitro model of lung fibrosis. Matrix Biol Plus 1:100005. https://doi.org/10.1016/J.MBPLUS.2019.04.002

15. Geevarghese A, Herman IM (2014) Pericyte-Endothelial Cross-Talk: Implications and Opportunities for Advanced Cellular Therapies. Transl Res 163(4):296. https://doi.org/10.1016/J.TRSL.2014.01.011

16. Bou-Gharios G, Ponticos M, Rajkumar V, Abraham D (2004) Extra-cellular matrix in vascular networks. Cell Prolif 37(3):207. https://doi.org/10.1111/J.1365-2184.2004.00306.X

17. Vigier S, Gagnon H, Bourgade K, Klarskov K, Fülöp T, Vermette P (2017) Composition and organization of the pancreatic extracellular matrix by combined methods of immunohistochemistry, proteomics and scanning electron microscopy. Curr Res Transl Med 65(1):31–39. https://doi.org/10.1016/J.RETRAM.2016.10.001

18. Tosti L, Hang Y, Debnath O, et al (2021) Single-Nucleus and In Situ RNA–Sequencing Reveal Cell Topographies in the Human Pancreas. Gastroenterology 160(4):1330-1344.e11. https://doi.org/10.1053/J.GASTRO.2020.11.010

19. Craig-Schapiro R, Li G, Chen K, et al (2025) Single-cell atlas of human pancreatic islet and acinar endothelial cells in health and diabetes. Nature Communications 2025 16:1 16(1):1338-. https://doi.org/10.1038/s41467-024-55415-3

20. Eguchi K, Nagai R (2017) Islet inflammation in type 2 diabetes and physiology. J Clin Invest 127(1):14. https://doi.org/10.1172/JCI88877

21. Hayden MR, Sowers JR, Tyagi SC (2005) The central role of vascular extracellular matrix and basement membrane remodeling in metabolic syndrome

and type 2 diabetes: the matrix preloaded. Cardiovasc Diabetol 4:9. https://doi.org/10.1186/1475-2840-4-9

22. Kilimnik G, Zhao B, Jo J, et al (2011) Altered Islet Composition and Disproportionate Loss of Large Islets in Patients with Type 2 Diabetes. PLoS One 6(11): e27445. https://doi.org/10.1371/journal.pone.0027445

23. Liu J, Tran V, Vemuri VNP, et al (2023) Concordance of MERFISH spatial transcriptomics with bulk and single-cell RNA sequencing. Life Sci Alliance 6(1). https://doi.org/10.26508/LSA.202201701

24. Patil AR, Schug J, Naji A, Kaestner KH, Faryabi RB, Vahedi G (2023) Single-cell expression profiling of islets generated by the Human Pancreas Analysis Program. Nat Metab 5(5):713. https://doi.org/10.1038/S42255-023-00806-X

25. Home | PANC-DB. https://hpap.pmacs.upenn.edu/

26. NABA_CORE_MATRISOME. https://www.gsea-msigdb.org/gsea/msigdb/human/geneset/NABA_CORE_MATRISOME.html

27. NABA_BASEMENT_MEMBRANES. https://www.gsea-msigdb.org/gsea/msigdb/human/geneset/NABA_BASEMENT_MEMBRANES.html

28. Naba A, Clauser KR, Hoersch S, Liu H, Carr SA, Hynes RO (2012) The matrisome: In silico definition and in vivo characterization by proteomics of normal and tumor extracellular matrices. Molecular and Cellular Proteomics 11(4). https://doi.org/10.1074/mcp.M111.014647

29. GSEA | MSigDB. https://www.gsea-msigdb.org/gsea/msigdb.

30. Liberzon A, Subramanian A, Pinchback R, Thorvaldsdóttir H, Tamayo P, Mesirov JP (2011) Molecular signatures database (MSigDB) 3.0. Bioinformatics 27(12):1739–1740. https://doi.org/10.1093/BIOINFORMATICS/BTR260

31. Liberzon A, Birger C, Thorvaldsdóttir H, Ghandi M, Mesirov JP, Tamayo P (2015) The Molecular Signatures Database (MSigDB) hallmark gene set collection. Cell Syst 1(6):417. https://doi.org/10.1016/J.CELS.2015.12.004

32. Jones RC, Karkanias J, Krasnow MA, et al (2022) The Tabula Sapiens: A multiple-organ, single-cell transcriptomic atlas of humans. Science 376(6594). https://doi.org/10.1126/SCIENCE.ABL4896

33. Muraro MJ, Dharmadhikari G, Grün D, et al (2016) A Single-Cell Transcriptome Atlas of the Human Pancreas. Cell Syst 3(4):385-394.e3. https://doi.org/10.1016/j.cels.2016.09.002

34. Slukvin II, Kumar A (2018) The mesenchymoangioblast, mesodermal precursor for mesenchymal and endothelial cells. Cellular and Molecular Life Sciences 75(19):3507–3520. https://doi.org/10.1007/s00018-018-2871-3

35. Chin CJ, Li S, Corselli M, et al (2018) Transcriptionally and Functionally Distinct Mesenchymal Subpopulations Are Generated from Human Pluripotent Stem Cells. Stem Cell Reports 10(2):436–446. https://doi.org/10.1016/j.stemcr.2017.12.005

36. Innovative Spatial Biology Technology | Vizgen. https://vizgen.com/

37. Schrimpe-Rutledge AC, Fontès G, Gritsenko MA, et al (2012) Discovery of novel glucose-regulated proteins in isolated human pancreatic islets using LC-MS/MS-based proteomics. J Proteome Res 11(7):3520–3532. https://doi.org/10.1021/pr3002996

38. Li Z, Tremmel DM, Ma F, et al (2021) Proteome-wide and matrisome-specific alterations during human pancreas development and maturation. Nature Communications 2021 12:1 12(1):1–12. https://doi.org/10.1038/s41467-021-21261-w

39. Abdulla S, Aevermann B, Assis P, et al (2025) CZ CELLxGENE Discover: a single-cell data platform for scalable exploration, analysis and modeling of aggregated data. Nucleic Acids Res 53(D1): D886–D900. https://doi.org/10.1093/NAR/GKAE1142

40. Pontén F, Jirström K, Uhlen M (2008) The Human Protein Atlas--a tool for pathology. J Pathol 216(4):387–393. https://doi.org/10.1002/PATH.2440

41. Virtanen I, Banerjee M, Palgi J, et al (2008) Blood vessels of human islets of Langerhans are surrounded by a double basement membrane. Diabetologia 51(7):1181–1191. https://doi.org/10.1007/S00125-008-0997-9/FIGURES/8

42. Smyth LCD, Rustenhoven J, Park TIH, et al (2018) Unique and shared inflammatory profiles of human brain endothelia and pericytes. J Neuroinflammation 15(1):138. https://doi.org/10.1186/S12974-018-1167-8

43. Gillespie M, Jassal B, Stephan R, et al (2022) The reactome pathway knowledgebase 2022. Nucleic Acids Res 50(D1): D687–D692. https://doi.org/10.1093/NAR/GKAB1028

44. Ribeiro AL, Kaid C, Silva PBG, Cortez BA, Okamoto OK (2017) Inhibition of Lysyl Oxidases Impairs Migration and Angiogenic Properties of Tumor-Associated Pericytes. Stem Cells Int 2017:4972078. https://doi.org/10.1155/2017/4972078

45. Janciauskiene S, Lechowicz U, Pelc M, Olejnicka B, Chorostowska-Wynimko J (2024) Diagnostic and therapeutic value of human serpin family proteins. Biomedicine & Pharmacotherapy 175:116618. https://doi.org/10.1016/J.BIOPHA.2024.116618

46. Wang D, Wang H, Zheng W, Wang H, Yu W, Du Q (2025) SERPINB6 Promotes Epithelial-Mesenchymal Transition via PI3K/AKT/mTOR Signalling Pathway in Glioma. J Cell Mol Med 29(13): e70711. https://doi.org/10.1111/JCMM.70711

47. Xiang D-N, Feng Y-F, Wang J, et al (2019) Platelet-derived growth factor-BB promotes proliferation and migration of retinal microvascular pericytes by up-regulating the expression of C-X-C chemokine receptor types 4. Exp Ther Med 18(5):4022. https://doi.org/10.3892/ETM.2019.8016

48. Wang Q yue, Guan Q hua, Chen F qin (2009) The changes of platelet-derived growth factor-BB (PDGF-BB) in T2DM and its clinical significance for early diagnosis of diabetic nephropathy. Diabetes Res Clin Pract 85(2):166–170. https://doi.org/10.1016/J.DIABRES.2009.05.008

49. Carbon S, Douglass E, Good BM, et al (2021) The Gene Ontology resource: enriching a GOld mine. Nucleic Acids Res 49(D1): D325–D334. https://doi.org/10.1093/NAR/GKAA1113

50. Hinderer S, Layland SL, Schenke-Layland K (2016) ECM and ECM-like materials — Biomaterials for applications in regenerative medicine and cancer therapy. Adv Drug Deliv Rev 97:260–269. https://doi.org/10.1016/J.ADDR.2015.11.019

51. Lammert E, Thorn P (2020) The Role of the Islet Niche on Beta Cell Structure and Function. J Mol Biol 432(5):1407–1418. https://doi.org/10.1016/J.JMB.2019.10.032

52. Kadono G, Ishihara T, Yamaguchi T, et al (2004) Immunohistochemical localization of type IV collagen alpha chains in the basement membrane of the pancreatic duct in human normal pancreas and pancreatic diseases. Pancreas 29(1):61–66. https://doi.org/10.1097/00006676-200407000-00057

53. Khan ST, Ahuja N, Taïb S, Vohra S, Cleaver O, Nunes SS (2024) Single-Cell Meta-Analysis Uncovers the Pancreatic Endothelial Cell Transcriptomic Signature and Reveals a Key Role for NKX2-3 in PLVAP Expression. Arterioscler Thromb Vasc Biol 44(12):2596. https://doi.org/10.1161/ATVBAHA.124.321781

54. Stratman AN, Davis GE (2012) Endothelial cell-pericyte interactions stimulate basement membrane matrix assembly: influence on vascular tube remodeling, maturation, and stabilization. Microsc Microanal 18(1):68–80. https://doi.org/10.1017/S1431927611012402

55. Armulik A, Genové G, Mäe M, et al (2010) Pericytes regulate the blood-brain barrier. Nature 468(7323):557–561. https://doi.org/10.1038/NATURE09522

56. Shirbaghaee Z, Sorenson CM, Sheibani N (2025) Pericytes and Diabetic Microangiopathies: Tissue Resident Mesenchymal Stem Cells with High Plasticity and Regenerative Capacity. Int J Mol Sci 26(11):5333. https://doi.org/10.3390/IJMS26115333

57. Miner JH (2012) The Glomerular Basement Membrane. Exp Cell Res 318(9):973. https://doi.org/10.1016/J.YEXCR.2012.02.031

58. Hung C, Linn G, Chow YH, et al (2013) Role of lung Pericytes and resident fibroblasts in the pathogenesis of pulmonary fibrosis. Am J Respir Crit Care Med 188(7):820–830. https://doi.org/10.1164/RCCM.201212-2297OC

59. Patel SN, Mathews CE, Chandler R, Stabler CL (2022) The Foundation for Engineering a Pancreatic Islet Niche. Front Endocrinol (Lausanne) 13:881525. https://doi.org/10.3389/FENDO.2022.881525/FULL

60. Khoshnoodi J, Pedchenko V, Hudson BG (2008) Mammalian Collagen IV. Microsc Res Tech 71(5):357. https://doi.org/10.1002/JEMT.20564

61. Nicholas A. K, Jacques P. B (2005) Internal Organization of Basement Membranes. Curr Top Membr 56:265–285. https://doi.org/10.1016/S1063-5823(05)56009-5

62. Warren E, Gerecht S (2023) Beyond the endothelium: the role of mural cells in vascular biology: In vitro systems to study endothelial/pericyte cell interactions. Vascular Biology 5(1): e220021. https://doi.org/10.1530/VB-22-0021

63. Hayden MR, Karuparthi PR, Habibi J, et al (2008) Ultrastructure of Islet Microcirculation, Pericytes and the Islet Exocrine Interface in the HIP Rat Model of Diabetes. Exp Biol Med (Maywood) 233(9):1109–1123. https://doi.org/10.3181/0709-RM-251

64. Lindblom P, Gerhardt H, Liebner S, et al (2003) Endothelial PDGF-B retention is required for proper investment of pericytes in the microvessel wall. Genes Dev 17(15):1835–1840. https://doi.org/10.1101/GAD.266803

65. Lee SJ, Kim S, Jo DH, et al (2021) Specific ablation of PDGFRβ-overexpressing pericytes with antibody-drug conjugate potently inhibits pathologic ocular neovascularization in mouse models. Communications Medicine 2021 1:1 1(1):1–12. https://doi.org/10.1038/s43856-021-00059-3

66. Brandhorst D, Brandhorst H, Lee Layland S, Acreman S, Schenke-Layland K, Johnson PRV (2022) Basement membrane proteins improve human islet survival in hypoxia: Implications for islet inflammation. Acta Biomater 137:92–102. https://doi.org/10.1016/J.ACTBIO.2021.10.013

67. Nilsson J, Fardoos R, Hansen L, et al (2019) Recruited fibroblasts reconstitute the peri-islet membrane: a longitudinal imaging study of human islet grafting and revascularisation. Diabetologia 2019 63:1 63(1):137–148. https://doi.org/10.1007/S00125-019-05018-1

68. Garcia PE, Scales MK, Allen BL, Di Magliano MP (2020) Pancreatic Fibroblast Heterogeneity: From Development to Cancer. Cells 9(11):2464. https://doi.org/10.3390/CELLS9112464

69. Wells RG (2014) The Portal Fibroblast—Not Just a Poor Man's Stellate Cell. Gastroenterology 147(1):41. https://doi.org/10.1053/J.GASTRO.2014.05.001

70. Liu K, Cui Y, Han H, et al (2025) Fibroblast atlas: Shared and specific cell types across tissues. Science Advances 11(14). https://doi.org/10.1126/SCIADV.ADO0173

71. Woodley DT (2017) Distinct Fibroblasts in the Papillary and Reticular Dermis: Implications for Wound Healing. Dermatol Clin 35(1):95–100. https://doi.org/10.1016/j.det.2016.07.004

72. Valenta T, Degirmenci B, Moor AE, et al (2016) Wnt Ligands Secreted by Subepithelial Mesenchymal Cells Are Essential for the Survival of Intestinal Stem Cells and Gut Homeostasis. Cell Rep 15(5):911–918. https://doi.org/10.1016/J.CELREP.2016.03.088

73. Plikus M V., Wang X, Sinha S, et al (2021) Fibroblasts: Origins, definitions, and functions in health and disease. Cell 184(15):3852–3872. https://doi.org/10.1016/J.CELL.2021.06.024

74. Dranoff JA, Wells RG (2010) Portal fibroblasts: Underappreciated mediators of biliary fibrosis. Hepatology 51(4):1438. https://doi.org/10.1002/HEP.23405

75. Driskell RR, Lichtenberger BM, Hoste E, et al (2013) Distinct fibroblast lineages determine dermal architecture in skin development and repair. Nature 2013 504:7479 504(7479):277–281. https://doi.org/10.1038/nature12783

76. Kaestner KH (2019) The Intestinal Stem Cell Niche: A Central Role for Foxl1-Expressing Subepithelial Telocytes. Cell Mol Gastroenterol Hepatol 8(1):111. https://doi.org/10.1016/J.JCMGH.2019.04.001

77. Santini-González J, Simonovich JA, Castro-Gutiérrez R, et al (2021) In vitro generation of peri-islet basement membrane-like structures. Biomaterials 273:120808. https://doi.org/10.1016/J.BIOMATERIALS.2021.120808

78. Irving-Rodgers HF, Ziolkowski AF, Parish CR, et al (2008) Molecular composition of the peri-islet basement membrane in NOD mice: A barrier against destructive insulitis. Diabetologia 51(9):1680–1688. https://doi.org/10.1007/S00125-008-1085-X

79. Korpos É, Kadri N, Kappelhoff R, et al (2013) The peri-islet basement membrane, a barrier to infiltrating leukocytes in type 1 diabetes in mouse and human. Diabetes 62(2):531–542. https://doi.org/10.2337/DB12-0432

80. Kalluri R (2003) Basement membranes: structure, assembly and role in tumour angiogenesis. Nature Reviews Cancer 2003 3:6 3(6):422–433. https://doi.org/10.1038/nrc1094

81. Leclech C, Natale CF, Barakat AI (2021) The basement membrane as a structured surface – role in vascular health and disease. J Cell Sci 133(18). https://doi.org/10.1242/JCS.239889/226247

82. Cabrera O, Berman DM, Kenyon NS, Ricordi C, Berggren P-O, Caicedo A (2006) The unique cytoarchitecture of human pancreatic islets has implications for islet cell function. 103

83. Öhlund D, Handly-Santana A, Biffi G, et al (2017) Distinct populations of inflammatory fibroblasts and myofibroblasts in pancreatic cancer. Journal of Experimental Medicine 214(3):579–596. https://doi.org/10.1084/JEM.20162024

84. Omary MB, Lugea A, Lowe AW, Pandol SJ (2007) The pancreatic stellate cell: a star on the rise in pancreatic diseases. J Clin Invest 117(1):50–59. https://doi.org/10.1172/JCI30082

85. Davidson S, Coles M, Thomas T, et al (2021) Fibroblasts as immune regulators in infection, inflammation and cancer. Nature Reviews Immunology 2021 21:11 21(11):704–717. https://doi.org/10.1038/s41577-021-00540-z

86. Pignatelli C, Campo F, Neroni A, Piemonti L, Citro A (2022) Bioengineering the Vascularized Endocrine Pancreas: A Fine-Tuned Interplay Between Vascularization, Extracellular-Matrix-Based Scaffold Architecture, and Insulin-Producing Cells. Transplant International 35:168. https://doi.org/10.3389/TI.2022.10555/BIBTEX

87. Yousef El-Gohary1 GG (2018) Structure of Islets and Vascular Relationship to the Exocrine Pancreas. Pancreapedia: The Exocrine Pancreas Knowledge Base. https://doi.org/10.3998/PANC.2017.10

88. Richards OC, Raines SM, Attie AD (2010) The Role of Blood Vessels, Endothelial Cells, and Vascular Pericytes in Insulin Secretion and Peripheral Insulin Action. Endocr Rev 31(3):343–363. https://doi.org/10.1210/ER.2009-0035

89. Murakami T, Fujita T, Taguchi T, Nonaka Y, Orita K (1992) The blood vascular bed of the human pancreas, with special reference to the insulo-acinar portal system. Scanning electron microscopy of corrosion casts. Arch Histol Cytol 55(4):381–395. https://doi.org/10.1679/AOHC.55.381

90. Memon B, Abdelalim EM (2021) ACE2 function in the pancreatic islet: Implications for relationship between SARS-CoV-2 and diabetes. Acta Physiol (Oxf) 233(4): e13733. https://doi.org/10.1111/APHA.13733

91. Cho H, Kozasa T, Bondjers C, Betsholtz C, Kehrl JH (2003) Pericyte-specific expression of Rgs5: implications for PDGF and EDG receptor signaling during vascular maturation. The FASEB journal: official publication of the Federation of American Societies for Experimental Biology 17(3):440–442. https://doi.org/10.1096/FJ.02-0340FJE

92. Xavier S, Sahu RK, Landes SG, et al (2017) Pericytes and immune cells contribute to complement activation in tubulointerstitial fibrosis. Am J Physiol Renal Physiol 312(3): F516. https://doi.org/10.1152/AJPRENAL.00604.2016

93. Miao Y, Wu S, Gong Z, et al (2024) SPARCL1 promotes chondrocytes extracellular matrix degradation and inflammation in osteoarthritis via TNF/NF-κB pathway. J Orthop Translat 46:116–128. https://doi.org/10.1016/J.JOT.2024.02.009

94. Tsilibary EC (2003) Microvascular basement membranes in diabetes mellitus. J Pathol 200(4):537–546. https://doi.org/10.1002/PATH.1439

95. Rafii S, Butler JM, Ding B Sen (2016) Angiocrine functions of organ-specific endothelial cells. Nature 529(7586):316–325. https://doi.org/10.1038/NATURE17040

96. Almaça J, Weitz J, Rodriguez-Diaz R, Pereira E, Caicedo A (2018) The Pericyte of the Pancreatic Islet Regulates Capillary Diameter and Local Blood Flow. Cell Metab 27(3):630-644.e4. https://doi.org/10.1016/J.CMET.2018.02.016

97. Harari N, Sakhneny L, Khalifa-Malka L, et al (2019) Pancreatic pericytes originate from the embryonic pancreatic mesenchyme. Dev Biol 449(1):14–20. https://doi.org/10.1016/J.YDBIO.2019.01.020

98. Hayden MR, Patel K, Habibi J, et al (2008) Attenuation of Endocrine-Exocrine Pancreatic Communication in Type 2 Diabetes: Pancreatic Extracellular Matrix Ultrastructural Abnormalities. J Cardiometab Syndr 3(4):234–243. https://doi.org/10.1111/J.1559-4572.2008.00024.X

99. Cao Z, Liu Y, Wang Y, Leng P (2023) Research progress on the role of PDGF/PDGFR in type 2 diabetes. Biomedicine & Pharmacotherapy 164:114983. https://doi.org/10.1016/J.BIOPHA.2023.114983

100. Cai Z, Xu S, Liu C (2024) Cathepsin B in cardiovascular disease: Underlying mechanisms and therapeutic strategies. J Cell Mol Med 28(17):e70064. https://doi.org/10.1111/JCMM.70064

101. Angel P, Karin M (1991) The role of Jun, Fos and the AP-1 complex in cell-proliferation and transformation. Biochim Biophys Acta 1072(2–3):129–157. https://doi.org/10.1016/0304-419X(91)90011-9

102. Somlyo AP, Somlyo A V. (2003) Ca2+ sensitivity of smooth muscle and nonmuscle myosin II: modulated by G proteins, kinases, and myosin phosphatase. Physiol Rev 83(4):1325–1358. https://doi.org/10.1152/PHYSREV.00023.2003

103. Tamayo A, Gonçalves LM, Rodriguez-Diaz R, et al (2022) Pericyte Control of Blood Flow in Intraocular Islet Grafts Impacts Glucose Homeostasis in Mice. Diabetes 71(8):1679. https://doi.org/10.2337/DB21-1104

104. Nyman LR, Wells KS, Head WS, et al (2008) Real-time, multidimensional in vivo imaging used to investigate blood flow in mouse pancreatic islets. Journal of Clinical Investigation 118(11):3790–3797. https://doi.org/10.1172/JCI36209

105. Tilton RG, Hoffmann PL, Kilo C, Williamson JR (1981) Pericyte degeneration and basement membrane thickening in skeletal muscle capillaries of human diabetics. Diabetes 30(4):326–334. https://doi.org/10.2337/DIAB.30.4.326

106. Williamson JR, Rowold E, Hoffman P, Kilo C (1976) Influence of fixation and morphometric technics on capillary basement membrane thickening prevalence data in diabetes. Diabetes 25(7):604–613. https://doi.org/10.2337/DIAB.25.7.604

107. Williamson JR, Kilo C (1977) Current status of capillary basement membrane disease in diabetes mellitus. Diabetes 26(1):69–73. https://doi.org/10.2337/DIAB.26.1.65

108. Williamson JR, Vogler NJ, Kilo C (1973) Early capillary basement membrane changes in subjects with diabetes mellitus. Adv Metab Disord 2. https://doi.org/10.1016/B978-0-12-027362-1.50044-3

109. Biernacka A, Frangogiannis NG (2011) Aging and Cardiac Fibrosis. Aging Dis 2(2):158

110. Gagliano N, Arosio B, Grizzi F, et al (2002) Reduced collagenolytic activity of matrix metalloproteinases and development of liver fibrosis in the aging rat. Mech Ageing Dev 123(4):413–425. https://doi.org/10.1016/S0047-6374(01)00398-0

111. Teuscher AC, Statzer C, Pantasis S, Bordoli MR, Ewald CY (2019) Assessing collagen deposition during aging in mammalian tissue and in Caenorhabditis elegans. Methods Mol Biol 1944:169. https://doi.org/10.1007/978-1-4939-9095-5_13

112. Marneros AG, Olsen BR (2005) Physiological role of collagen XVIII and endostatin. FASEB J 19(7):716–728. https://doi.org/10.1096/FJ.04-2134REV

113. Molina C, Tsukui T, Khan IS, et al (2025) Clonal expansion of alveolar fibroblast progeny drives pulmonary fibrosis in mouse models. J Clin Invest 135(22). https://doi.org/10.1172/JCI191826

114. Usama M, Deng Y, Chen Y, Milland T, Malleshaiah M, Aghazadeh Y (2025) Navigating challenges in human pluripotent stem cell-derived islet therapy for type 1 diabetes. Front Immunol 16:1625439. https://doi.org/10.3389/FIMMU.2025.1625439

115. Jun Y, Nguyen-Ngoc KV, Sai S, et al (2025) Engineered vasculature induces functional maturation of pluripotent stem cell-derived islet organoids. Dev Cell 60(18):2455-2469.e7. https://doi.org/10.1016/j.devcel.2025.04.024

116. Li G, Craig-Schapiro R, Redmond D, et al (2025) Vascularization of human islets by adaptable endothelium for durable and functional subcutaneous engraftment. Sci Adv 11(5):5302. https://doi.org/10.1126/SCIADV.ADQ5302

117. Sackett SD, Tremmel DM, Ma F, et al (2018) Extracellular matrix scaffold and hydrogel derived from decellularized and delipidized human pancreas. Scientific Reports 2018 8:1 8(1):1–16. https://doi.org/10.1038/s41598-018-28857-1

118. Wan J, Huang Y, Zhou P, et al (2017) Culture of iPSCs Derived Pancreatic í µí»½-Like Cells In Vitro Using Decellularized Pancreatic Scaffolds: A Preliminary Trial. https://doi.org/10.1155/2017/4276928

119. Stendahl JC, Kaufman DB, Stupp SI (2009) Extracellular matrix in pancreatic islets: Relevance to scaffold design and transplantation. Cell Transplant 18(1):1–12. https://doi.org/10.3727/096368909788237195

120. Dhandapani V, Boabekoa P, Vermette P (2026) Extracellular matrix from decellularized porcine organs as scaffolds for insulin-secreting cells and pancreatic islets. Front Endocrinol (Lausanne) 16:1722536. https://doi.org/10.3389/FENDO.2025.1722536/

121. Irving-Rodgers HF, Choong FJ, Hummitzsch K, Parish CR, Rodgers RJ, Simeonovic CJ (2014) Pancreatic Islet basement membrane loss and remodeling

after mouse islet isolation and transplantation: Impact for allograft rejection. Cell Transplant 23(1):59–72. https://doi.org/10.3727/096368912X659880

122. Cross SE, Vaughan RH, Willcox AJ, et al (2017) Key Matrix Proteins Within the Pancreatic Islet Basement Membrane Are Differentially Digested During Human Islet Isolation. American Journal of Transplantation 17(2):451–461. https://doi.org/10.1111/ajt.13975

123. Kuncha J, Veeraswamy SD, Darden CM, et al (2026) Engineering Stem Cells for Islet Replacement Therapy: Recent Advances and Barriers for Clinical Translation. Cells 2026, Vol 15, 15(6). https://doi.org/10.3390/CELLS15060532

124. Ito T, Itakura S, Todorov I, et al (2010) Mesenchymal stem cell and islet co-transplantation promotes graft revascularization and function. Transplantation 89(12):1438–1445. https://doi.org/10.1097/TP.0B013E3181DB09C4

125. Dewalkar LP (2026) Experimental models in diabetes research. Laboratory Animal Research 2026 42:1 42(1):25-. https://doi.org/10.1186/S42826-026-00286-6

126. Lawrence E, Sims J, Gander A, et al (2020) The Barriers and Motivators to Using Human Tissues for Research: The Views of UK-Based Biomedical Researchers. Biopreserv Biobank 18(4):266. https://doi.org/10.1089/BIO.2019.0138

127. Edwards J, Belvisi M, Dahlen SE, Holgate S, Holmes A (2015) Human tissue models for a human disease: What are the barriers? Thorax 70(7):695–697. https://doi.org/10.1136/THORAXJNL-2014-206648

128. Li Y, Du Y, Li R, et al (2024) Spatial transcriptomics in pancreatic cancer: Advances, prospects and challenges. Crit Rev Oncol Hematol 203:104430. https://doi.org/10.1016/J.CRITREVONC.2024.104430

129. Khaliq AM, Rajamohan M, Saeed O, et al (2024) Spatial transcriptomic analysis of primary and metastatic pancreatic cancers highlights tumor microenvironmental heterogeneity. Nature Genetics 2024 56:11 56(11):2455–2465. https://doi.org/10.1038/s41588-024-01914-4

130. Zhang P, Lehmann BD, Shyr Y, Guo Y (2017) The Utilization of Formalin Fixed-Paraffin-Embedded Specimens in High Throughput Genomic Studies. Int J Genomics 2017:1926304. https://doi.org/10.1155/2017/1926304

131. Masuda N, Ohnishi T, Kawamoto S, Monden M, Okubo K (1999) Analysis of chemical modification of RNA from formalin-fixed samples and optimization of molecular biology applications for such samples. Nucleic Acids Res 27(22):4436–4443. https://doi.org/10.1093/NAR/27.22.4436

132. Bilous M, Buszta D, Bac J, et al (2026) Resolving sensitivity, specificity and signal contamination in Xenium spatial transcriptomics. Nature Methods 2026 1–11. https://doi.org/10.1038/s41592-026-03089-8

133. Ting DT, Wittner BS, Ligorio M, et al (2014) Single-Cell RNA Sequencing Identifies Extracellular Matrix Gene Expression by Pancreatic Circulating Tumor Cells. Cell Rep 8(6):1905–1918. https://doi.org/10.1016/J.CELREP.2014.08.029

134. Fu N, Drinnenberg I, Kelso J, et al (2007) Comparison of Protein and mRNA Expression Evolution in Humans and Chimpanzees. PLoS One 2(2): e216. https://doi.org/10.1371/JOURNAL.PONE.0000216

135. Chen X, Nadiarynkh O, Plotnikov S, Campagnola PJ (2012) Second harmonic generation microscopy for quantitative analysis of collagen fibrillar structure. https://doi.org/10.1038/nprot.2012.009

136. Figueiredo RG, Patino CM, Ferreira JC (2025) Cross-sectional studies: understanding applications, methodological issues, and valuable insights. Jornal Brasileiro de Pneumologia 51(1): e20250047. https://doi.org/10.36416/1806-3756/E20250047

137. Wassmer C-H, Lebreton F, Bellofatto K, et al (2022) Bio-Engineering of Pre-Vascularized Islet Organoids for the Treatment of Type 1 Diabetes. Transplant International 35:10214. https://doi.org/10.3389/TI.2021.10214

138. Venning FA, Wullkopf L, Erler JT (2015) Targeting ECM Disrupts Cancer Progression. Front Oncol 5(OCT):224. https://doi.org/10.3389/FONC.2015.00224

139. Metikala S, Warkala M, Casie Chetty S, et al (2022) Integration of vascular progenitors into functional blood vessels represents a distinct mechanism of vascular growth. Dev Cell 57(6):767-782.e6. https://doi.org/10.1016/j.devcel.2022.02.015

140. Xu J, Nuno K, Litzenburger UM, et al (2019) Single-cell lineage tracing by endogenous mutations enriched in transposase accessible mitochondrial DNA. Elife 8. https://doi.org/10.7554/ELIFE.45105

141. Yagnik G, Liu Z, Rothschild KJ, Lim MJ (2021) Highly Multiplexed Immunohistochemical MALDI-MS Imaging of Biomarkers in Tissues. J Am Soc Mass Spectrom 32(4):977–988. https://doi.org/10.1021/JASMS.0C00473

142. Parra ER (2018) Novel Platforms of Multiplexed Immunofluorescence for Study of Paraffin Tumor Tissues. J Cancer Treatment Diagn 2(1):43–53. https://doi.org/10.29245/2578-2967/2018/1.1122

143. Page-McCaw A, Ferrell N (2025) Basement Membrane Structure and Function: Relating Biology to Mechanics. Matrix Biol 141:16. https://doi.org/10.1016/J.MATBIO.2025.08.004

144. Lin Z, Chen Y, Zhang P, Jin M, Zha Y, Zhao Z (2026) Spatiotemporal dynamics and regulation of suture morphology and collagen remodeling during trans-sutural distraction osteogenesis. npj Regenerative Medicine 2026 11:1 11(1):4-. https://doi.org/10.1038/s41536-025-00448-5

145. Wolf FA, Angerer P, Theis FJ (2018) SCANPY: large-scale single-cell gene expression data analysis. Genome Biol 19(1). https://doi.org/10.1186/S13059-017-1382-0

146. Palla G, Spitzer H, Klein M, et al (2022) Squidpy: a scalable framework for spatial omics analysis. Nature Methods 2022 19:2 19(2):171–178. https://doi.org/10.1038/s41592-021-01358-2

147. Lopez R, Regier J, Cole MB, Jordan MI, Yosef N (2018) Deep generative modeling for single-cell transcriptomics. Nature Methods 2018 15:12 15(12):1053–1058. https://doi.org/10.1038/s41592-018-0229-2

148. Fang Z, Liu X, Peltz G (2023) GSEApy: a comprehensive package for performing gene set enrichment analysis in Python. Bioinformatics 39(1). https://doi.org/10.1093/BIOINFORMATICS

149. Zhu Q, Jiang Z, Zuckerman B, Weinberger L, Thomson M, Gartner ZJ (2026) Revealing a coherent cell-state landscape across single-cell datasets with CONCORD. Nature Biotechnology 2026 1–15. https://doi.org/10.1038/s41587-025-02950-z

150. Schindelin J, Arganda-Carreras I, Frise E, et al (2012) Fiji: an open-source platform for biological-image analysis. Nature Methods 2012 9:7 9(7):676–682. https://doi.org/10.1038/nmeth.2019

151. Bankhead P, Loughrey MB, Fernández JA, et al (2017) QuPath: Open source software for digital pathology image analysis. Sci Rep 7(1):16878. https://doi.org/10.1038/S41598-017-17204-5

152. Pachitariu M, Stringer C (2022) Cellpose 2.0: how to train your own model. Nature Methods 2022 19:12 19(12):1634–1641. https://doi.org/10.1038/s41592-022-01663-4

153. Stauffer W, Sheng H, Lim HN (2018) EzColocalization: An ImageJ plugin for visualizing and measuring colocalization in cells and organisms. Scientific Reports 2018 8:1 8(1):15764-. https://doi.org/10.1038/s41598-018-33592-8

154. Sari AIP, Copeland K, Nuwongsri P, et al (2025) RNAscope Multiplex FISH Signal Assessment in FFPE and Fresh Frozen Tissues: The Effect of Archival Duration

on RNA Expression. Journal of Histochemistry and Cytochemistry 73(1–2):9. https://doi.org/10.1369/00221554241311971

2.10 Supplemental Files

2.10.1 Chapter 2_Source_Data.xlsx

Publishing Agreement

It is the policy of the University to encourage open access and broad distribution of all theses, dissertations, and manuscripts. The Graduate Division will facilitate the distribution of UCSF theses, dissertations, and manuscripts to the UCSF Library for open access and distribution. UCSF will make such theses, dissertations, and manuscripts accessible to the public and will take reasonable steps to preserve these works in perpetuity.

I hereby grant the non-exclusive, perpetual right to The Regents of the University of California to reproduce, publicly display, distribute, preserve, and publish copies of my thesis, dissertation, or manuscript in any form or media, now existing or later derived, including access online for teaching, research, and public service purposes.

DocuSigned by:
Luisa Kimberly Meneses
F1F9DC6AE989428...
Author Signature

08/06/2026
Date